The Pennsylvania State University

The Graduate School

Department of Energy and Mineral Engineering

INORGANIC-BASED PROTON CONDUCTIVE COMPOSITE MEMBRANES FOR ELEVATED TEMPERATURE AND REDUCED RELATIVE HUMIDITY PEM FUEL CELLS

A Dissertation in

Energy and Geo-Environmental Engineering

by

Chunmei Wang

Submitted in Partial Fulfillment
of the Requirements
for the Degree of

Doctor of Philosophy

May 2010

The dissertation of Chunmei Wang has been reviewed and approved* by the following:

Serguei N. Lvov
Professor of Energy and Mineral Engineering and
Material Science and Engineering
Dissertation Advisor
Chair of Committee

Sridhar Komarneni
Distinguished Professor of Clay Mineralogy
Dissertation Co-Advisor

Derek Elsworth
Professor of Energy and Mineral Engineering

T.C. Mike Chung
Professor of Material Science and Engineering

Yaw D. Yeboah
Professor of Energy and Mineral Engineering
Head of the Department of Energy and Mineral Engineering

*Signatures are on file in the Graduate School

ABSTRACT

Proton exchange membrane (PEM) fuel cells are regarded as highly promising energy conversion systems for future transportation and stationary power generation and have been under intensive investigations for the last decade. Unfortunately, cutting edge PEM fuel cell design and components still do not allow economically commercial implementation of this technology. The main obstacles are high cost of proton conductive membranes, low-proton conductivity at low relative humidity (RH), and dehydration and degradation of polymer membranes at high temperatures.

The objective of this study was to develop a systematic approach to design a high proton conductive composite membrane that can provide a conductivity of approximately 100 mS cm^{-1} under hot and dry conditions (120 °C and 50 % RH). The approach was based on fundamental and experimental studies of the proton conductivity of inorganic additives and composite membranes. We synthesized and investigated a variety of organic-inorganic Nafion-based composite membranes. In particular, we analyzed their fundamental properties, which included thermal stability, morphology, the interaction between inorganic network and Nafion clusters, and the effect of inorganic phase on the membrane conductivity.

A wide range of inorganic materials was studied in advance in order to select the proton conductive inorganic additives for composite membranes. We developed a conductivity measurement method, with which the proton conductivity characteristics of solid acid materials, zirconium phosphates, sulfated zirconia (S-ZrO_2), phosphosilicate gels, and Santa Barbara Amorphous silica (SBA-15) were discussed in detail.

Composite membranes containing Nafion and different amounts of functionalized inorganic additives (sulfated inorganics such as S-ZrO_2, SBA-15, Mobil Composition of Matter MCM-41, and S-SiO_2, and phosphonated inorganic P-SiO_2) were synthesized with different

methods. We incorporated inorganic particles within Nafion clusters either by mixing inorganic gels or solutions with Nafion solution followed by membrane casting or by blending inorganic powders with Nafion solution. The membrane properties, such as acidity, swelling, water uptake, thermostability, proton conductivity, and electrochemical performance, were explored in depth. We characterized the inorganic phase inside composite membranes and its interaction with the Nafion matrix by scanning electron microscopy (SEM) and Fourier transform infrared spectroscopy (FT-IR). Furthermore, we discussed the effect of these inorganic conductors' properties, such as particle size, conductivity, and interaction between functional groups and the Nafion, on the membrane conductivity. The contribution of hydrophilic inorganic particles in improving the membrane fuel cell performance was numerically analyzed by Tafel plot.

Finally, the proton conductivity phenomena in composite membranes were simulated with two proton-transport models; one was based on the rule of mixtures, and the other was described by generalized Stefan-Maxwell equations. In the simulation, we proposed a new route in rational design of high proton-conductive composite membranes.

TABLE OF CONTENTS

LIST OF FIGURES

LIST OF TABLES

NOMECLATURE

A	Cross-section area perpendicular to the ion flow (cm^2), or surface area of inorganic materials (cm^2)
B	Tafel slope
c	Total concentration of liquid mixture (mol cm^{-3})
$c_{AH,0}$	Acid-group concentration of Nafion membrane (mol cm^{-3})
C_{cell}	Geometrical cell capacitance (F)
C_{H+}^{α}	Concentration of protons participating in the diffusion mechanism α (mol cm^{-3})
c_{i}	Concentration of species i (mol cm^{-3} pore solution)
C_{int}	Interface capacitance (F)
$c_{ZH,0}$	Acid-group concentration of inorganic particles (mol cm^{-3})
$c_{ZH_0}^{*}$	Surface acid site density of the additive (mol cm^{-2})
d_Z	Particle size of inorganic additives (cm)
d	Diameter of the pellet (cm)
D_{H+}^{α}	Diffusion coefficient of protons for the diffusion mechanism α ($cm^2\ s^{-1}$)
D_{ij}	Mutual diffusion coefficient for species i and j ($cm^2\ s^{-1}$)
D_{iM}	Diffusion coefficient for interaction of species i and matrix M ($cm^2\ s^{-1}$)
D_{ij}^{e}	Effective mutual diffusion coefficient of species i and j within membrane, = $K_1 D_{\text{ij}}$ ($cm^2\ s^{-1}$)

D_{iM}^{e}	Effective diffusion coefficient for interaction of species *i* and matrix *M*, = $K_0 D_{iM}$ ($cm^2\ s^{-1}$)
E_η	Activation energy for viscosity of water ($kJ\ mol^{-1}$)
F	Faraday constant, 96485 ($C\ mol^{-1}$)
g	Weight of dry material (g)
h	Thickness of the pellet or membrane (cm)
j	Electric current density ($A\ cm^{-2}$)
$K_{A,C}$	Equilibrium constant for proton salvation in terms of concentrations
K_0	Structural constant for the matrix diffusion coefficient
K_1	Structural constant for the mutual diffusion coefficient
l	Distance between electrodes (cm), or mean step distance between steps, (nm)
m	The number of CF_2 units in Nafion
pK	Acid strength of the membrane
$P(T_h)$	Saturated water pressure at the humidification saturator temperature
$P(T_c)$	Saturated water pressure at the conductivity cell temperature
q	Bruggeman or critical exponent predicted to be 1.5
r	Ratio of partial molar volume of membrane to that of water, or area-specific resistance, $\Omega\ cm^2$
R	Molar gas constant ($8.314\ J\ mol^{-1}\ K^{-1}$)
R_e	Electronic resistance through the pellet (Ω)
R_i	Ionic resistance across the pellet (Ω)
R_{int}	Resistance of the interface (Ω)
T_{cell}	Temperature of the conductivity cell (°C)

t_e	Transport number of electrons
t_i	Transport number of ions
T_{hu}	Temperature of the humidifier saturator (°C)
T_g	Glass-transition temperature of membrane (°C)
U	Volume of the titrated NaOH solution (ml)
V	Cell potential
V_0	Open circuit voltage
v_i^D	Diffusional velocity of species *i* with respect to the mixture mass-average velocity (cm s^{-1})
$\overline{V}_i$	Partial molar volume of species *i*, (cm^3 mol^{-1})
W	Warburg impedance (S)
W_s	Width of the sample (cm)
x	Weight percent of the inorganic additive or polymer solution

Greek

α	Degree of acid-group dissociation
α_{AH}	Degree of acid-group dissociation in Nafion membrane
α_{ZH}	Degree of acid-group dissociation in inorganic additives
ε_i	Porosity of the membrane
σ	Proton conductivity (S cm^{-1})
σ_{H+}^{Σ}	Proton conductivity in the surface of membrane (S cm^{-1})
σ_{H+}^{G}	Proton conductivity by Grotthuss diffusion in the membrane (S cm^{-1})
σ_{H+}^{E}	Proton conductivity by *en mass* diffusion in the membrane (S cm^{-1})

σ_P	Proton conductivity in a pore of membrane (S cm^{-1})
δ_{AH}	Ratio of mutual to Nafion matrix effective diffusion coefficients
δ_{ZH}	Ratio of mutual to inorganic additive matrix effective diffusion coefficients
ΔH^0	Enthalpy of proton solvation (kJ mol^{-1})
ϵ	Volume fraction of water in hydrated membrane, or wet porosity
ϵ_0	Percolation threshold volume fraction of water in hydrated membrane
κ	Dimensionality constant of random-walk
ζ_{ij}	Friction coefficient for interaction between species *i* and *j* (J s cm^{-5})(cm^3 mol^{-1})^2
ζ_{iM}	Friction coefficient for interaction between species *i* and matrix *M* (J s cm^{-5})(cm^3 mol^{-1})^2
λ_1^0	Equivalent conductivity of hydronium ions in water (S cm^2)
λ	Ionic conductivity (S m^2 mol^{-1}) or water loading, that is number of water molecules per $-SO_3H$ group
λ_{H+}	Equivalent conductivity of the proton at infinite dilution (S cm^2)
ρ	Pellet resistivity (Ω cm)
ρ_0	Density of dry membrane (g cm^{-3})
τ	Tortuosity factor
τ_D	Mean time between successive jumps (ps)
μ	Chemical potential (J mol^{-1})
μ_i^e	Electrochemical potential of species *i* (J mol^{-1})
ω	Frequency

Abbreviations

α-ZP	Alpha zirconium phosphate
BET	Brunauer-Emmett-Teller
CTAB	Cetyltrimethylammonium bromide, $(C_{16}H_{33})N(CH_3)_3Br$
DFM	Dusty-fluid model
DMFC	Direct methanol fuel cell
DOE	Department of Energy
DPTS	Diethylphosphatoethyltriethoxysilane, $(C_2H_5O)_3SiCH_2CH_2PO(OC_2H_5)_2$
EERE	Energy Efficiency & Renewable Energy
EIS	Electrochemical impedance spectroscopy
EW	Equivalent weight of the membrane
FT-IR	Fourier transform infrared spectroscopy
HPAs	Heteropoly acids
IEC	Ion-exchange capacity (mmol g^{-1})
MCM-41	Mobil Composition of Matter
MEA	Membrane-electrode assembly
MPMS	Mercaptopropyl trimethoxysilane, $(CH_3O)_3SiHS$
NPS	Nafion/phosphosilicate gels composite membrane
PEM	Proton exchange membrane
P-SiO_2	Phosphosilicate gels
PTFE	Polytetraflouroethylene
RH	Relative humidity
SBA-15	Santa Barbara Amorphous silica

SEM	Scanning electron microscopy
SSA	Specific surface area
S-ZrO_2	Sulfated zirconia
TEOS	Tetraethoxysilane, $Si(C_2H_5O)_4$
TFE	Tetrafluoroethylene
TGA	Thermogravimetric analysis
VDF	Vinylidene difluoride
XRD	X-ray diffraction

ACKNOWLEDGEMENTS

I would like to show my upmost appreciation to my thesis advisors, Dr. Serguei Lvov and Dr. Sridhar Komarneni, for their suggestions and support on my Ph.D. study at Penn State. I am very thankful to Dr. Lvov that he proposed such an interesting research project as my thesis topic. His smart advice nourished my mental development. I am also very grateful for his teaching in fundamentals of electrochemistry, which build the knowledge foundation for my research.

I sincerely appreciate Dr. Komarneni for his encouragement and research guidance. And many thanks to Dr. Komarneni and his research group that provided inorganic materials and their characterization with XRD and SEM images.

I am very thankful to Dr. Elena Chalkova, who has guided me with many useful and practical suggestions on experimental system development, composite membrane synthesis, various operations in our laboratory, and data analysis. Her knowledge and experience contributed greatly to this thesis.

Special thanks are to our research group members. I thank Dr. Viktor Balashov for his patient help in developing the impedance open circuit modeling. Dr. Mark Fedkin always provided elaborated comments on all research reports and presentations. Dr. John Lee cooperated on carrying out the PEM fuel cell performance measurements with our fabricated composite membranes. I also thank Christopher Lute for his help to design the sample holder for inorganic material conductivity measurements. Justin Beck and Mark LaBarbera proofread the thesis.

I thank my doctoral committee members for their encouragement and advice on my research. In addition, I am very thankful to Dr. Harold Schobert and Dr. Andre Boehman for their great help to guide me to pursue my Ph.D. study from aspects of fundamental theory.

I also thank many sisters and brothers in the Chinese Alliance Church for their consistent sincere help and pray.

Last but not least, I am really thankful to my parents and two sisters, who have strongly supported me and helped me overcome difficulties, sadness, and loneliness during my study abroad.

I acknowledge the U.S. Department of Energy (contract No. DE-FG36-06GO16036) for the financial support of this project.

Chapter 1

Introduction

1.1 Problem statement

We need to develop new membrane materials operating at elevated temperatures (100 ~130 °C) and reduced relative humidity (RH) in order to fulfill the implementation of PEM fuel cell technology. PEM fuel cells have a great potential for a small-scale stationary power generation and for future transportation, owing to their inherently high energy efficiency and low emission of environmental pollutants and green house gases, such as CO_2. However, the commercialization of PEM fuel cells is hamstrung by the limitations of available polymer electrolyte membranes. The traditional polymer membranes (perfluorinated and aromatic sulfonated membranes) have low glass transition temperatures and usually limit operation temperatures to below 60-80 °C. At these temperatures, impurities in fuels, such as CO, can poison the Pt catalysts [1]. At concentration level as low as 5-10 ppm, CO poisons the Pt anode electrocatalysts and the current drops dramatically at higher voltages [2]. However, the tolerance for CO increases dramatically with increasing temperature. Therefore, a higher operating temperature is very desirable. Currently, researchers world-wide have begun to seek suitable alternatives to traditional polymer membranes that might operate at higher temperatures. The Department of Energy (DOE) Energy Efficiency & Renewable Energy (EERE) program has established a High Temperature Membrane Working Group, including universities, national labs, small business, and industry, to provide a forum for greater interactions. The program put the effort to develop high-temperature membranes for PEM fuel cells [3].

The requirement to keep the polymer membranes hydrated places an additional limitation in their applications in PEM fuel cell technology. Traditional polymer membranes cannot operate properly at temperatures above 100 °C because they dehydrate and degrade rapidly [4-7], resulting in substantially decreased proton conductivity. Conductivity lower than 100 mS cm^{-1} is not acceptable for use in PEM fuel cells [6]. Presently, only fully-hydrated sulfonic acid membranes are known to have sufficient conductivity [8]. The proton conductivity of polymeric membranes decreases logarithmically with the RH of membranes. At low humidity, most conductive polymers have very low proton conductivity. For example, the current standard for PEMs is Nafion, a perfluorosulfonic acid membrane that presents only a conductivity of 2 mS cm^{-1} at 100 °C and 20 % RH [4]. A fully hydrated membrane requires using an external humidifier, which results in a more complex and expansive fuel cell system. Thus, a limitation of the water-thermal management is imposed on PEM fuel cells. To address these problems, we need new membrane materials with sufficient proton conductivity operating at low humidity and temperatures above 100 °C.

We also need to solve another problem: the thermo-mechanical properties of membranes must be improved. Many polymer membranes swell up upon hydration, which causes mechanical stress and deteriorates membranes' mechanical properties. Furthermore, methanol easily permeates these polymer membranes, which limits the performance of direct methanol fuel cells (DMFC) [9]. These membranes also exhibit poor thermal and chemical stability and limited durability in operational environments. A suitable membrane is the main obstacle in the PEM fuel cell technology and requires further development.

1.2 Objectives

The creation of new high-temperature membrane with desired performance characteristics requires significant fundamental research and development. The membrane has to be thermally and dimensionally stable, be resistant to fuel permeation, and be highly proton-conductive under high temperature and low RH conditions. The main objective of our research was to carry out extensive fundamental studies to design a composite membrane with the desired proton conductivity at elevated temperatures and reduced RH. To fulfill this objective we

1) designed an experimental method to study the conductivity of inorganic conductors;
2) developed an experimental system for reliable measurements of the proton conductivity;
3) investigated highly proton conductive inorganic materials as additives to increase the membrane conductivity up to 100 mS cm^{-1} at 120 °C and 50 % RH;
4) produced a composite membrane fabrication method to allow the incorporation of inorganic particulate materials into Nafion matrix with a suitable compatibility;
5) explored the proton transport mechanisms in inorganic materials and composite membranes;
6) studied the PEM fuel cell performance of the newly developed composite membranes.

A proton conductive inorganic standard, α-zirconium phosphate (α-ZP), was proposed in this study on the basis of the literature study and our laboratory measurements. Three solid acid inorganic conductors were extensively studied: phosphosilicate gels (P-SiO_2), sulfated zirconia (S-ZrO_2), and sulfonic acid-functionalized Santa Barbara Amorphous silica (SBA-15). We chose them because they are highly surface-hydrophilic and acidic. Three main composite membrane synthesis methods were developed. The research systematically examined the conductivities of

composite membranes with different inorganic additives and different inorganic contents. The results explored the fundamental components of the membrane conductivity, such as inorganic phase within membranes, membrane properties, and the interaction between inorganic phase and membrane matrix. The proton transport phenomena were simulated from the kinetic theory. All inorganic materials studied in this research, except phosphosilicate gels, were provided by Dr. Komarneni's research lab.

1.3 Hypothesis

The present critical technical requirement for elevated-temperature membranes is to maintain or enhance water content to achieve the proton conductivity at 120 °C [3]. Hydrophilic inorganic additives were investigated to aid in water management and to improve overall membrane performance [10-13]. This study examined the use of surface functionalized acidic inorganic additives. Those inorganic materials composed of oxyanion groups, such as SO_4 and PO_4, when doped in Nafion membrane, could preserve a very thin surface layer of adsorbed water at elevated temperatures and low RH, which increased the proton conductivity by 10 %. Also, retaining the water made continuous channels throughout the membrane and would enhance the fuel cell performance at low RH. In order to check the hypothesis, we studied the surface properties of acidic inorganic additives. The proton conductivities and fuel cell performance of Nafion-based composite membranes were measured and compared with recast Nafion at 120 °C and different RH.

1.4 Thesis structure

This thesis consists of seven chapters. Chapter 1 provides the reader with an introduction to the concepts relevant to this study. This chapter lays out clearly the problems that exist in current technology and the proposed methodology to address these problems. Next, a breakdown of the objectives and hypothesis specific to this study are provided.

Chapter 2 generates a literature review on the topic, which introduces the background information on the proton conductivity of inorganic materials and Nafion-based composite membranes. The main focuses of this literature analysis are the proton conductivity characteristics of inorganic materials, proton transport mechanisms and models of membranes.

Chapter 3 describes the designed measurement method and developed experimental system for measuring the conductivity of inorganic proton conductors over wide ranges of temperature and relative humidity. The chapter also addresses the analytical techniques used to characterize inorganic materials and composite membranes. The characterized properties of inorganic conductors include the inorganic phase, the surface area, the morphology, and the ion-exchange capacity (IEC). For composite membranes, the analysis includes synthesis techniques, thermal stability, swelling, IEC, morphology, physicochemical properties, and electrochemical fuel cell performance. The chapter describes the protocols for the proton conductivity measurements of the inorganic materials and the composite membrane as well.

Chapter 4 presents the literature study and the experimental results of proton conductivity of α-ZP, P-SiO_2, S-ZrO_2, and SBA-15, respectively. The electronic conductivity and impedance characteristics of these inorganic conductors are also discussed.

Chapter 5 provides experimental results of the proton conductivity and fuel cell performance of Nafion-based composite membranes. The membrane properties, such as acidity, swelling, water uptake, thermostability, physic-chemical properties, and morphology, are studied

extensively. We discuss the interaction of inorganic's functional groups with Nafion matrix, and conclude the fundamental relationship between membrane properties and the proton conductivity. The membrane fuel cell performance is analyzed from aspects of ohmic loss and activation polarization.

Chapter 6 addresses the modeling of the proton conductivity in composite membranes. Two theoretical models are developed. One is based on the modified rule of mixtures, which estimates the proton conductivities of composite membranes from the conductivity of the Nafion and inorganic additives. The second approach simulates the proton transfer in composite membranes on the basis of generalized Stefan-Maxwell equations.

Chapter 7 gives an overall summary of the completed research, draws the most important conclusions, and provides suggestions for the future work.

Chapter 2

Literature Review

This chapter introduces the background information on the proton conductivity of inorganic materials and Nafion-based composite membranes. The contents will cover the information available in published sources on four topics: the conductivity measurement method of inorganic materials, the characteristics of solid acid conductors, the development of composite proton-exchange membranes, the proton transport mechanism, and modeling of composite membranes.

2.1 Proton conductivity of inorganic materials

2.1.1 The method for measuring proton conductivity in inorganic materials

AC impedance spectroscopy measurements on dense pellets have been widely used to study the proton conductivity of inorganic materials [14-28]. Different materials have served as blocking electrodes: platinum disks, brass discs, graphite slices, or gold foils. Ionic conductive materials were cold pressed into pellets at room temperature. A sealed-off cell or resin was used to avoid evaporation of water. An example of the sample arrangement is shown in Figure **2-1**. At the early stage of the research, the assembly was put into an oven or a furnace to provide high operational temperatures. The procedures proved to have several limitations when it came to getting reliable conductivity measurements. For example, using a resin to seal the sample allowed the measurements to be performed only at room temperature in water or at 100 % RH [15, 16]. Moreover, putting the sealed-off cell into the oven or furnace hindered the adjustment of the RH

inside the cell. Before the measurements, pellets were equilibrated for a week at a controlled RH [17, 21, 22]. This method did not permit the adjustable RH experimental condition. As a result, experiments could not provide a wide range of conditions with desired RHs. In the most recent method, the conductivity cell is connected to a water reservoir; adjusting the temperature in the water tank permits a wide range of RH in the cell [27]. Instead to heat up the whole water tank, in our study, we introduced a saturator (BT-104 BekkTech saturator) to improve the accuracy of the RH adjustment. The accurate control of temperature and RH proved to be the issue in the study of the proton conductivity of inorganic materials.

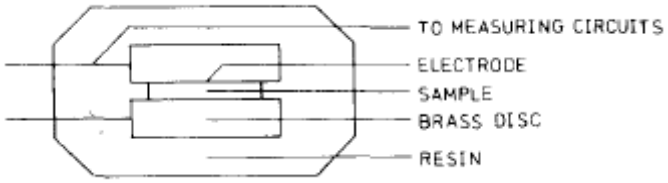

Figure **2-1**: Original arrangement of a sample for conductivity measurements [15].

2.1.2 Proton conductive inorganic materials

A material is defined as a proton conductor if protons can be transferred through the material and converted to hydrogen gas at the cathode [29]. In principle, the conducting species include protons, oxonium, ammonium NH_4^+, hydrazinium ions $N_2H_5^+$, or hydroxyl groups. Inorganic conductors proved to be thermal stable, oxidation resistant, and inert to ionizing radiation. These conductors have been used in diverse processes, such as photosynthesis in green plants and electricity production in a fuel cell. Colomban divided inorganic protonic conductors

into five classifications according to the preparation method, the structural dimensionality and the conductivity mechanism [29]. They are

(1) mineral acids, e.g. HCl and H_3PO_4;

(2) heteropoly acids (HPAs), e.g. $H_3PW_{12}O_{40}{\cdot}nH_2O$ or sulfonated zirconium phosphonates;

(3) acid phosphates, e.g. $Zr(HPO_4)_2{\cdot}H_2O$ and $HUO_2PO_4{\cdot}4H_2O$;

(4) hydroscopic oxides, e.g. silica, titania, alumina, $ZrO_2{\cdot}nH_2O$, $SnO_2{\cdot}nH_2O$, and $Sb_2O_5{\cdot}nH_2O$; and

(5) aluminosilicates, e.g. zeolites, clays, micas, and felspars [8, 15].

Mineral acids presented the highest proton conductivity with values $\sigma > 100$ mS cm^{-1} up to nearly 200 °C. Heteropoly acids have a decreasing order of conductivity. The structural characteristics of inorganic components determine their proton conduction. Superacidic HPAs have structural groups of polyoxometalates, which bring forth the stable proton conductivity of 20 ~ 100 mS cm^{-1} at room temperature [30, 31]. Phosphosilicate gels with a P_2O_5-SiO_2 network consist of thermally stable silica and phosphate. Phosphate has a strong affinity for water molecule adsorption, and is reported to reach a high proton conductivity of 15 mS cm^{-1} at 130 °C and 0.7 % RH [24]. Hydrated ZrO_2 having a fast ion-exchange property is of particular significance in the constitution of its particle surface, on which the surface oxygen is associated with protons. Terminal oxygens belong to H_2O and bridging oxygen belongs to OH^- ions. At 27 °C, the proton conductivity of hydrous ZrO_2 can reach as high as 0.1 mS cm^{-1} [15]. $CsHSO_4$ and other oxoacid salts have a super-protonic phase transition. When the temperature is above 150 °C, their proton conductivities increase by several orders of magnitude up to 10 mS cm^{-1} [32, 33].

Thampan et al reported that inorganic conductive materials when doped in a conventional polymer electrolyte membrane can enhance the acidity and water sorption of the membrane,

especially at low RH [34]. Several classes of inorganic proton conductors were investigated as candidates for the new composite membranes [35], which were

(1) layer-structured phases of hydrogen phosphates with high proton contents up to ~7 meq g^{-1}, such as α-$Zr(HPO_4)_2 \cdot H_2O$, γ- $Zr(HPO_4)_2 \cdot 2H_2O$, α-$Ti(HPO_4)_2 \cdot H_2O$, and γ-$Ti(HPO_4)_2 \cdot 2H_2O$;

(2) three-dimensional network phases of hydrogen phosphates with the ability to retain water up to 300 °C, like $HZr_2(PO_4)_3$, $H(Zr_{2-x}Sn_x)(PO_4)_3$, $HTi_2(PO_4)_3$, and $H_3OTi_2(PO_4)_3$;

(3) mesoporous oxide materials with the specific surface areas up to 400 m^2 g^{-1}, for example Al_2O_3, SiO_2, TiO_2, and ZrO_2;

(4) porous titanosilicates, e.g. $Na_2Ti_2O_3SiO_4 \cdot 2H_2O$, $H_2Ti_2O_3SiO_4 \cdot 1.5H_2O$; and

(5) solid acid materials, such as sulfated ZrO_2, sulfated SiO_2, SiO_2 phosphates, and $CsHSO_4$.

In order to enhance the interaction between the inorganic phase and polymer clusters, some inorganic materials were surface functionalized. Recently, acid-functionalized proton conductors based on mesostructured silica have been prepared by postgrafting [36] or co-condensing functional silica precursors [27, 37]. These materials exhibit promising proton conductivity at elevated temperatures and low RH due to superior water adsorption properties of the porous structure. Marschall [38] synthesized SO_3H-functionalzied nanoparticles of Si-MCM-41 by co-condensation of mercaptopropyl trimethoxysilane (MPMS, $(CH_3O)_3SiHS$)) and tetraethoxysilane (TEOS, $Si(C_2H_5O)_4$) with a pre-hydrolysis step. At 140 °C and 100 % RH, this sample reached a high proton conductivity of 50 mS cm^{-1}. In these mesoporous proton conductors, sulfonic acid acted as the protogenic group. Alternatively, phosphoric acid and phosphonic acid can serve as the functionalization agent. Amphoteric phosphoric/phosphonic acids are found to be advantageous over sulfonic acid in that they can facilitate proton conduction in the dry state by forming dynamic hydrogen bond networks [39]. Jin [28] developed

microporous MCM-41 by the co-condensation of diethylphosphatoethyltriethoxysilane (DPTS, $(C_2H_5O)_3SiCH_2CH_2PO(OC_2H_5)_2$) and TEOS using surfactant cetyltrimethylammonium bromide (CTAB, $(C_{16}H_{33})N(CH_3)_3Br$) as a template. Then, the sample was phosphonated with the phosphoric-acid acidification. The MCM-41 showed a proton conductivity of 0.3 to 15 mS cm^{-1} at 130 °C with RH increased from 20 to 100 %.

2.2 Composite proton-exchange membranes

2.2.1 Proton-exchange polymer membranes

A proton-exchange membrane (PEM) consists of the polymer backbone, chemical cross-links, side chains, and the pendant acid group [34]. The backbone of polymers is fluorinated or hydro-carbonated. The acid groups include as (1) sulfonic acid ($-SO_3H$), (2) carboxylic acid (-COOH), (3) phosphonic acid ($-PO_3H_2$), and (4) sulfonyl imide ($-SO_3NHSO_2CF_3$). The number (equivalent weight, EW) and strength (p*K*) of acid groups determine the conductivity of the PEM. The backbone along with cross-links confers the PEM thermomechanical properties and the extent of swelling.

Nafion, a perfluorosulfonic acid membrane, has been widely used because of its excellent proton conductivity and electrochemical stability. In this study, we chose a Nafion ionomer to fabricate the composite membranes. The influence of inorganic additives on the proton conductivity of composite membranes was extrapolated on the basis of an understanding of the structure and proton transport mechanisms of Nafion.

Nafion is generated by copolymerization of a perfluorinated vinyl ether comonomer with tetrafluoroethylene (TFE). The chemical structure and the morphology network are shown in Figure **2-2**. Nafion is characteristic of a cluster-network containing ionic clusters within a

semicrystalline matrix. The ionic clusters are approximately spherical in shape and are interconnected by narrow channels for ionic transportation. Under hydration, clusters expand in sizes when the sulfonated sites redistribute to yield fewer clusters. The EW of Nafion is the number of grams of dry Nafion per mole of sulfonic acid groups, which indicates the distribution of CF_2 units [40]. Commonly, the designation "117" for Nafion 117 refers to a membrane having the 1100 EW and a nominal thickness of 0.007 in.

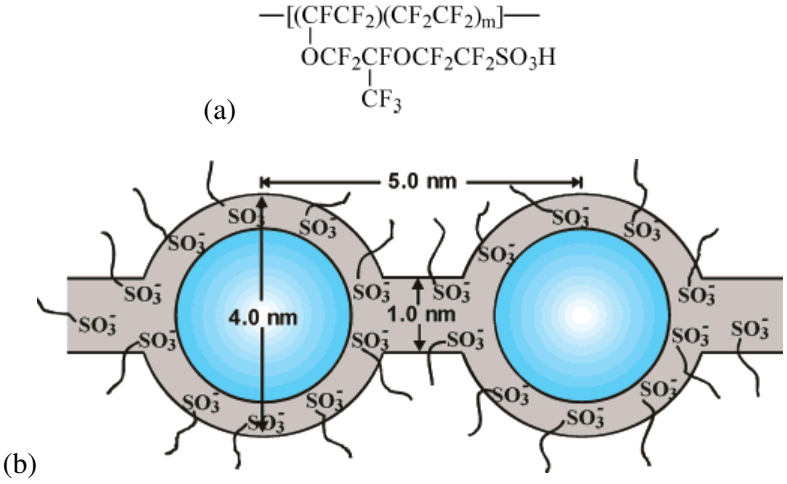

Figure **2-2**: The chemical structure (a) and the morphology cluster-network of hydrated Nafion (b) [40].

The proton transport mechanisms in Nafion are believed to occur through the mixture of surface hoping, vehicle transport and Grotthuss diffusion [41]. In the vehicle mechanism, protons are transferred by riding along with the diffusing H_2O complexes, such as hydronium ions, or through the electro-osmotic drag, in which protons are strongly bonded with water molecules in the first hydration shell. In the Grotthuss mechanism, protons hop from one solvent molecule to the adjacent one. This process involves the stretching of an OH bond on an H_3O^+ ion, which

creates a dipolar field that orients a neighboring H_2O molecule. As the energies before and after a hop become equal, the orientation becomes correct and proton tunneling occurs from H_3O^+ to H_2O.

The proton conductivity in Nafion strongly depends on water content, on structural variables such as porosity and tortuosity, on proton diffusion coefficients, and on the distribution of protons. A simplified picture of the proton diffusion in Nafion is shown in Figure **2-3**. Porosity is the volume fraction of absorbed water, and tortuosity is a factor of proton concentrations in the surface region and in the bulk. When Nafion sorbs a large amount of water, the membrane pores become larger and less tortuous. This increases the conductivity of protons in the membranes. The distribution of protons between the surface and the pore bulk is important and depends on the acid strength of the functional groups. The Grotthuss diffusion coefficient was calculated to be around 7.05×10^{-5} cm^2 s^{-1} and was four times higher than the vehicle diffusion coefficient of 2.26×10^{-5} cm^2 s^{-1} [13]. Choi et al concluded that the Grotthuss diffusion is the dominant proton transport mechanism within Nafion.

The thermomechanical properties of Nafion substantially affect its operation in PEM fuel cells. Researchers found that the swelling of Nafion is mostly determined by its elasticity. The Young's modulus of Nafion at different temperatures as a function of RH was reported and is shown in Figure **2-4** [13]. The relationship between RH and the water activity is that RH (%) equals to the water activity multiplying 100. The Young's modulus declines when either temperature or RH increases. The dependence on the temperature becomes more apparent when the temperature is close to the glass-transition temperature (T_g). T_g for Nafion-112 membrane is around 110 °C. As the Young's modulus decreases, the amount of water absorbed increases owing to the reduced swelling pressure. As a result, the water sorption for Nafion increases gradually with temperature increasing.

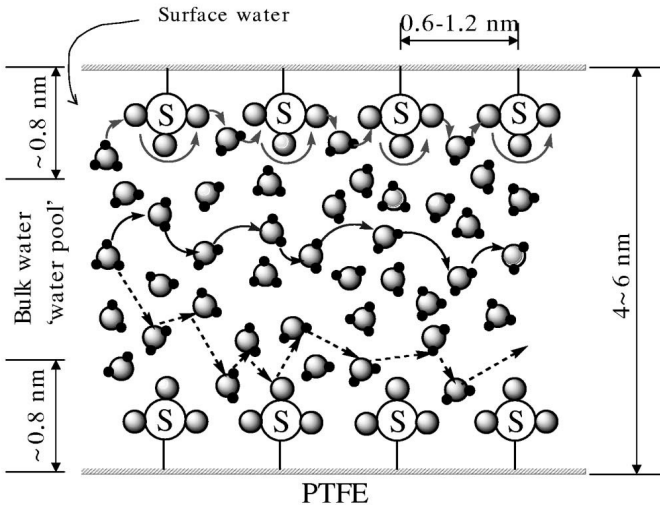

Figure **2-3**: Proton transfer in Nafion in fully hydrated state [41].

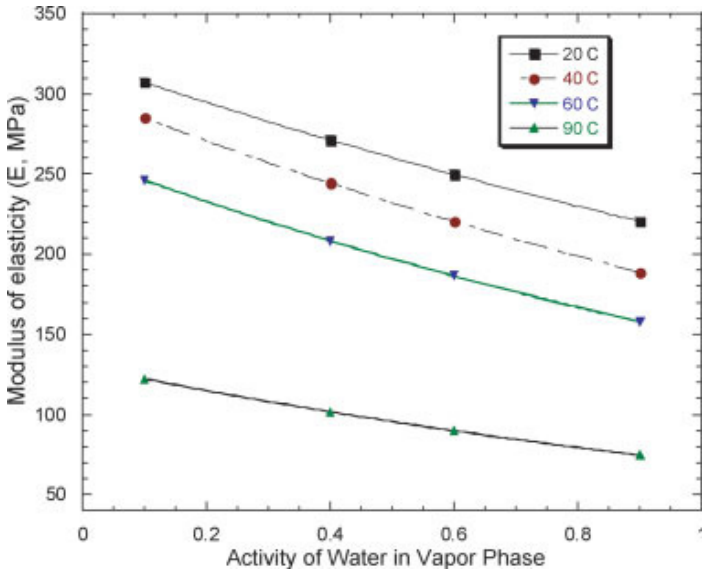

Figure **2-4**: Experimental results of Young's modulus of Nafion as a function of water activity (RH) [13].

2.2.2 Nafion-based composite proton-exchange membranes

In order to develop a desirable PEM, a well known approach has been explored to synthesize composite polymer electrolyte membranes. That is membranes were prepared by the incorporation of functional additives into conventional PEMs. To select an appropriate functional additive for a composite proton-exchange membrane, the following factors need to be considered: (1) the hydrophilicity of inorganic materials, (2) the acid site density and strength on the inorganic particles surface, (3) the particle size or the specific surface area of inorganic particles, (4) the amount of the inorganic loading, and (5) the compatibility of inorganic particles with the polymer electrolyte.

In Nafion-based composite membranes, Nafion is employed as the host membrane to direct the morphology, the particle growth, and the size of additives in the PEM matrix. A variety of solid acids, such as SiO_2, TiO_2, ZP, $H_3PW_3O_{40}$, ZrO_2, S-ZrO_2, and silica phosphates, are used as the functional additives [10, 11, 34, 42-58]. Researchers developed two main methods to prepare composite membranes, i.e. dispersion of inorganic particles in an ionomer solution followed by film casting, and growth of inorganic particles within a performed membrane or in an ionomer solution [8]. The effect of inorganic additives on the membrane proton conductivity depends on the particle size, the amount, the uniformity of dispersion, the acid site density, the acid strength, and interactions between inorganic elements and polymer backbone and acid sites.

Composite proton-exchange membranes have shown some promise in the proton conductivity and PEM fuel cell performance at high temperatures with low water content. The inorganic additives play a key role in holding water within the membrane, especially at higher temperatures and lower RHs. Some hygroscopic oxides, such as SiO_2, Al_2O_3, ZrO_2, and TiO_2, doped in Nafion have substantially enhanced the water retention properties of Nafion and, as a result, the performance of the PEM fuel cells. It was found that the variation in the conductivity

and electrochemical performance of three different TiO_2-doped composite membranes was mainly due to the difference in their specific surface areas. A larger specific surface area favored for high water sorption [49]. Superacidic S-ZrO_2 has an acid strength stronger than 100 % H_2SO_4 and, when incorporated into Nafion membranes, the amount of water uptake increases by establishment of specific Lewis acid-base interactions [26]. The nanostructured Nafion/S-ZrO_2 composite membranes exhibited an increase of ~ 40 % in water sorption, and ~ 5 % enhancement in conductivity vs. unmodified Nafion 112 at 120 °C and 40 % RH [34]. Other solid acid inorganic materials, such as heteropoly acids (HPAs) with structure groups of polyoxometalates and stable proton conductivity at high temperature, have been applied in high temperature/low RH PEM fuel cells applications [56]. When HPAs are doped into perfluorosulfonic acid polymers, the composite membranes show improved proton conductivity at higher temperatures (80 -120 °C) and all RH levels up to 80 % [31]. Zirconium hydrogen phosphate (ZHP) in Nafion/ZHP composite membranes proved as a hygroscopic agent for water retention at elevated temperature [54]. Water molecules within composite membranes were effectively coordinated by the surface groups of inorganic additives. Those inorganic particles with a larger surface area increase water sorption. However, increased water sorption does not necessarily lead to proportionately increased proton conductivity. This is because the ratio of adsorbed water to free water has a strong effect on the proton-conduction process.

A uniform and continuous distribution of the inorganic phase in composite membranes has been shown to improve fuel cell performance. Yang et al reported that a Nafion/zirconium phosphate (ZP) composite membrane presented substantially less ohmic resistance than Nafion or Nafion/sulfated zirconia membranes. The ZP seemed to form a continuous network which connected the ion-clusters of Nafion. On the contrary, when the particulate S-ZrO_2 was not evenly dispersed in Nafion, no conductivity enhancement was observed [59].

Nafion/inorganic-conductor composites have more advantages than unmodified Nafion. They significantly increase CO tolerance, decrease fuel permeability, and increase T_g. Composite membranes are thermomechanically more stable than Nafion membrane. The glass transition temperatures, T_g, for Nafion/SiO_2, Nafion/TiO_2, and Nafion/ZrO_2 membranes were about 118, 122, and 135 °C, respectively, compared with 110 °C for Nafion 112 [13].

Finally, polymer/inorganic-additive composite membranes realize cost reduction when compared with pure polymer electrolyte membrane. Inorganic additives are cost-effective, the addition of which allows a cost saving because of the reduction of the volume ratio of polymer. Also, inorganic additives enhance polymer strength, which permits the fabrication of thinner membranes. The reduced thickness of the membrane scales down the cost of polymer ionomer. Furthermore, composite membranes reduce fuel/oxygen crossover, resulting in decreased fuel consumption for the same level of power output, which provides a cost savings benefit [60].

2.2.3 Modeling of proton transport in composite membranes

At present, an understanding and modeling of the proton transport through Nafion and composite proton-exchange membranes are not yet adequately developed. A theoretical model of proton-exchange membranes includes a structural model and a transport model. The cluster-network model (Figure **2-2**) provides a suitable structural framework for the development of proton transport in Nafion and Nafion-based composite membranes. Three approaches have been reported to construct the proton transport model, i.e. (1) phenomenological models based on nonequilibrium thermodynamics, (2) models based on the Nernst-Planck equations, and (3) models based on the Stefan-Maxwell equations [61]. In the models based on the Nernst-Planck equations, different diffusion coefficients are involved; while in the models based on Stefan-Maxwell equations, the frictional coefficients are incorporated.

The proton conductivity (σ) is described by the Nernst-Einstein relation in terms of diffusion coefficient

$$\sigma_{H+}^{\alpha} = \frac{F^2}{RT} D_{H+}^{\alpha} C_{H+}^{\alpha} \qquad [2\text{-}1]$$

where F is Faraday constant (96485 C mol^{-1}), R is the molar gas constant (8.314 J mol^{-1} K^{-1}), T is thermodynamic temperature (K), D_{H+}^{α} is the diffusion coefficient of protons related to the diffusion mechanism α, and C_{H+}^{α} is the concentration of protons participating in the diffusion mechanism α [62]. The proton conductivity in a pore σ_P can be written based on different proton-transport mechanisms

$$\sigma_P = \sigma_{H+}^{\Sigma} + \sigma_{H+}^{G} + \sigma_{H+}^{E} \qquad [2\text{-}2]$$

where σ_{H+}^{Σ}, σ_{H+}^{G}, and σ_{H+}^{E} represent the proton conductivity from the surface, Grottthuss, and *en masse* or so called vehicular diffusion mechanisms, respectively.

The diffusion coefficient of protons is given by the Einstein-Smoluchowski equation

$$D_{H+} = \frac{l^2}{\kappa \tau_D} \qquad [2\text{-}3]$$

where κ is a constant dependent upon the dimensionality of random-walk (κ = 2, 4, or 6 for a one-, two-, or three-dimensional walk, respectively), l is the mean step distance, and τ_D is the mean time between successive steps. Taking into account the tortuous nature of membrane pores, the effective diffusion coefficient is obtained by multiplying the diffusion coefficient for a single pore by ε_i / τ, where $\varepsilon_i = \lambda/(\lambda + r)$, λ is water loading, which is the moles of water sorbed per acid site, $r = \overline{V}_M / V_{H2O}$, that is the ratio of partial molar volume of membrane to that of water, and τ is the tortuosity factor. The partial molar volume is defined as $V_B = (\partial V / \partial n_B)_{T,p,n_j \neq B}$ [63]. The surface diffusion coefficient is calculated by assuming that the electrostatic columbic-

energy between the sulfonic ion and the hydronium ion is equal to the effective Gibbs free energy of activation for surface diffusion; the Grotthuss diffusion coefficient can be found based on classical treatment of water rotation and microhydrodynamics; and the *en masse* diffusion coefficient of hydronium ion is calculated by the Stokes-Einstein equation.

On the other hand, the diffusion of protons can be described with the generalized Stefan-Maxwell equation, in which the electrochemical potential gradient is the driving force. When applied to diffusional transport within an ion-exchange membrane, the equation is written as

$$\frac{-c_i}{RT}\nabla_T \mu_i^e = \sum_{\substack{j=1 \\ j\neq i}} \frac{c_i c_j}{c D_{ij}^e}(v_i^D - v_j^D) + \frac{c_i}{D_{iM}^e} v_i^D \quad (i = 1, 2, \ldots, n) \qquad [2\text{-}4]$$

where c_i is the concentration of species i (mol cm^{-3} pore solution), μ_i^e is the electrochemical potential of species i (J mol^{-1}), c is the total concentration of liquid mixture (mol cm^{-3}), D_{ij}^e is the effective mutual diffusion coefficient of species i and j within membrane (cm^2 s^{-1}), v_i^D is the diffusional velocity of species i with respect to the mixture mass-average velocity (cm s^{-1}), D_{iM}^e is the effective diffusion coefficient for interaction of species i and matrix M (cm^2 s^{-1}), and n is the number of conducting species [61]. The effective and continuum diffusion coefficient are interrelated through

$$D_{ij}^e = K_1 D_{ij} \qquad [2\text{-}5]$$

With the structural constant for the molecular diffusion coefficient $K_1 = (\epsilon - \epsilon_0)^q$, where ϵ is the volume fraction of water in hydrated membrane, ϵ_0 is the percolation threshold volume fraction of water in hydrated membrane, and q is the Bruggeman or critical exponent. The effective membrane diffusion coefficient may similarly written as

$$D_{iM}^e = K_0 D_{iM} \qquad [2\text{-}6]$$

where K_0 is the constant for the matrix diffusion coefficient.

From the correlation between the flux of protons and the current density, the proton conductivity is induced to be

$$\sigma = \frac{F^2}{RT} D_{12}^e (1 + \frac{D_{12}^e}{D_{1M}^e})^{-1} c_{HA,0} \alpha \qquad [2\text{-}7]$$

with the subscripts of 1 as species of hydronium ion and 2 as water. $c_{HA,0}$ is the concentration of membrane acid groups, and α is the degree of acid-group dissociation. By introducing the definition $D_{12}^e / D_{1M}^e = \zeta_{1M} / \zeta_{12} = (K_1 / K_0)(D_{12} / D_{1M}) \equiv \delta$, the proton conductivity finally is

$$\sigma = (\varepsilon - \varepsilon_0)^q (\frac{\lambda_1^0}{1+\delta}) c_{HA,0} \alpha \qquad [2\text{-}8]$$

where λ_1^0 is the of hydronium ions in water, and $\lambda_1^0 \equiv F^2 D_{12} / RT$ [61]. ζ_{1M} is the friction coefficient for interaction between hydronium ions and matrix *M* (J s cm^{-5})(cm^3 mol^{-1})^2, and ζ_{12} is the friction coefficient for interaction between hydronium ions and water (J s cm^{-5})(cm^3 mol^{-1})^2.

In this study, we developed the proton-transport model, using the generalized Stefan-Maxwell equations, to simulate the proton conductivity of Nafion-based composite membranes. This modeling approach explored the proton transfer phenomena within composite membranes and key parameters affecting the membrane conductivity. The simulation enhanced the fundamental understanding of proton transport mechanisms in composite membranes.

Chapter 3

Experimental Techniques

The experimental techniques include the proton conductivity studies of inorganic materials and composite membranes. Inorganic proton conductors were characterized from phase purity, surface area, morphology, and IEC; composite membranes were tested with thermal stability, swelling, IEC, morphology, and physicochemical property.

3.1 Proton conductivity study of inorganic materials and composite membranes

This section describes the proton conductivity measurement method, the conductivity data analysis, and the proton conductivity measurement protocol for inorganic materials and composite membranes.

3.1.1 Inorganic material proton conductivity measurement

3.1.1.1 Method

On the basis of previous literature studies, we developed the method for measuring the proton conductivity of inorganic conductors, which consists of a newly constructed conductivity cell, a commercial RH control system, and the sample preparation procedures. The cell includes the newly designed inorganic sample holder and the BekkTech conductivity cell hardware. The sample holder was assembled in the BekkTech conductivity cell, which was connected with a water supply system (BT-301 pressurized deionized water system) and the saturator. Note that the

BekkTech conductivity cell was previously developed and successfully used in our laboratory for in-plane conductivity measurements of a verity of polymeric and composite proton conductive membranes. One of the features of the cell is a relatively small cell chamber, and this allowed for better control of the sample's RH. In our measurements, the RH was calculated from the ratio between the pressure of saturated water vapor at the temperature of the humidification saturator P(T_h) and the conductivity cell P(T_c) as follows:

$$RH(\%) = P(T_h) / P(T_c) \times 100 \qquad [3\text{-}1]$$

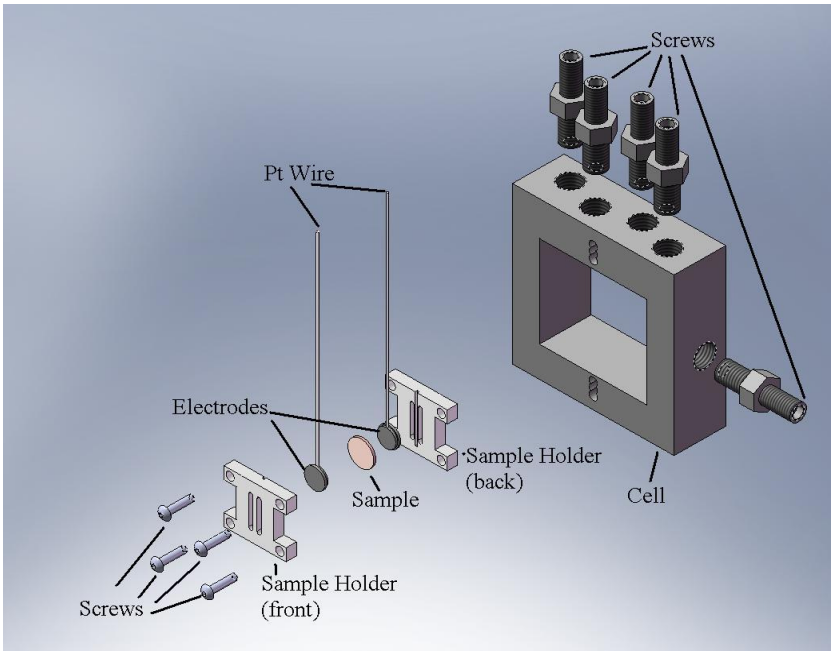

Figure **3-1**: Schematic of the inorganic sample assembly[1].

A two-electrode through-plane conductivity measurement method was developed in this study. Inorganic pellet samples were sandwich-held between sample holders. Figure **3-1** shows

[1] I acknowledge the participation of Chris Lute to have helped to design the sample holder.

the schematic of the sample assembly. An inorganic sample was prepared by pressing 300 mg of powder into a pellet of 13 mm in diameter and 1-2 mm in thickness under the pressure of about 5 t cm^{-2}. The pellet was then annealed at 200 °C for 6 hours. On each side of the pellet surface Ag was painted to serve as electrodes. The designed Teflon sample holders and two flat Ag plates soldered with two Pt wires were used to sandwich-hold the pellets and then assembled in the BekkTech hardware. A Gamry Electrochemical Impedance Spectroscopy (EIS) system with a frequency range of 0.2 to 100 kHz was used to measure the AC conductivity of the inorganic samples. A linear 2-electrode DC sweeping from -10mV to +10mV was used to check the electron conductivity of the samples. If the sweeping at low potential produced a linear response, the inorganic sample was considered to conduct electrons because the over-potential was insufficient to begin splitting water and to generate protons [64]. We found that the designed method can be used for reliable conductivity measurements over wide ranges of temperatures (25 – 120 °C) and RHs (1 – 100 %). The precision of temperature control was ± 0.2 °C and the calculated error estimate of RH was ± 0.1 %.

3.1.1.2 Conductivity data analysis

The EIS equivalent circuit modeling approaches were commonly used to treat the impedance spectroscopy data and to retrieve proton conductivity values for inorganic materials [18, 65, 66]. In this study, based on the physical characteristics of the inorganic sample assembly, we newly introduced the geometrical cell capacitance. Figure **3-2** shows two equivalent circuit models consisting of resistors and capacitors. An EIS Nyquist plot consists of a y-axis being the negative imaginary impedance and an x-axis representing the real impedance (resistance). Each point is the impedance value for one frequency value, ω. The simple model M1 was used when the complex impedance Nyquist plots simply consisted of a semi-arc and a low-frequency tail.

Under other conditions, when the Nyquist plots had more than one semi-arc, the model M2 was applied. In the model b, to our best knowledge, the ionic resistance and the electronic resistance were retrieved simultaneously by using one equivalent circuit. Furthermore, we found that the retrieved electronic resistance was consistent with DC measured resistance.

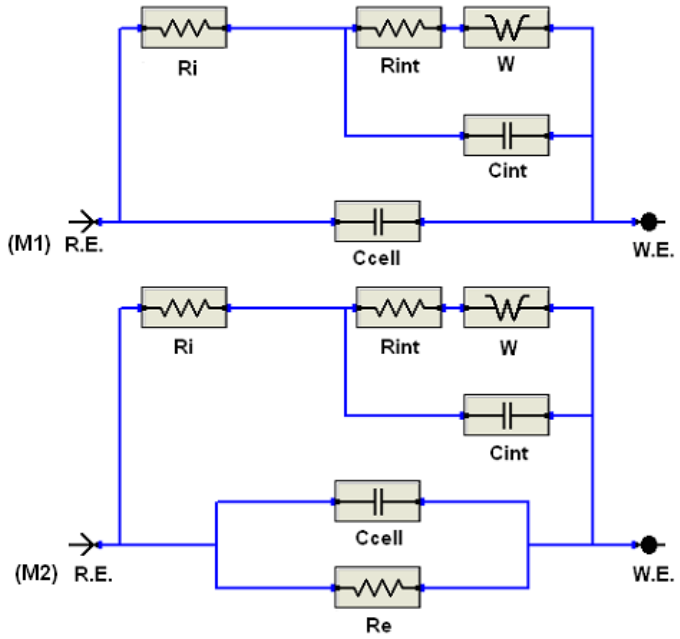

Figure **3-2**: The schematic of the EIS equivalent circuits M1 and M2.

In the models, R_{int} is the resistance of the interface (Ω), R_i is the ionic resistance across the pellet (Ω), R_e is the electronic resistance through the pellet (Ω), W is the Warburg impedance (S), C_{int} is the interface capacitance (F), and C_{cell} is the geometrical cell capacitance (F). The Warburg impedance W and the interface capacitance C_{int} can be defined as [67]:

$$W = \sigma\omega^{-1/2} - j(\sigma\omega^{-1/2}) \qquad [3\text{-}2]$$

$$C_{int} = \frac{1}{\sigma\omega^{1/2}} \qquad [3\text{-}3]$$

where ω is the frequency (s^{-1}) and σ is a diffusion transport parameter that takes into account of diffusion coefficients ($\Omega\ s^{1/2}$). The typical values of C_{int}, C_{cell} and W are 10^{-8} F, 10^{-10} F and 10^{-6} S for inorganic materials impedance data treatment. We calculated R_i using a fitting procedure based on a non-linear least-squares analysis of the complex impedance.

Proton conductivity, σ (S cm^{-1}), of the inorganic pellet was calculated from R_i and pellet physical parameters, diameter, d (cm), and thickness, h (cm), using the following equation

$$\sigma = \frac{1}{\rho} = \frac{h}{\pi R_i \times d^2 / 4} \qquad [3\text{-}4]$$

where ρ was pellet resistivity (Ω cm).

The electrical charge transported within inorganic materials can be carried either by electrons and/or by protons. The application of a proton conductive inorganic conductor as an additive in composite membranes requires that the charge transport is predominantly related to the proton conductivity. One can use the Hittorf transport number to describe the contributions of protons or electrons to the total charge transport in the pellet. The transport number (t) is defined as the fraction of the total electrical current that is carried by a particular species when an electrical potential difference is imposed upon the adjacent electrodes [66]. Defined by International Union of Pure and Applied Chemistry (IUPAC), the transport number is calculated with [63]

$$t_B = \lambda_B c_B / \sum_i \lambda_i c_i = j_B / \sum_i j_i \qquad [3\text{-}5]$$

where λ is the ionic conductivity (S m^2 mol^{-1}), c is the concentration (mol m^{-3}), and j is the electric current density (A m^{-2}). Thus, the transport number of protons as t_i and electrons as t_e are:

$$t_i = \frac{j_i}{j_i + j_e} = \frac{R_e}{R_i + R_e} \qquad [3\text{-}6]$$

$$t_e = \frac{j_e}{j_i + j_e} = \frac{R_i}{R_i + R_e} \qquad [3\text{-}7]$$

with R_i retrieved from AC Nyquist plots and R_e either read from DC polarization curves or retrieved from the equivalent circuit modeling M2. For the purpose of the application, it is desired that the proton transport number t_i be relatively large (> 0.95), and the electron transport number t_e be relatively small (< 0.05). In the research, we quantitatively measured the electron conductivities of inorganic materials and their proton conductivities as well. The conductance nature of the inorganic conductors was clearly defined.

3.1.1.3 Conductivity measurement protocol

The proton conductivity measurement protocol for inorganic materials was as follows:

- Measure the thickness of the pellet
- Assemble the inorganic pellet into the designed conductivity cell. And then assemble the cell into the conductivity test system
- Control the N_2 flow rate at around 350 cm^3 min^{-1}
- Monitor the back-pressure of the system at around 18.3 psi
- Condition the sample at 70 % RH for around 6 hours
- Adjust the RH step by step to 60 %, 50 %, 40 %, 30 %, 20 % and then 95 %. Allow 3-4 hours of stabilization at each condition. The temperature set up for the conductivity cell and the humidifier saturator under different operating conditions is listed in Table **3-1**.
- Apply EIS AC sweeps to measure the proton conductivity
- Sweep a DC linear voltage sweep from 10 mV to -10mV to measure the electron conductivity

At each RH, the conductivity measurement was completed at the stabilized condition in which measured resistance of inorganic pellets was kept constant.

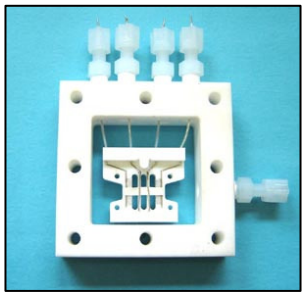

Figure **3-3**: Sample assembly of the BekkTech conductivity cell.

Table **3-1**: Dew point of the humidifier saturator at 100 and 120 °C under different RH.

T_{cell}	100 °C						
RH (%)	20	30	40	50	60	70	95
T_{hu} (°C)	60.4	69.4	76.2	81.7	86.3	90.3	98.6
T_{cell}	120 °C						
RH (%)	20	30	40	50	60	70	95
T_{hu} (°C)	75.7	86	93	99.4	104.5	109.1	118.4

3.1.2 Composite membrane proton conductivity measurement

3.1.2.1 Method

The membrane's conductivity was measured by using a 4-electrode in-plane method in a BekkTech conductivity cell (BT 115). The cell was assembled in the ElectroChem fuel cell hardware. Figure **3-3** shows the sample assembly of the cell. We cut composite proton-exchange

membranes into a rectangular piece around 4.0 mm in width and 25.0 mm in length. The thickness of the piece was measured using a micrometer (Starrett, V216MXFL-25). When the thickness of the sample was less than 100 μm the membrane was put under the electrodes to improve the solid contact between the electrodes and the membrane sample. A linear DC sweeping from -100 mV to +100 mV was applied to measure the proton conductivity of composite membranes. The slop of the DC polarization curve indicated the ionic resistance, R_i.

3.1.2.2 Conductivity data analysis

The membrane conductivity was calculated using the ionic resistance (R_i) and the geometric dimensions of the sample with the following equation

$$\sigma = \frac{1}{\rho} = \frac{l}{R_i \times A} = \frac{l}{R_i \times W_s \times h} \qquad [3\text{-}7]$$

where, A is the cross-section area perpendicular to the ion flow (cm^2), l is the distance between electrodes (cm), W_s is the width of the sample (cm), and h is the thickness of the membrane (cm).

3.1.2.3 Conductivity measurement protocol

The proton conductivity measurement protocol for composite membranes was similar to that for inorganic materials except the following difference:

- Dry membranes in a desiccator overnight
- Cut a sample with 4.0 mm × 20 mm
- Measure the width of the membrane sample, and measure the thickness of the sample at different points. The average value of the thickness was used to calculate the proton conductivity.
- Condition the sample at 120 °C and 70 % RH for 2 hours
- Adjust the RH to 50 % and 20 %, allowing 1 hour of stabilization at each RH

- A DC linear sweep from 100 mV to -100 mV was performed to measure the proton conductivity

3.1.3 Proton conductivity measurement system

We constructed an experimental conductivity measurement system. Figure **3-4** shows the schematic of the system. It consisted of three main sections: the humidification system, the conductivity cell, and the back-pressure control section.

A BekkTech humidification system having a BT-301 pressurized deionized water system and a BT-104 saturator was installed to auto control RH from 1 to 100 %. Nitrogen was used to carry humidified moisture into the conductivity cell. We controlled the flow rate of N_2 at around 350 cm^3 min^{-1}.

A back-pressure control system was consisted of an Omega pressure meter and a Swagelok needle valve. We adjusted the back pressure to be higher than the saturated water vapor pressure at each RH to pressurize the conductivity cell. In order to avoid blocking the needle valve, the moisturized exhaust gas out of the conductivity cell was cooled and passed through a water trap. The captured water was emptied out of the water trap periodically, while the dry gas was passed through the pressure meter then released into air.

Three temperatures – the conductivity cell temperature, the cell inlet temperature, and the saturator temperature – needed to be adjusted according to different operating conditions. The PID control method was applied with Omega temperature controllers. We adjusted the cell inlet temperature to be higher than that of the conductivity cell to avoid water condensation in the connecting tube. The system allowed the conductivity measurements in the temperature range from 25 to 120 °C.

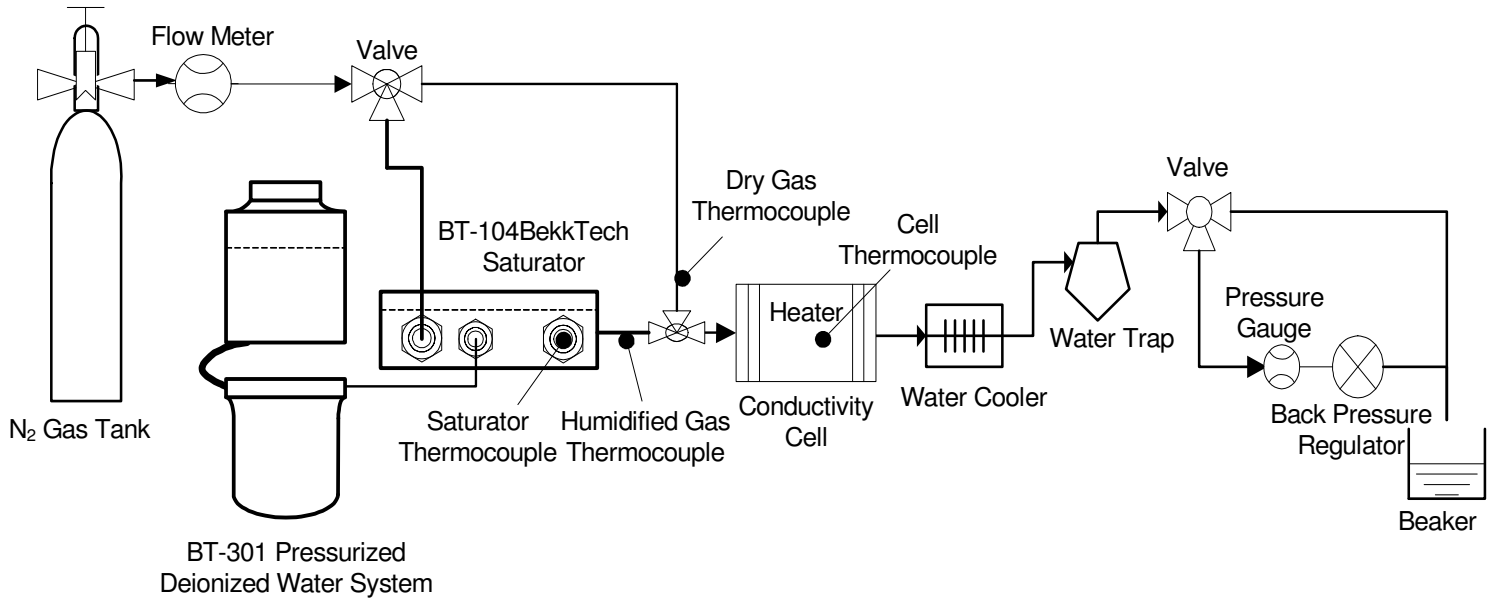

Figure **3-4**: Schematic of the conductivity measurement system.

3.2 Inorganic proton conductor characterization

Surface area, morphology, and the ion-exchange capacity of proton conductive inorganic materials were determined.

X-ray diffraction (XRD) measurement

The solid phases were characterized by using a computer-assisted x-ray diffractometer with CuK_{α} radiation (Scintag, Inc., Cupertino, CA, currently Thermo Scientific). XRD data of inorganic powders were obtained using samples loaded in the cavity of a zero background slide in the 2θ range of 4-40° at a scanning speed of 5° min^{-1}.

Surface area measurement

Inorganic surface area and pore-size distribution were determined from the nitrogen adsorption-desorption isotherms using an Autosorb 1 instrument (Quantachrome Co, Ronkonkoma, NY, USA). Before the adsorption measurement, the samples were degassed at 120 - 300 ^{o}C for 3 hours.

Scanning electron microscopy (SEM) measurement

The morphology and particle size of inorganic materials were observed on the Hitachi S-3500N VP scanning electron microscope.

IEC measurement

The IEC was defined as the ratio between the number of the surface ionogenic groups (in mmol) and the weight of the dry materials [42]. The inorganic powder was first dried in the oven at 60 ^{o}C overnight. Around 100 mg of dry inorganic powder was then mixed with 40 ml of NaCl (aq) solution (0.01 M) for counter-ion exchange for two days. IEC was measured by titration with NaOH (aq) solution (0.01 M) after the completion of the ion exchange [68]. The solution pH was

checked in the titration procedure repeatedly until it became stable at neutral pH = 7. The IEC was calculated using the following equation

$$IEC = \frac{U \times C}{g} \qquad [3\text{-}8]$$

where U was the volume of titrated NaOH solution (ml), C is the concentration of NaOH solution (10 mM), g was the weight of dry material (g), and IEC was in mmol g^{-1}.

3.3 Composite membrane characterization

This section introduces the synthesis and characterization of Nafion-based composite membranes.

3.3.1 Composite membrane fabrication method

Taking into account inorganic material surface properties, inorganic material components, and inorganic additive concentrations, Nafion-based composite membranes were synthesized by three main methods:

Method I: in-situ formation of inorganic particles by dispersing inorganic sol-gel in the Nafion solution followed by membrane casting;

Method II: in-situ poly-condensation of inorganic network in the Nafion matrix by mixing inorganic precursor solutions with the Nafion solution followed by sol-gel heat treatment and membrane casting; and

Method III: blending of inorganic powders in the Nafion solution followed by casting and annealing.[2]

[2] I acknowledge the participation of Dr. Chalkova to have developed this method.

In method I, an inorganic sol-gel was formed first following the inorganic material synthesis procedure. Then, a certain amount of the sol-gel was mixed with an appropriate amount of commercial 5 % Nafion solution (Aldrich), which needed to be sonicated in an ultrasonic bath for 4 hours. The inorganic content in the composite membrane determined the amount of the sol-gel and the Nafion solution. The suspension was poured into a 5×5 cm Teflon dish and cast at 80 °C with a slow heating rate until it was dry. The recast composite film was peeled off and hot-pressed at a low pressure (less than 2 bar) at 150 °C for 10 min, then purified using a standard procedure.

In method II, appropriate amount of inorganic precursor solutions was mixed with proportional Nafion solution. The function of the Nafion solution was to replace ethanol in the precursors. Then, the mixture was heated to start the sol-gel reaction. The heating temperature and time followed the procedure of inorganic material sol-gel reaction. The procedure to cast and anneal composite membranes was the same as method I.

In method III, a certain weight of commercial inorganic powder or synthesized inorganic materials by Dr.Komarneni's lab was mixed with the Nafion solution. The treatment of the mixture followed the same procedure described in method I.

The names of composite membranes were defined from the inorganic additive concentration, inorganic components, and the synthesize method. For example, 10NPS I meant 10 % of P-SiO_2 were mixed with the Nafion solution by method I. In our composite membranes, the concentration of inorganic additives was relative to the Nafion solution. The thickness of composite membranes was about 80 - 100 μm. As a comparison, a pure Nafion membrane (called recast-Nafion membrane) was prepared using the Nafion solution without the addition of inorganic precursors.

The composite membranes were cleaned using a standard procedure, in which they were boiled in a 3 % (by volume) hydrogen peroxide solution to remove any residual organic

impurities, in deionized water, in 0.5 M H_2SO_4 to remove any possible inorganic contaminants, and in deionized water, respectively. Each step took at least one hour [69].

3.3.2 Composite membrane characterization

Thermogravimetric analysis (TGA)

The thermal stability and thermo-decomposition analysis were carried out on a thermogravimetric system (2960 STD V3 DSC-TGA) in the temperature range of 303-873 K at a heating rate of 10 °C min^{-1} in an inert N_2 atmosphere.

Swelling measurement

The water swelling of membranes was determined as the weight percent of water in fully water equilibrated membranes per dry membrane weight at room temperature.

IEC measurement

Ion-exchange capacities of composite membranes were measured by back titration method. At first, the samples were dried in a desiccator until the weight was constant. Then, each sample was soaked in 50 ml of 0.01 M NaOH solution for two days followed by three hours of sonication in an ultrasonic bath to exchange sodium ions with protons in composite membranes. Back titration was accomplished by titrating the remaining NaOH in solution with 0.01 M HCl solution. The IEC values were obtained by subtracting the added volume of 0.01 M HCl from the initial NaOH volume.

SEM measurement

The morphologies of composite membranes were measured on the Hitachi S-3500N VP scanning electron microscopy. The particle size distribution of inorganic particles was observed in micrometer (μm) scales.

Fourier transform infrared spectroscopy (FT-IR) characterization

The spectra were recorded on a model Nicolet NEXUS 470 FT-IR spectrophotometer from 4000 to 650 cm^{-1} at 298 K with a resolution of 4 cm^{-1}. This vibration investigation was performed to elucidate: 1) the interactions between inorganic particles and Nafion matrix; 2) the water domain distributions in the composite membranes and; 3) the effect of interactions between sulfonated functional group $–SO_3H$ in Nafion and inorganic network structure on the proton conductivity of membranes.

Fuel cell performance

Composite membranes fuel cell performance and resistance were tested using a H_2/Air Fuel Cell in a Scribner 850e-Multi-Range Fuel Cell Test Station under the same temperature and RH as the proton conductivity measurement.

Chapter 4

Proton Conductive Inorganic Materials

This chapter introduces experimental results, characterization, proton and electron conductivity, proton transport mechanisms, and impedance characteristics of solid acid materials, such as α-zirconium phosphate, sulfated zirconia, phosphosilicate gels, and sulfonic-functionalized SBA-15.

4.1 α-Zirconium phosphate

We proposed α-ZP to be used as a reference material for calibrating the newly developed conductivity cell. The α-ZP is a well known proton conductor with a layered-structure [70]. The first crystalline zirconium phosphate, α-$Zr(HPO_4)_2 \cdot H_2O$, was synthesized by Clearfield and Stynes in 1964 [71]. In its layered structure, metal atoms lie nearly in a plane and are bridged by phosphate groups. The protons are situated in the inter-layers and are attached to the PO_4 tetrahedra, which are surrounded by water molecules. The α-ZP is a surface proton conductor and is thermally stable up to 450 °C [72]. Its surface counter-ions move 10^4 times fasters than the internal ones do. At room temperature, the proton conductivity is in the range of 10^{-3} – 10^{-2} mS cm^{-1}. Since the proton conductivity of α-ZP has been investigated intensively, for the purposes of this research, its measured conductivities were compared with literature values under the same conditions to check the reliability of the designed conductivity measurement method and system. In this study, α-ZP donated by Toagosei Co. Ltd of Japan was used.

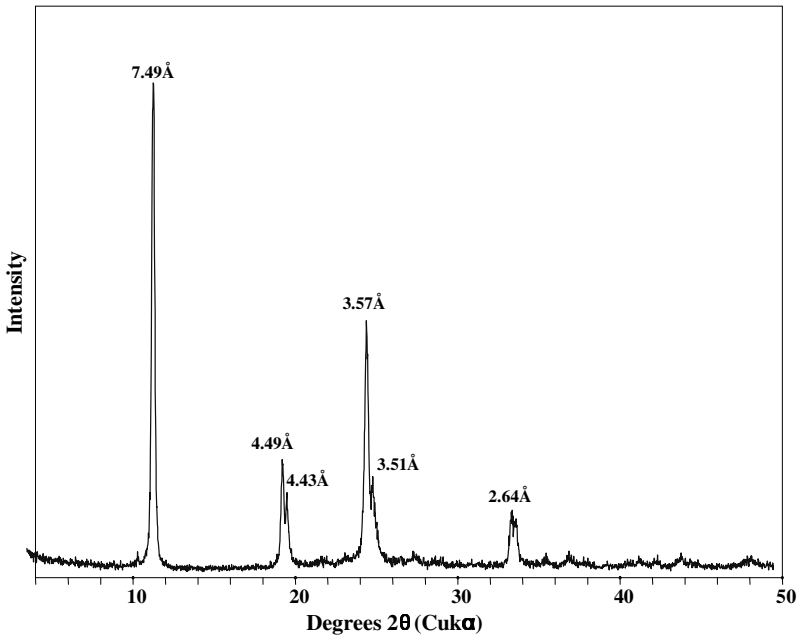

Figure **4-1**: XRD pattern of α-ZP.

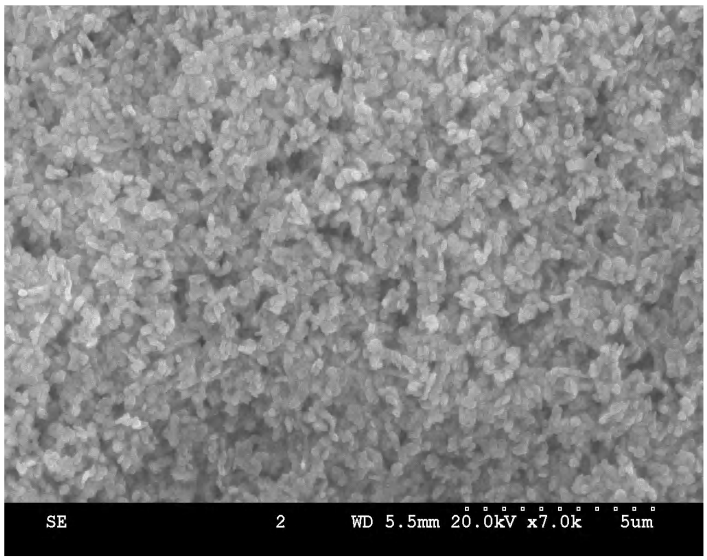

Figure **4-2**: SEM image of α-ZP.

The phase purity of α-ZP was checked by powder XRD. Figure **4-1** shows the XRD pattern. Crystals of α-ZP were hexagonal with a d(001) spacing of 7.49 Å. The surface area was evaluated as 11 m^2g^{-1} (Table **4-1**). SEM image (Figure **4-2**) of α-ZP displayed its platy morphology.

Table **4-1**: Surface area and IEC characterization of inorganic proton conductors.

	α-ZP	S-ZrO_2	P-SiO_2 (P: Si)			SBA-15
			0.5	1	1.5	
Surface Area (m^2 g^{-1})	11	5.0	9	5.2	3	629
IEC ($mmolg^{-1}$)	6.64	0.22	2.66	4.22	4.75	0.8

The proton conductivity of α-ZP measured using the designed method at 100 °C and different RH was compared with literature data and is shown in Figure **4-3**. Results show that the measured proton conductivity is consistent with all literature data over the entire RH range. Based on this comparison we conclude that the developed method and the experimental system are applicable for reliable through-plane conductivity measurements. In Figure **4-3**, data set #1 was obtained with a home-made humidifier, which was a stainless steel column to be heated up as a saturator. It could provide around 340 ml of deionized water for one fill up. Data set #2 was measured using a new humidification system, which was purchased from BekkTech. The pressurized deionized water system provided water vapor continuously into the cell. The two experimental systems with different humidification systems were calibrated with Nafion 212 under different RH at 30, 80, 100, and 120 °C. The measured results were compared with those from BekkTech. The comparison indicated that the home-made humidifier under-evaluated the

proton conductivity at low RH (20 %). The new humidification system provided more accurate conductivity data. In the figure, the deviated experimental point at 20 % RH with the new humidification system might come from the measurement error.

Little [73] or no conductivity of α-ZP has been previously measured at elevated temperatures. To provide such data, we measured the proton conductivity of α-ZP at 120 °C under different RHs. The results of our measurements are presented in Figure **4-4**. At 120 °C, α-ZP exhibited the similar Nyquist plots at different RH with smaller arc of semi-circles. In DC measurements we did not find an evidence of electronic conductivity. Thus, at 120 °C, α-ZP provides the conduction mainly through protons. The proton conductivity is approximately one hundred times higher than the electron conductivity (Table **4-2**). At a lower temperature (100 °C), the electron conductivity is about one-tenth that of the proton conductivity.

Table **4-2**: Hittorf proton and electron transport numbers for proton conductive inorganic materials at 120 °C and RH from 20 to 70 %.

Inorganic	RH, %					
	20		50		70	
	t_i	t_e	t_i	t_e	t_i	t_e
α-ZP	0.973	0.027	0.983	0.017	0.986	0.014
S-ZrO_2	0.848	0.152	0.924	0.076	0.974	0.026
P-SiO_2 P:Si = 0.5	0.968	0.032	0.995	0.005	0.987	0.013
P-SiO_2 P:Si = 1.5	0.994	0.006	0.997	0.003	0.998	0.002
SBA-15	0.927	0.073	0.964	0.036	0.987	0.013

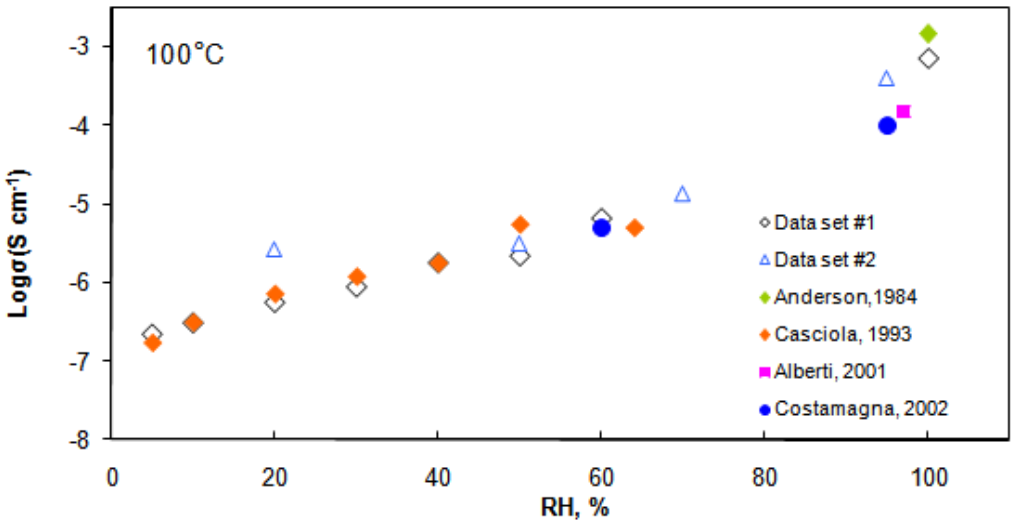

Figure **4-3**: The comparison of measured proton conductivity of α-ZP with literature data at 100 °C and different RH.

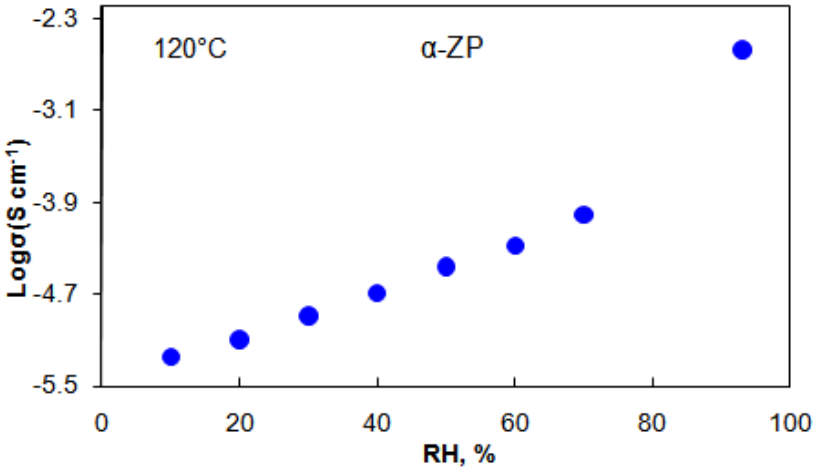

Figure **4-4**: Proton conductivity of α-ZP at 120 °C and different RH.

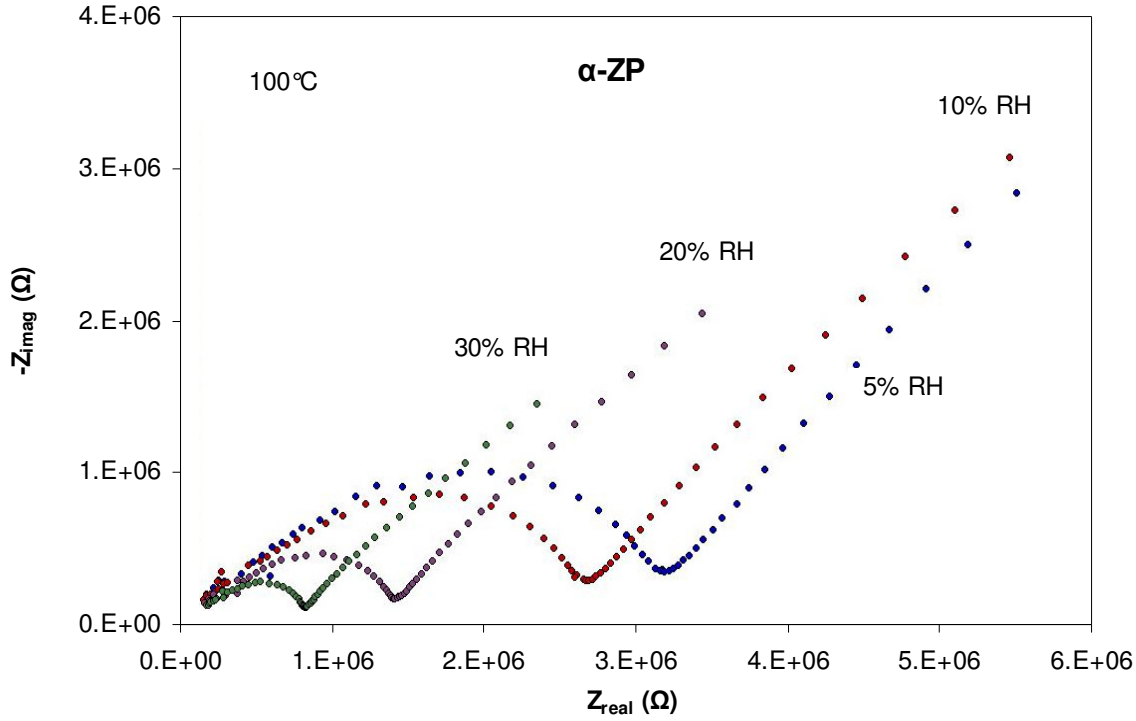

Figure **4-5**: The impedance Nyquist plots of α-ZP at 100 °C and different RH.

The proton conductivity of zirconium phosphate with respect to the structure characteristic was checked with α-zirconium phosphate, 3-dimensional zirconium phosphate, and amorphous zirconium phosphate. Figure **4-6** shows their proton conductivities. The data implied that the layered structure of α-ZP reached the highest conductivity. The mechanism of the proton transport along the surface of α-ZP is not yet well understood in literatures [18]. Water molecules on the surface of α-ZP seem to form bridges among P-OH groups and protons diffuse along the hydrated surface. The number and the arrangement of water molecules determine the characteristics of the proton transport. Researchers have studied the proton transfer between H_3O^+ ions and H_2O molecules. They found that the reorientation of the H_2O molecules in the hydration sheath of the H_3O^+ ion, as the proton passes through the water, is a rate-determining step in the proton conductance [69]. Furthermore, the liberation of both the H_3O^+ ion and rotated H_2O is

important, since the proton transfer occurs only during some fraction of the period when H_3O^+ and H_2O are free. When the water content is increased, the degree of H_3O^+ ion liberation significantly extends and the strength of the hydrogen bonds enlarges rapidly. The proton conduction increases with enhanced hydrogen bond strength. Thus, from the liberation of water and hydrogen bonding strength, higher RH promotes the proton conductivity [13].

The impedance Nyquist plots for α-ZP at 100 °C and different RH are shown in Figure **4-5**. The Nyquist plot of α-ZP typically consists of a semi-circle representing the bulk resistance of the specimen and a low-frequency tail reflecting the proton diffusion within the pellet. The amplitude of the pellet resistance at different RH can be estimated roughly by extrapolating the semi-circle to the Z_{real} axis [74]. In addition, observation shows that when RH is increased, the pellet resistance decreases accordingly. At 120 °C, α-ZP presentes the similar Nyquist plots at different RH with smaller arc of the semi-circles than those at 100 °C. α-Zirconium phosphate was adopted as an additive for a functionalized and cross-linkable vinylidene difluoride (VDF)/tetrafluoroethylene (TFE) polymer. Its contribution in the membrane conductivity is shown in Appendix **A**.

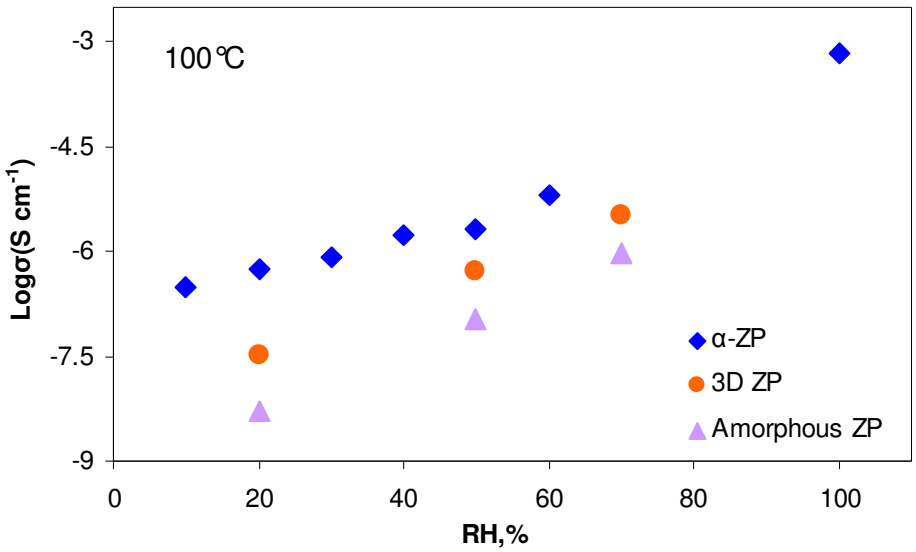

Figure **4-6**: Proton conductivity of zirconium phosphates with different structural characteristics at 100 °C and different RH.

4.2 Sulfated zirconia

Sulfated zirconia (S-ZrO_2) is the strongest solid acid and has a Hammett acid strength, H_0, of -16.03, whereas Nafion shows only about -12 [75]. Therefore, we were interested to check the conductivity of S-ZrO_2 with the newly developed measurement system.

To prepare S-ZrO_2 samples, zirconium oxychloride hydrate ($ZrOCl_2 \cdot 8H_2O$) was used as the starting material, and aqueous ammonia (NH_4OH) and sulfuric acid (H_2SO_4) were used as the precipitating agent and sulfating agent, respectively. Concentrated water several times in the centrifuge until the absence of chloride ions was confirmed by the silver nitrate ($AgNO_3$) test. Then 100 ml 0.2 M H_2SO_4 was added to the zirconia sol and stirred for 6 hours. The final

colloidal solution was filtered and dried in air at 60 °C followed by calcination at 620 °C for 3 hours. The IEC of S-ZrO_2, a surface-dominant conductor, was found to be 0.22 mmol g^{-1} (Table **4-1**). The low IEC value could be caused by the small surface area of 5.0 m^2 g^{-1}. Figure **4-**7 presents the XRD pattern of dried material at 60 °C. The S-ZrO_2 is a very poorly crystalline phase consisting of agglomerated fine particles (Figure **4-8**) prior to the calcination at 620 °C.aqueous ammonia solution (~28 %) was gradually dropped into 100 ml 0.20 M aqueous $ZrOCl_2 \cdot 8H_2O$ solution until the pH was adjusted to 10. The precipitated white-colored $ZrO_2 \cdot nH_2O$ sol was washed with distilled

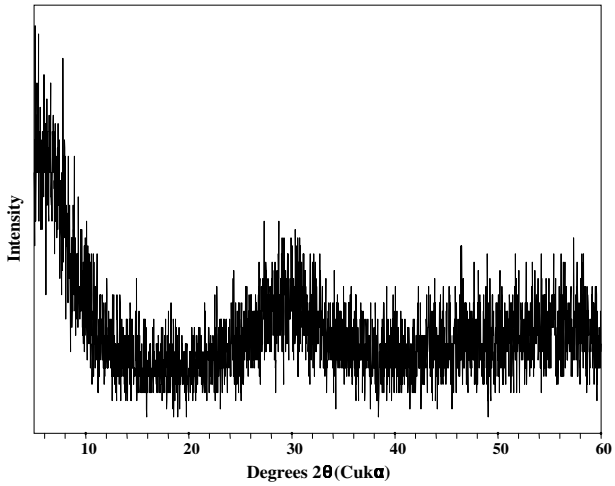

Figure **4-7**: XRD pattern of S-ZrO_2.

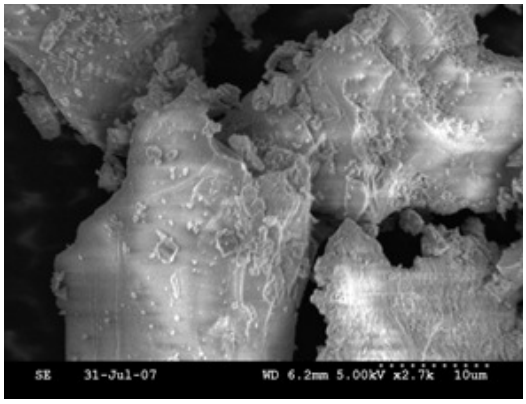

Figure **4-8**: SEM images of S-ZrO_2.

After stabilization the pellet humidification condition for 8-16 hours at each RH, we measured the proton conductivity of S-ZrO_2 at different temperatures. RH dependence of the S-ZrO_2 conductivity at 100 °C and 120 °C is shown in Figure **4-9**. Results showed that at elevated temperatures, a fully-hydrated (RH = 100 %) S-ZrO_2 can provide a high proton conductivity of about 10 mS cm^{-1}. From the infrared spectra of S-ZrO_2 obtained in Ref. [26], Hara et al found that the SO_x groups exist on the ZrO_2 surface. The SO_x groups are electron-withdrawing and strengthen the Lewis and Brønsted acidities of Zr; the feature enhances the proton conductivity. At a low RH, S-ZrO_2 cannot hold the water and the conductivity drops substantially. At a high RH, the Lewis acid sites can easily convert to Brønsted acid sites. Some of the SO_x groups on S-ZrO_2 have been released from the surface forming free SO_4^{2-} owing to the change of bond strength, which leads to a high proton conductivity [26]. At 70 % RH, the protonic transport number of S-ZrO_2 is around 40 times higher than the electronic transport number (Table **4-2**). At lower RH, the electron conductivity is around one-tenth of its proton conductivity. At both temperatures, DC polarization curves for S-ZrO_2 did not present the linear electron conductivity characteristic. As a conclusion, sulfated zirconia is a proton-conductivity dominant material.

The impedance Nyquist plots of S-ZrO_2 at 100 °C and different RH are shown in Figure **4-10**. At a low RH ranging from 20 to 50 %, the Nyquist plots consist of a relatively large semi-arc of the resistance of the pellet and a short tail of the proton diffusion in the low frequency range. So that we conclude that the proton transport in the S-ZrO_2 pellet is a kinetically sluggish process [67]. When RH is increased to 70 %, the proton kinetic mass transfer is a dominant mechanism of proton conductivity, and therefore, the pellet resistance decreases.

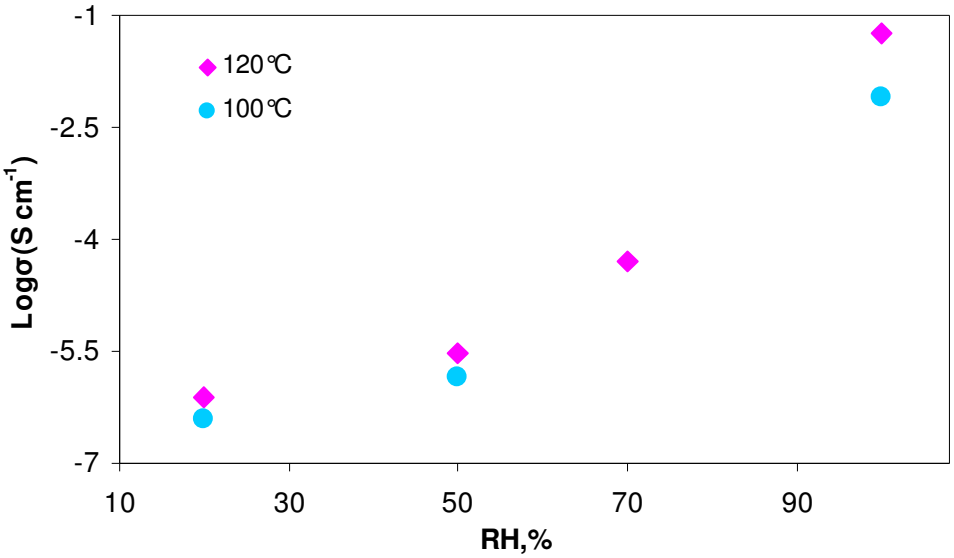

Figure **4-9**: Proton conductivity of S-ZrO_2 at 100 °C and 120 °C different RH.

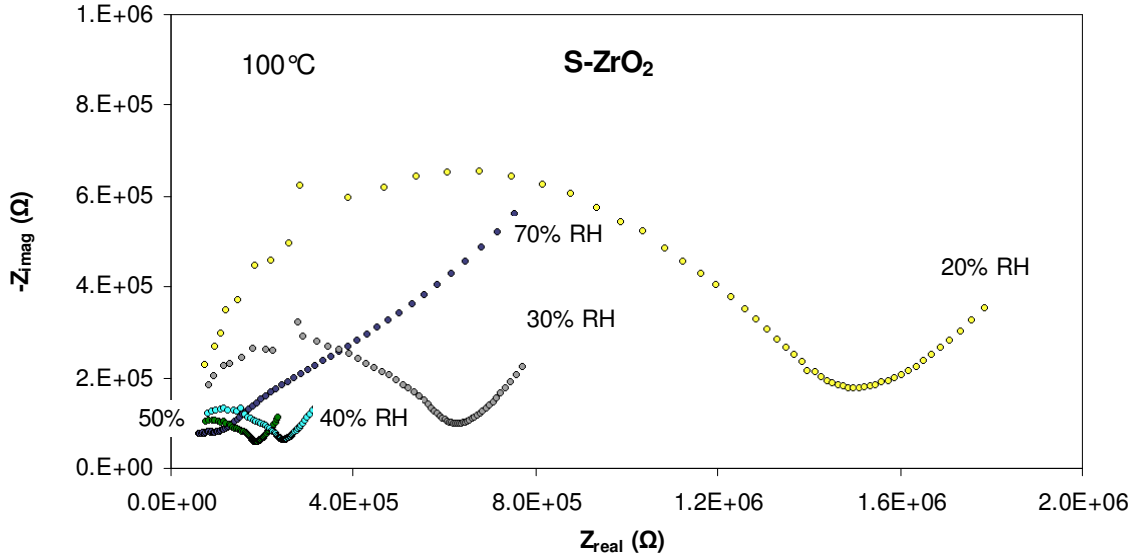

Figure **4-10**: The impedance Nyquist plots of S-ZrO_2 at 100 °C and different RH.

4.3 Phosphosilicate gels

Phosphosilicate gels with a P_2O_5-SiO_2 network structure consist of thermally stable silica and phosphate. Phosphate has a strong affinity for water molecule adsorption. Thus, phosphosilicate gels can be expected to attain a high proton conductivity even at higher temperatures (>100 °C) and lower RH. Matsuda and co-authors reported that at 130 °C and 0.7 % RH phosphosilicate gels reached a high proton conductivity of 15 mS cm^{-1} [24]. Their proton conductivity at elevated temperatures and over a wide range of RH is not reported in the literatures yet. Thus, in this research, we tested the proton conductivity of phosphosilicate gels with different P:Si ratios at higher temperatures under different RH.

Several phosphosilicate gels with P:Si mole ratios of 0.5, 1.0 and 1.5 were prepared based on the previously described procedures [24]. Tetraethoxysilane (TEOS), $Si(OC_2H_5)_4$, was first diluted with ethanol (EtOH) and then hydrolyzed with H_2O containing HCl (pH = 0.3) while stirring at room temperature for 10 min. A stoichiometric amount of H_3PO_4 (85 % aqueous solution) was added to the above hydrolyzed solution followed by stirring at room temperature for 3 hours. The mole ratio of TEOS: EtOH: H_2O: H_3PO_4 was 1: 8: 4: x (x=0.5, 1.0 or 1.5). The obtained sols were kept at 50 °C in a closed Teflon vessel to form wet phosphosilicate gels. The wet gels were subsequently dried at 50 °C for an additional week in the Teflon vessel in open air. The dried gels were pulverized into powders with an agate mortar and a pestle followed by heating in an oven at 150 °C for 5 hours.

The three powders were characterized from the aspects of the surface area, IEC, and XRD analysis. Results are listed in Table **4-1** and shown in Figure **4-11**. Phosphosilicate gels with a P:Si ratio of 1.5 have the highest IEC, and this may indicate their highest proton conductivity. Powder XRD showed the formation of silicon phosphate oxide, $Si_5O(PO_4)_6$ (2θ = 25). Crystal $Si_5O(PO_4)_6$ could be readily hydrolyzed at high RH, forming isolated phosphoric acid and

Si-O-POH groups, which are beneficial for enhancement of the proton conductivity [76]. We measured the proton conductivity of P-SiO_2 at 120 °C and different RH. Figure **4-12** shows measured data. P-SiO_2 with the P:Si ratio of 1.5 has a better proton conductivity than the gel with the P:Si ratio of 0.5. At 120 °C and 70 % RH, P-SiO_2 with the P:Si ratio of 1.5 reaches a high conductivity value of 100 mS cm^{-1}, which is higher than that of Nafion. Nafion NRE-212 was reported to have a conductivity value of 80 mS cm^{-1} at the same condition [64]. The peak height of $Si_5O(PO_4)_6$ in XRD for phosphosilicate gels with a P:Si ratio of 1.5 is higher than those with the P:Si ratio of 0.5, so it indicates that a higher amount of $Si_5O(PO_4)_6$ crystal is formed. Both IEC and XRD analyses explain the better conductivity of P-SiO_2 with the P:Si ratio of 1.5. Furthermore, at low RH, a higher amount of phosphate in the phosphosilicate gels with the P:Si ratio of 1.5 retains more water and leads to a better conductivity.

Phosphosilicate gels are primarily proton-conductive materials (Table **4-2**). Figure **4-13** shows the impedance Bode plots of P-SiO_2 with a P:Si ratio of 0.5 at 120 °C and different RH. At a high frequency, P-SiO_2 conducts protons as pure conductors, because the impedance phase angles keep around 0˚.

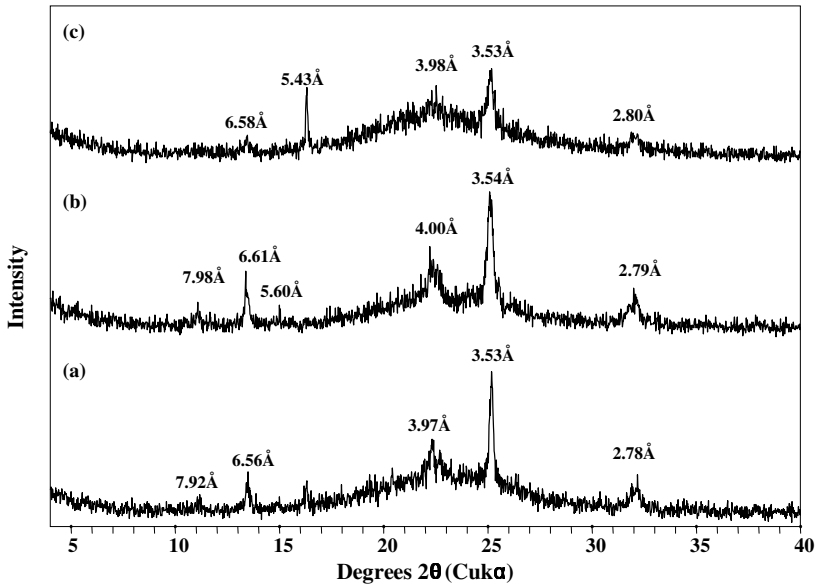

Figure **4-11**: Powder XRD patterns of P-SiO_2 with different P:Si mole ratios of 1.5 (a), 1.0 (b) and 0.5 (c).

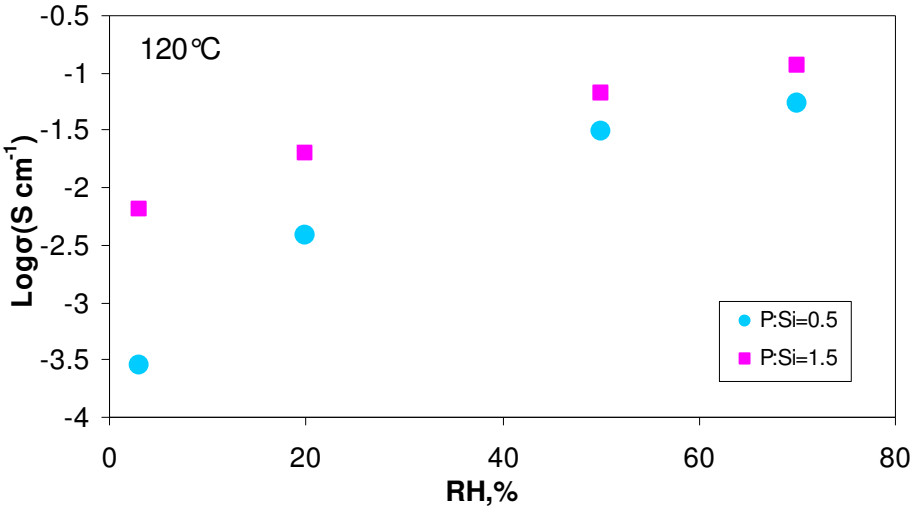

Figure **4-12**: Proton conductivity of P-SiO_2 with different P: Si ratios at 120 °C and different RH.

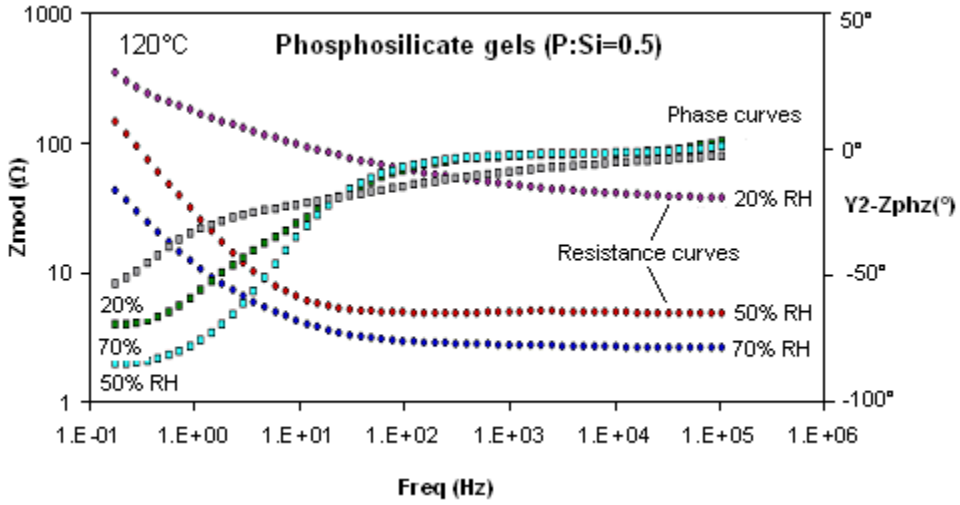

Figure **4-13**: The impedance Bode plots of P-SiO_2 with the P:Si ratio of 0.5 at 120 °C and different RH.

4.4 Sulfonic-functionalized SBA-15

Functionalized Santa Barbara Amorphous silica SBA-15 containing sulfonic acid groups has uniform pore sizes, high surface area, high thermal and hydrothermal stability, and relatively high acid strength, all of which are appealing properties for the electrolyte membrane application in PEM fuel cells [36, 77-79]. However, the proton conductivity is not well described in the literature and is of the concern of this study.

To synthesize periodic ordered sulfonic functionalized SBA mesostructures, poly(ethylene oxide)–poly(propylene oxide)–poly-(ethylene oxide) block copolymer species (Pluronic 123) was used as the templating surfactant. The one-step procedure of co-condensation of TEOS and 3-mercaptopropyltrimethoxysilane (MPTMS), with Pluronic 123 species was used as follows: 4g of Pluronic123 was dissolved in 125 ml of 2M HCl at room temperature. The

solution was heated to 40ºC before adding 7.4 g of TEOS. After 4 hours of stirring, 1.6 g of MPTMS was added. The resulting mixture was stirred at 40ºC for 20 hours, after which the mixture was aged hydrothermally at 100ºC for 24 hours. The solid product was recovered by centrifugation and washed with distilled water and dried at 60ºC. The above material was then treated hydrothermally at 90ºC for 24 hours with H_2O_2, ethanol, and HCl. The thiol groups of MPTMS were oxidized with H_2O_2 to form sulfonic groups. Ethanol and HCl (aq, 2M) were used to remove template in a one-step. The structure schematic of propylsulfonic-acid-modified SBA-15 is shown in Figure **4-14**. In this meso-structured material, the siloxane $[Si(OSi)_n\text{-}(OH)_{4-n}$, n = 2-4] and organosiloxane $[HO_3S(CH_2)_3Si(OSi)_m\text{-}(OH)_{3-m}$, m = 1-3] units were observed. The sulfonic groups were covalently attached on pore walls of the silica. The acid-synthesized sulfonic-functionalized SBA-15 has pore sizes up to 38 Å (Figure **4-15**). Figure **4-16** shows the adsorption-desorption isotherms, which indicates its mesoporous nature. This SBA-15 material has a surface area of 629 $m^2\ g^{-1}$ and an acid exchange capacity of 0.8 mmol of H^+ per g SiO_2.

We measured the proton conductivity of SBA-15 at 120 °C and different RH (Figure **4-17**) and the obtained values were not very high. At 70 % RH, SBA-15 reached a conductivity value of 0.04 mS cm^{-1}, which was not as high as those of other inorganic conductors. However, its high surface area and the presence of sulfonic acid functional groups seem beneficial to be compatible with polymer membranes. The siloxane groups Si-O-Si-OH and sulfonic groups $-SO_3H$ on the mesopore surfaces provide proton diffusion through the sample. At low RH (20 %), the proton conductivity decreases by almost two orders of magnitude because of the decrease of the transport media: water molecules.

The electron conductivity of SBA-15 was measured by DC sweeps. Figure **4-18** shows an example of DC polarization curve at 120 °C and 70% RH. Observation indicates that the curve follows the linear electron-conductive characteristic, suggesting that SBA-15 partially conducts

electrons. The magnitude of the electron conductivity compared with the proton conductivity, represented by transport numbers, was calculated under different RH and results are shown in Table **4-2**. The table displays that in a wide range of RH the electron conductivity of SBA-15 is less than 1 % of the proton conductivity. This indicates that SBA-15 is mainly a proton-conducting material. The conductive characteristic of SBA-15 can be observed in the AC impedance Nyquist plots as well. Figure **4-**19 provides the Nyquist plots at 120 °C and different RH. All plots present a first small curve and part of the second big arc. The first curve reflects the resistance of ionic transport. Owing to the limited frequency range, the second big arc was not produced fully. However, this part of arc would demonstrate the large electronic resistance. On the whole, SBA-15 is considered as a proton-conductivity dominant material.

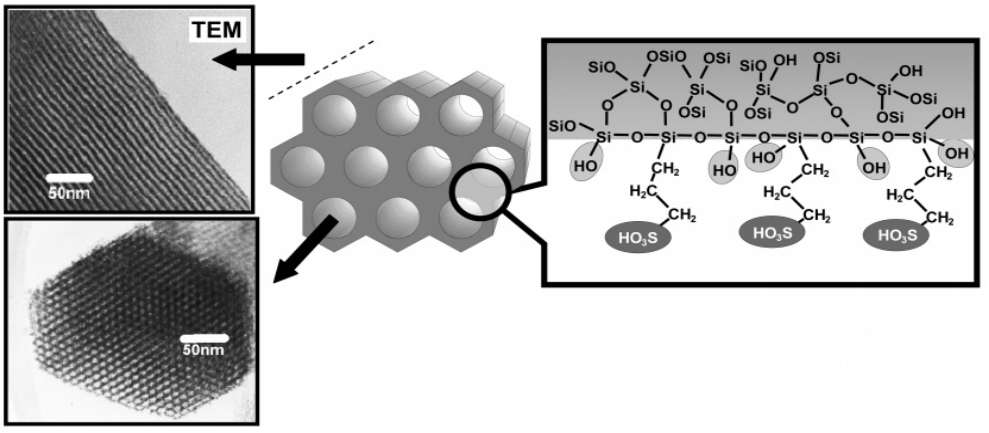

Figure **4-14**: The structure schematic of propylsulfonic-acid-modified SBA-15 [36].

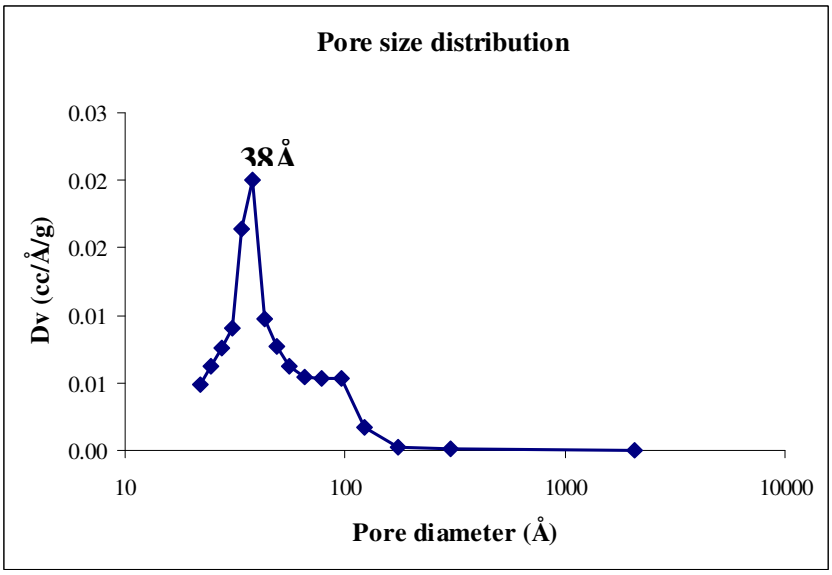

Figure **4-15**: Pore size distribution of sulfonic functionalized SBA-15 degassed at 120 °C.

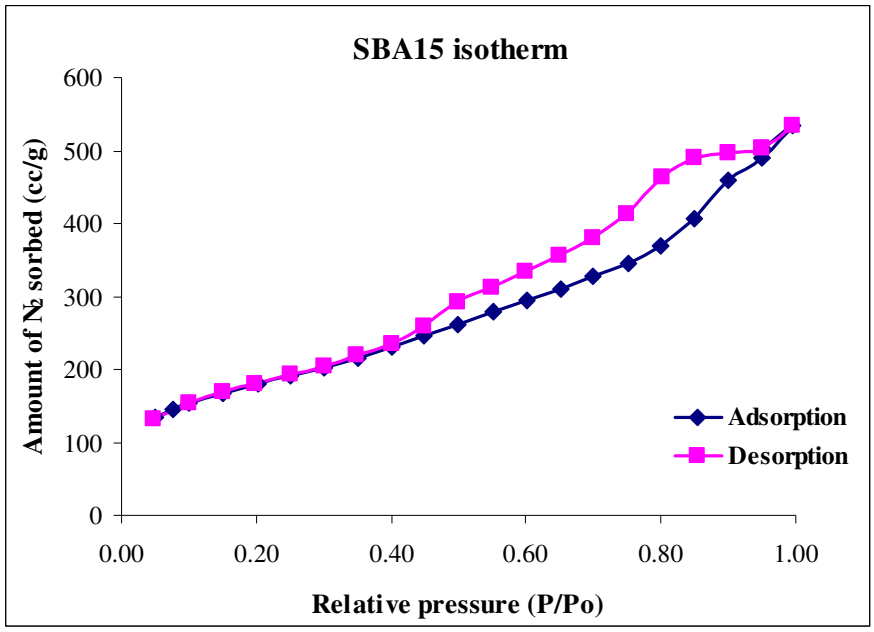

Figure **4-16**: Nitrogen adsorption-desorption isotherms of SBA-15.

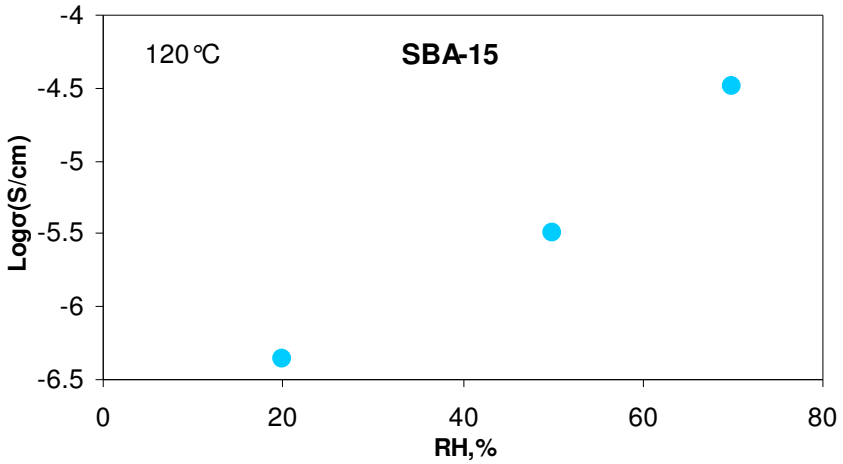

Figure **4-17**: Proton conductivity of SBA-15 at 120 °C and different RH.

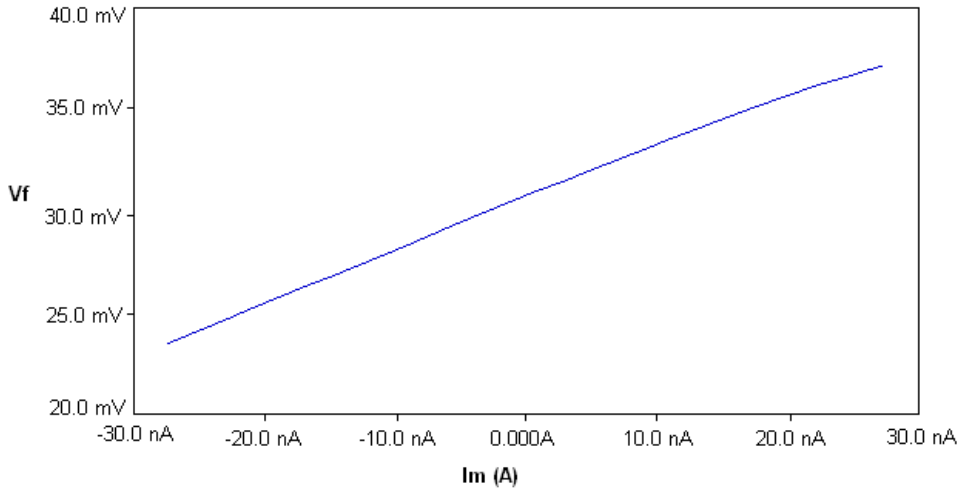

Figure **4-18**: The DC polarization curve of SBA-15 at 120 °C and 70% RH.

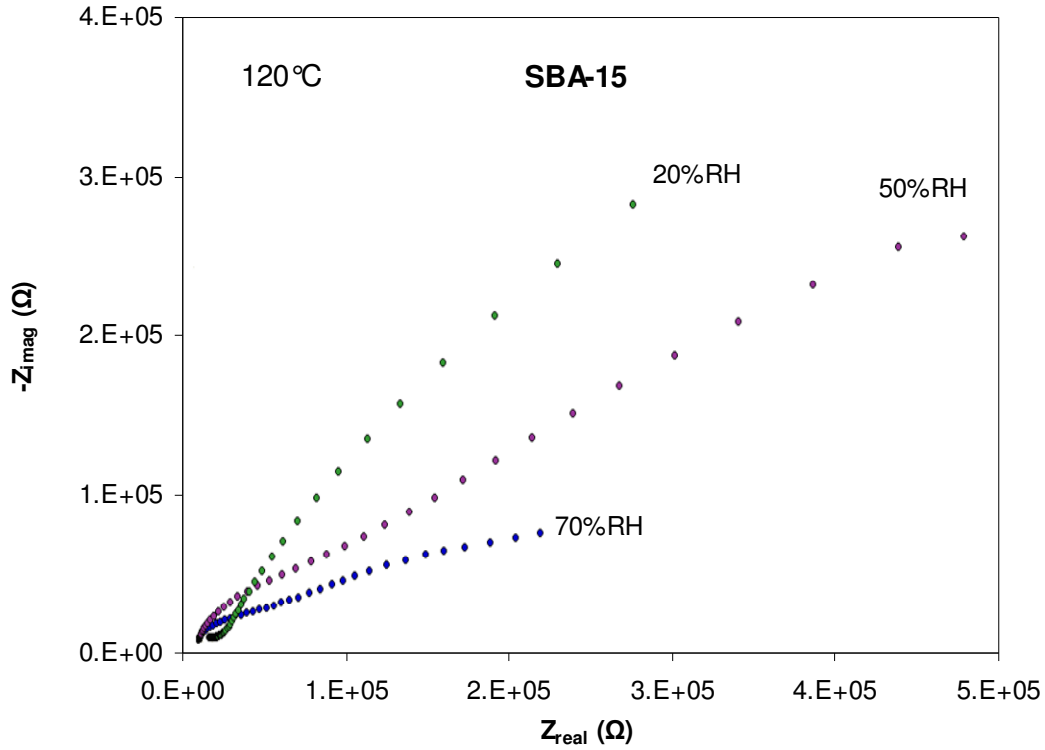

Figure **4-19**: The impedance Nyquist plots of SBA-15 at 120 °C and different RH.

Chapter 5

Proton Conductive Nafion-Based Composite Membranes

This chapter describes different Nafion/inorganic additive composite membranes with their thermodynamic, morphological, and physicochemical properties. The introduction of well-dispersed hydrophilic particles in Nafion improves the membrane thermal stability and fuel cell performance.

5.1 Nafion/sulfonated-inorganic composite membranes

Composite membranes of Nafion/10 % sulfonated-inorganic (S-ZrO_2, SBA-15, MCM-41, S-SiO_2)[3] synthesized by method III are discussed in detail in their water sorption ability, acidity, morphology, and proton conductivity. Table **5-1** presents results of the swelling and IEC measurements on recast Nafion and Nafion/sulfonated-inorganic composite membranes. Figure **5-1** shows proton conductivities of these composite membranes at 80 and 120 °C under different RH. We found that the acidity (IEC) of all composite membranes was higher than that of recast Nafion. However, none of the conductivities were higher than that of Nafion. The composite membranes Nafion/S-ZrO_2 and Nafion/SBA-15 presented the highest acidity. Their proton conductivities were found comparably high also. The proton conductivities of the composite membranes were in agreement with their acidity. No correlation between the proton conductivity and swelling was found.

[3] Inorganic powders of S-ZrO_2, SBA-15, and MCM-41 were prepared by Dr.Komarneni research group. The S-SiO_2 called Si-propylsulfonic acid derived silica gel was purchased from Silicycle.

None of these sulfonated inorganic conductors enhanced the conductivity of Nafion. The water uptakes of recast Nafion and Nafion/sulfonated-inorganic composite membranes at 120 °C were calculated from TGA curves (Figure **5-2**), and the results are listed in Table **5-1**. On the whole, the water content of all of these composite membranes was lower than that of pure Nafion, indicating that the composite membrane fabrication method of simply mixing solid acid inorganic particles with Nafion solution did not improve the water uptake and the proton conductivity of membranes. The lower water uptake of composite membranes explained their lower proton conductivity compared with recast Nafion. Thus, we needed to develop a new fabrication method to improve the acidity and water uptake of composite membranes.

Table **5-1**: Water sorption properties and acidity of recast Nafion and Nafion/sulfonated-inorganic composite membranes.

Membrane	Swelling, weight %	IEC, mmol g^{-1}	Water uptake at 120 °C, weight %
Recast Nafion	27.6	1.07	4.26
10N/S-ZrO_2	25.5	1.96	3.72
10N/SBA-15	28.3	1.77	3.96
10N/MCM-41	30.3	1.68	3.69
10N/S-SiO_2	26	1.44	

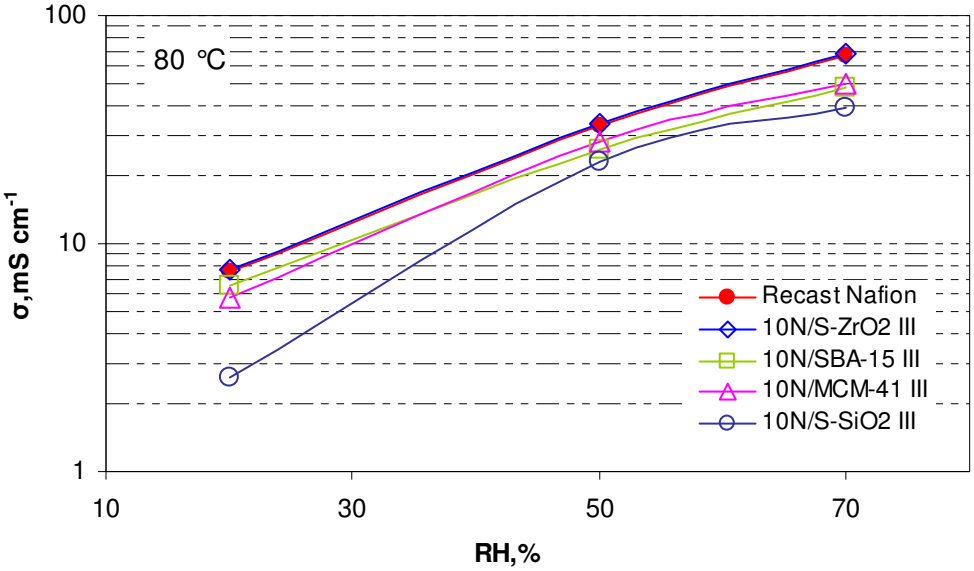

(a)

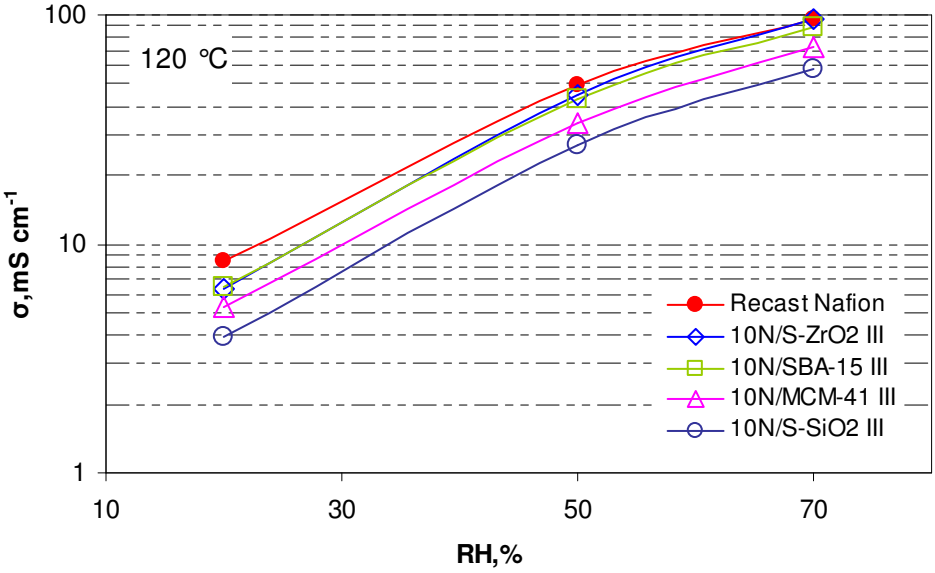

(b)

Figure **5-1**: Proton conductivity of Nafion/10 % sulfonated-inorganic composite membranes at 80 °C (a) and 120 °C (b) with different RH.

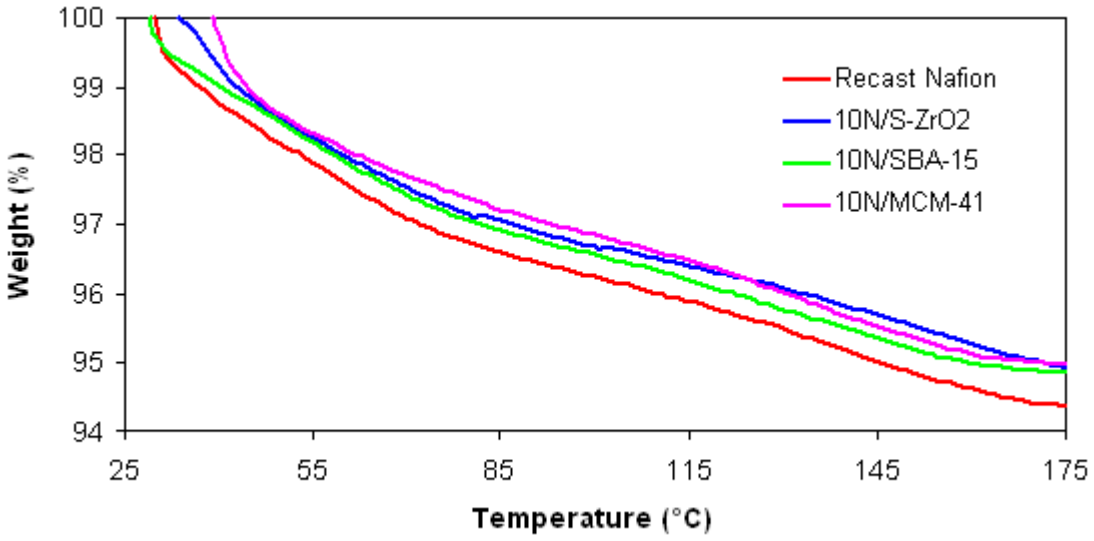

Figure **5-2**: TGA curves for recast Nafion and Nafion/sulfonated-inorganic composite membranes at the temperature range of 25 to 175 °C.

(a) 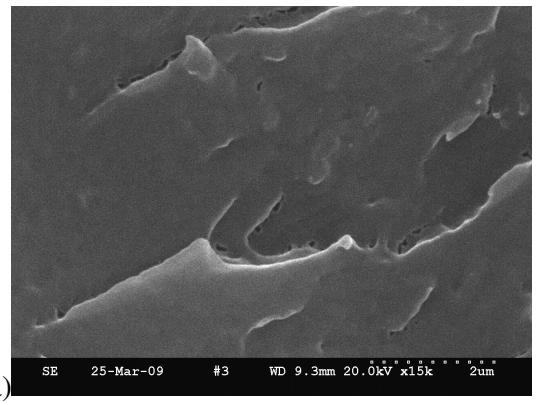

(b) 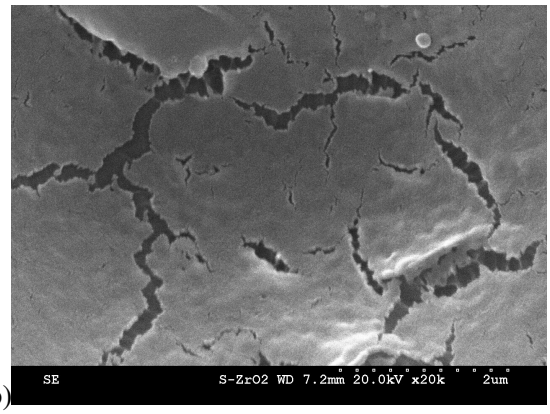

Figure **5-3**: Cross-section SEM images of Nafion (a) and 10N/S-ZrO_2 (b).

The inorganic phase was checked by using SEM images. Figure **5-3** shows the cross-section of SEM images of recast Nafion and 10N/S-ZrO_2. No obvious particle agglomerations were found. Inorganic particles of S-ZrO_2 well dispersed in the Nafion matrix.

We adjusted the concentration of S-SiO_2 and measured the membrane conductivity to examine the effect of inorganic additive content on the membrane conductivity. The varied S-SiO_2 contents ranged from around 10 % to 50 %. Figure **5-4** shows the proton conductivity of composite membranes under different conditions. Table **5-2** lists the deduction of the membrane conductivity of membranes with different content of S-SiO_2 on the basis of the proton conductivity of the membrane with 10 % of S-SiO_2 at 80 and 120 °C under different RH. The observation indicated that the proton conductivity decreased gradually as the inorganic content increased above 10 %. Inorganic particle agglomerates at higher content of the inorganic additive appeared and impeded the proton transport. These agglomerates filled up the polymer pores, blocked the proton transfer path, and reduced the water sorption substantially. In the meantime, the decrease of the proton conductivity of these membranes came from the reduced Nafion content. As the Nafion content decreased, the membrane conductivity decreased.

We discussed the function of the inorganic content and the Nafion content affecting the membrane conductivity. Figure **5-5** shows the rate of the conductivity decrease at different concentration of Nafion. It suggested that the conductivity decrease was most severe at a Nafion concentration around 70 % for all RHs, which indicated the proton conductivity of Nafion played a key role in contributing to the membrane conductivity. The decrease of Nafion concentration brought the drop of the membrane conductivity. Thus, as the Nafion concentration was below 70 %, the membrane conductivity reduction was mainly due to the decrease of the Nafion concentration. When the Nafion content was above 70 %, the decrease of the membrane conductivity was partly from the reduced Nafion concentration. At the same time, S-SiO_2 particle agglomerates impeded the proton transport.

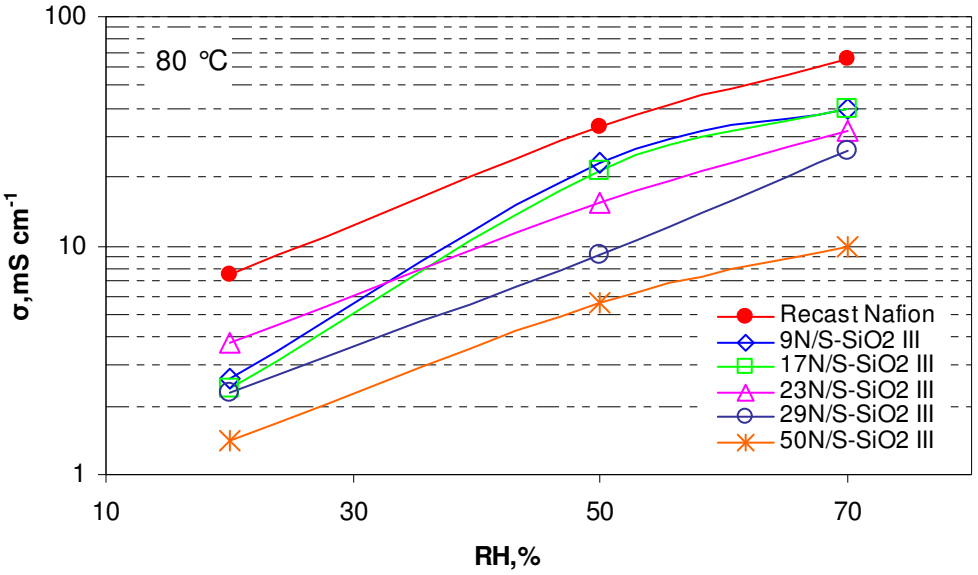

(a)

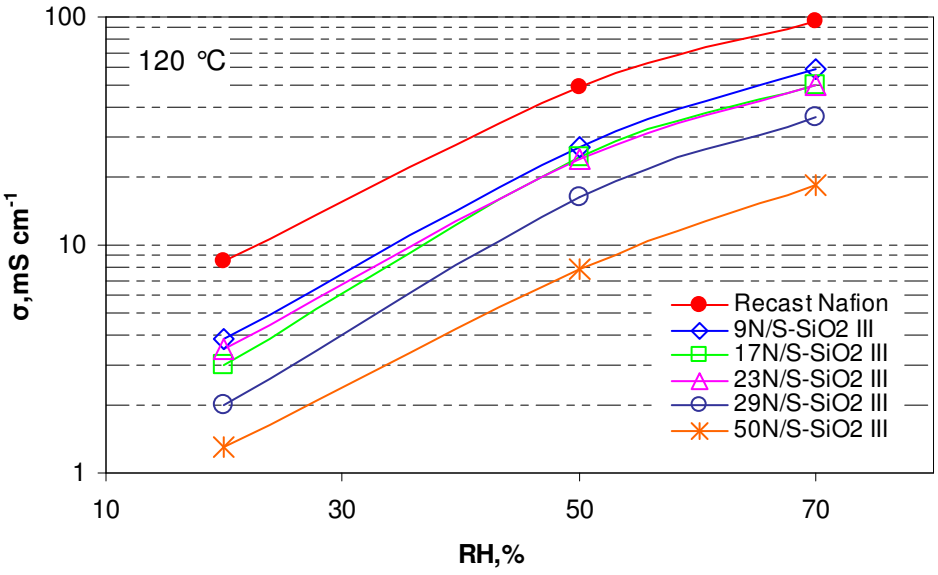

(b)

Figure **5-4**: Proton conductivity of Nafion/S-SiO_2 composite membranes with different content of S-SiO_2 at 80 °C (a) and 120 °C (b) under different RH.

Table **5-2**: Percent reduction (%) of the proton conductivity of Nafion/S-SiO_2 composite membranes with different contents of S-SiO_2 on the basis of the conductivity of 10 % of S-SiO_2 at 80 and 120 °C with different RH.

S-SiO_2 concentration	80 °C (RH)			120 °C (RH)		
	20	50	70	20	50	70
17	8.8	7.4	0.3	23.1	9.0	13.5
23	0.1	33.5	19.0	10.3	11.9	13.5
29	11.5	60.4	33.5	48.7	38.8	37.7
50	46.2	75.7	74.6	66.7	70.5	68.9

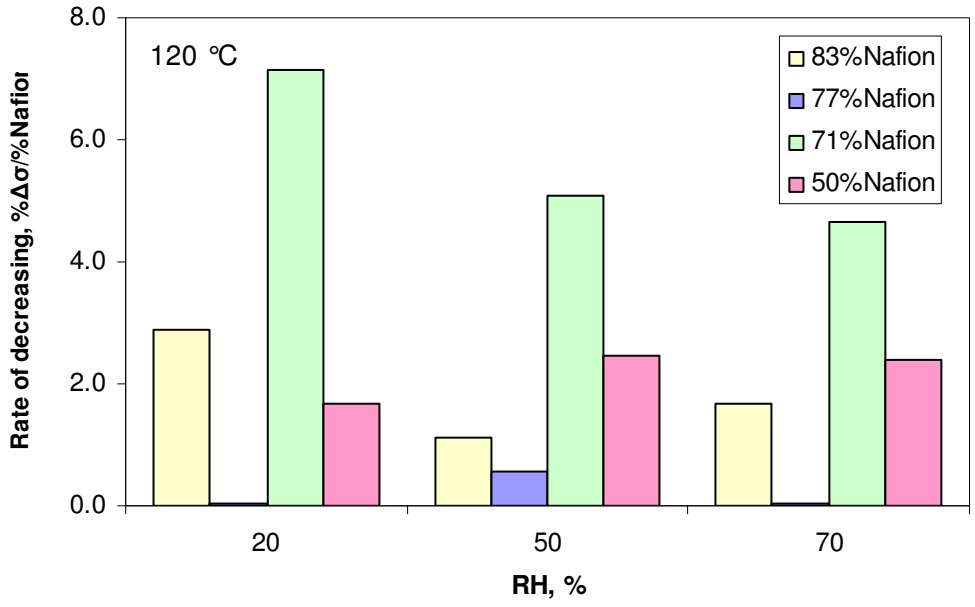

Figure **5-5**: Rate of the proton conductivity decrease in Nafion/S-SiO_2 composite membranes with different contents of Nafion at 120 °C.

5.2 Nafion/phosphosilicate gels composite membranes

This research extensively investigated composite membranes of Nafion/P-SiO_2 (NPS). Membranes were synthesized by different fabrication methods with different phosphor to silicate (P:Si) ratios. We studied their thermal stability, morphology, physicochemical properties, and proton conductivity. Figure **5-6** shows the proton conductivity of NPS composite membranes, in which P-SiO_2 was controlled with P:Si ratio at 1. The results showed that the composite membrane 10NPS II demonstrated a substantial increase in the proton conductivity at 120 °C under all RH compared with that of recast Nafion; at 70 % RH the increase was around 30 %, at 50 % RH it was 37 %, and at 20 % RH it was 30 %. The reason for the high membrane conductivity of 10NPS II was explored through the membrane water uptake, morphology, and physicochemical properties.

Table **5-**3 presents values of the water uptake of NPS composite membranes at 120 °C. We found that the water uptake for composite membranes 10NPS II and 10NPS III were relatively high compared with recast Nafion and other composite membranes. The high water uptake of 10NPS II contributed to its high proton conductivity. However, the proton conductivity of 10NPS III was not as high as that of 10NPS II. We analyzed physicochemical properties of these composite membranes using Fourier transform infrared spectroscopy (FT-IR) and expected to explain the conductivity difference between 10NPS II and 10NPS III. Figure **5-**7 shows the spectra. Table **5-4** lists the assigned components at different frequencies [69, 80-84].

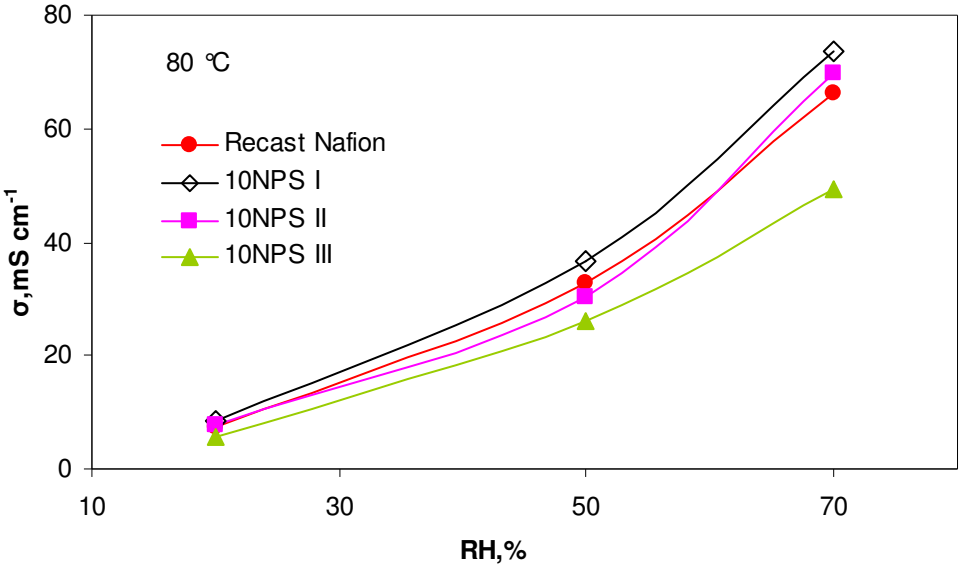

(a)

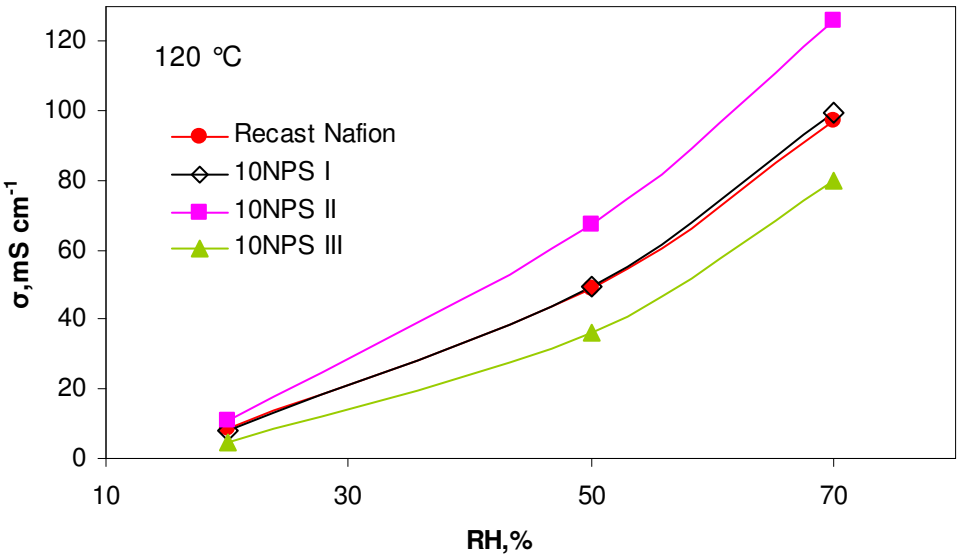

(b)

Figure **5-6**: Proton conductivity of 10NPS composite membranes with different synthesis methods at 80 °C (a) and 120 °C (b) under different RH.

Table **5-3**: Water uptakes of recast Nafion and Nafion/P-SiO_2 composite membranes at 120 °C.

Membrane	Recast Nafion	10NPS I	10NPS II	10NPS III	10$NP_{0.5}$S III
Water uptake at 120 °C (%)	4.26	3.66	4.47	4.58	3.67

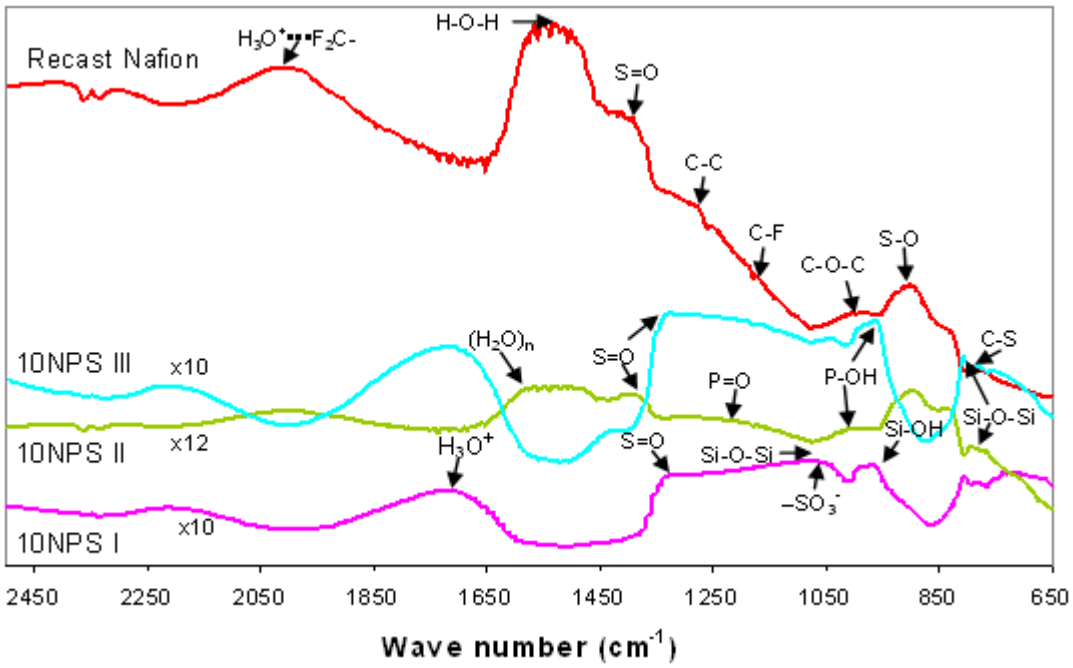

Figure **5-7**: FT-IR spectra of recast Nafion and NPS composite membranes with different fabrication methods.

Table **5-4**: FT-IR characteristic bands for recast Nafion and Nafion/P-SiO_2 composite membranes.

Wave number (cm^{-1})	Assignment
2200 – 2250	POH combination vibration
2000	$H_3O^+ \cdots F_2C$-
1720 – 1750	H_3O^+, $H_5O_2^+$ asymmetric bending
1600	$(H_2O)_n$
1500 – 1580	H-O-H
1450	C-F stretching in amorphous polytetrafluoroethylene
1400 – 1430	S=O asymmetric stretching
1299	C-C stretching
1260	C-F asymmetric stretching
1210-1250	P=O in P_2O_5 network structure
1180	C-F symmetric stretching
1070, 810-837	Si-O-Si stretching in SiO_2 network structure
1057	$–SO_3^-$ asymmetric stretching
980-1000	C-O-C stretching
970-1000	P-OH in $(HPO_4)^{2-}$, $(H_2PO_4)^-$
968	Si-OH stretching
916	S-O stretching of the $–SO_2OH$ groups
810	C-S stretching

In the FT-IR spectra, the peak frequency value, corresponding to the maximum adsorption, identifies components of composite membranes. The line-shift and the line-broadening indicate the interaction between phosphosilicate gels and the Nafion matrix [32]. The P-OH peak in 10NPS III at 980 cm^{-1} shifted to a high vibration frequency of 1000 cm^{-1} in 10NPS II, which indicated that the P-OH bond was lengthened in 10NPS II. This enhanced the proton conductivity of 10NPS II. The physicochemical properties of composite membranes were consistent with their proton conductivities. The H_3O^+ peaks at 1600 – 1750 cm^{-1} in Nafion and all composite membranes were broad, which demonstrated the strong bonding between water molecules and acid groups [80]. The observed spectra were consistent with those in studies of the Nafion and phosphosilicate gels composite membranes [69, 81, 83, 84].

We further investigated the structure and morphology of composite membranes. The Nafion membrane consists of a hydrophobic tetrafluoroethylene backbone with pendant side-chains of perfluoronated vinyl-ethers terminated by sulfonic groups. In the IR spectra of NPS composite membranes, peaks of Si-OH, P=O, Si-O-Si, and P-OH appeared around the same frequency range of Nafion C-O-C, S-O, and $-SO_3^-$ stretching frequencies. Noto et al suggested the SiO_2-P_2O_5 network reacted with the Nafion side-chain clusters and formed dynamic crosslinks of SiO_2-P_2O_5···HSO_3- [84]. On the basis of this understanding, we proposed a schematic of NPS composite membranes. Figure **5-8** shows this schematic. The silica and phosphate groups were connected with –O– bonds and reacted with sulfonic groups through –OH and –O– bonds. The morphologies of NPS composite membranes were measured by SEM. Figure **5-**9 shows the images. The cross-section figures showed that in 10NPS I, around 20-40 nm particles were dispersed in the Nafion matrix; in 10NPS II, even smaller particles were observed; and in 10NPS III, particle agglomerates were found. In 50NPS II, P-SiO_2 particles agglomerated, which partially destroyed the Nafion matrix. By comparing the inorganic phase in the composite membranes with different fabrication methods, method I and II realized particles to uniformly

distribute in the Nafion clusters. These particles, especially the smaller particles in 10NPS II, retained water with their high surface area and provided additional paths for proton transport.

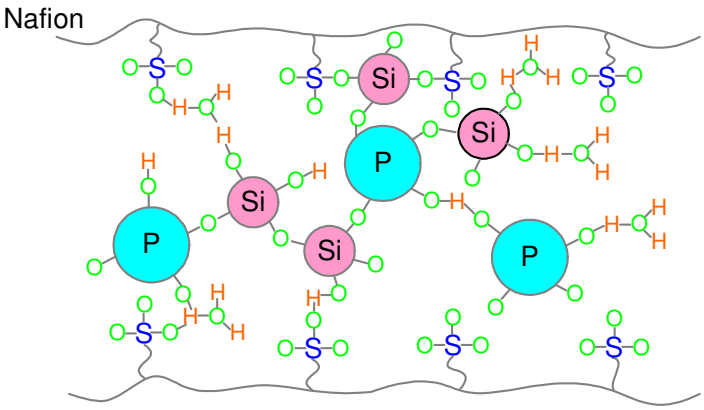

Figure **5-8**: Proposed schematic view of the NPS composite membranes.

(a) 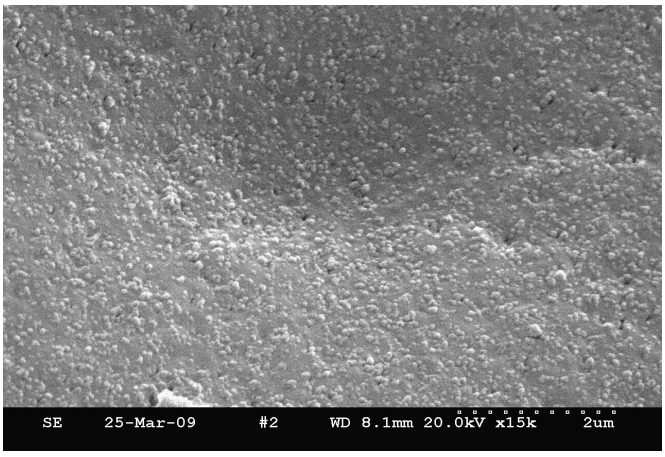

(b)

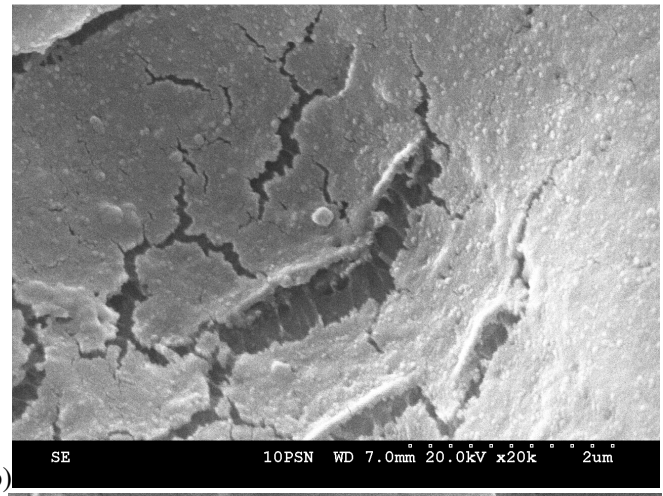

(c)

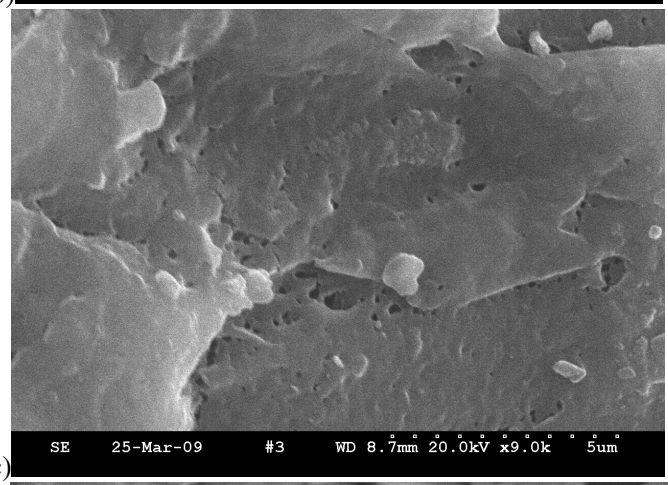

(d)

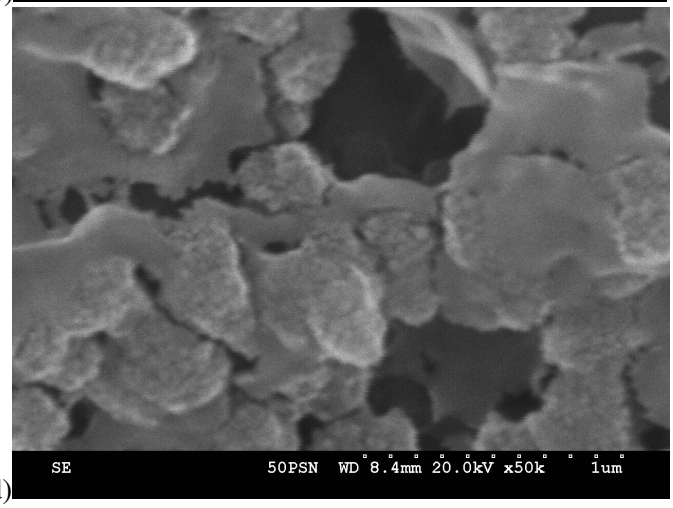

Figure **5-9**: Cross-section of 10NPS I (a), 10NPS II (b), 10NPS III (c), and 50NPS II (d).

We studied the thermo-stability of composite membranes with their TGA curves. Figure **5-10** shows weight changes of 10NPS composite membranes from 25 to 560 °C. The mass loss of 7.4 % when heating from 25 to 299 °C was attributed mainly to the loss of the H_2O molecules. From 290 to 560 °C there appeared three stages for membrane decomposition: 1) weight loss of around 19 % in the range of 290 - 400 °C which was associated with a desulfonation process; 2) weight loss from 400 to 490 °C was related to the side chain decomposition; and 3) weight loss from 490 to 560 °C was from the polytetraflouroethylene (PTFE) backbone decomposition. All composite membranes presented similar thermo-stability to Nafion in all temperature ranges except in the temperature range of 400 to 490 °C. Figure **5-10** shows the amplified mass loss in this range. We found that the slop of 10NPS II was not the same as Nation; it showed a lower slope of decomposition compared with Nafion and other composite membranes. This might indicate that 10NPS II has better thermal stability. Figure **5-11** shows the magnified mass change in the lower temperature range of 25 to 180 °C. The figure presented the same results as those listed in Table **5-3** that at around 120 °C, 10NPS II and 10NPS III attained more water than recast Nafion and other composite membranes.

In the inorganic material conductivity research, results showed that phosphosilicate gel with a P:Si ratio of 1.5 reached a better conductivity than the gel with a P:Si ratio of 0.5. Therefore, the study examined the performance of these phosphosilicate gels in contributing to the membrane conductivity. We measured the proton conductivity of NPS membranes with different P:Si ratios (0.5, 1, and 1.5) prepared by method III. Figure **5-12** shows tested results. The membrane $10NP_{0.5}S$ III demonstrated the highest performance, which was better than that of recast Nafion at both 80 and 120 °C. The measurements pointed out that P-SiO_2 with a P:Si ratio of 0.5 presented the highest surface area (9.0 m^2g^{-1} in Table **4-1**). This high surface area provided extra water-rich surface inside the membrane, resulting in improved membrane conductivity.

Furthermore, the FT-IR analysis revealed that this high surface area facilitated the inorganic network to react with Nafion sulfonic groups, which enhanced the hydrogen bonds.

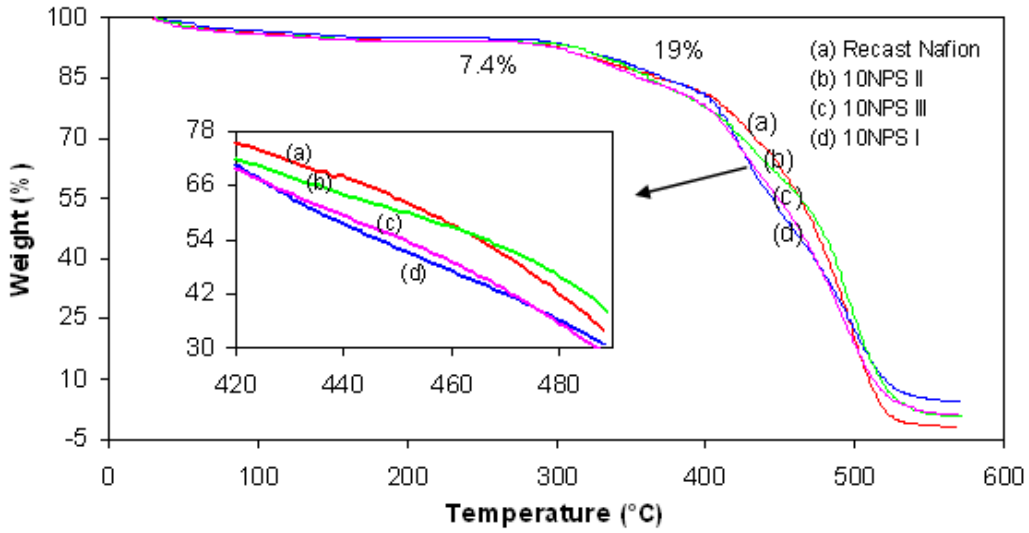

Figure **5-10**: Thermogravimetric analysis of 10NPS composite membranes.

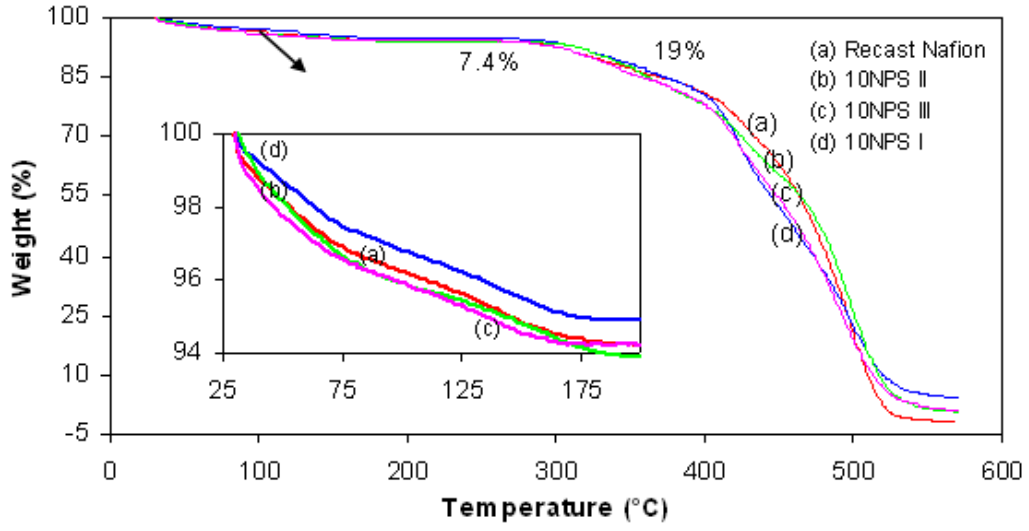

Figure **5-11**: TGA curves of 10NPS composite membranes amplified at low temperature ranges (25 – 180 °C).

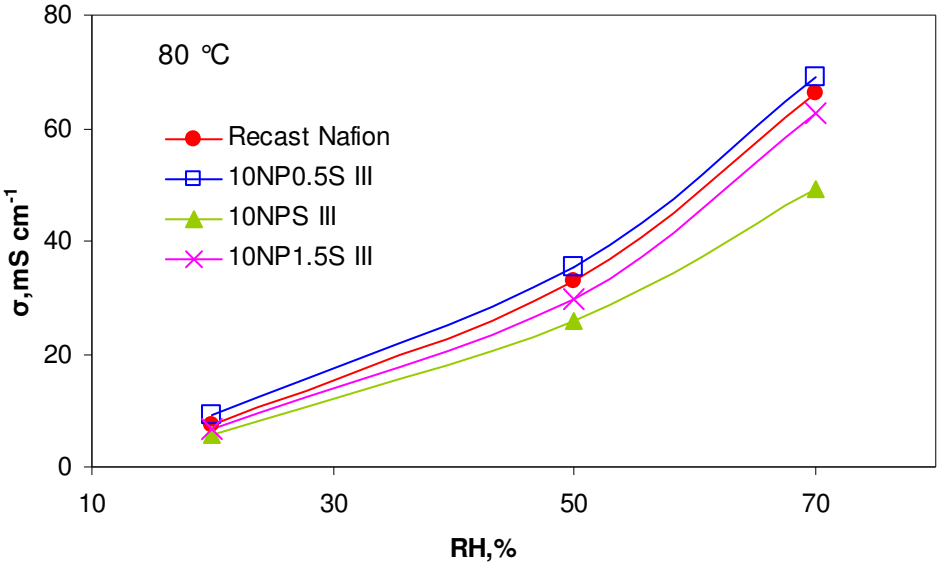

(a)

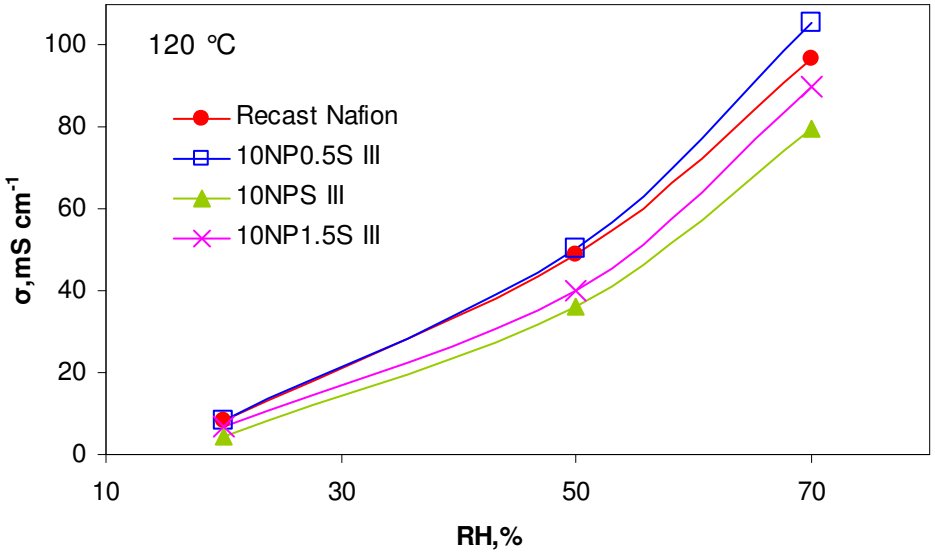

(b)

Figure **5-12**: Proton conductivity of 10NPS composite membranes synthesized by method III with different P:Si ratios at 80 °C (a) and 120 °C (b) under different RH.

Figure **5-13** shows the FT-IR spectra of composite membranes with different P:Si ratios. The P-OH band at 980 cm^{-1} in $10P_{0.5}SN$ III presented to be broader compared with the band in other composite membranes, indicating the P-OH bonding was the strongest. We believed this broader band partially contributed to the highest proton conductivity of $10P_{0.5}SN$ III in NPS composite members. Also, the Si-O-Si peak shifted from 810 cm^{-1} in 10NPS III to high vibration frequency of 837 cm^{-1} in $10P_{0.5}SN$ III, which meaned the Si-O-Si bond was lengthened in $10P_{0.5}SN$ III. Sulfonic acid groups $–SO_3H$ intercalated into the network of SiO_2-P_2O_5 and made it more disordered, which might improve the proton transfer between acid sites by means of the Grotthuss transport mechanism [85].

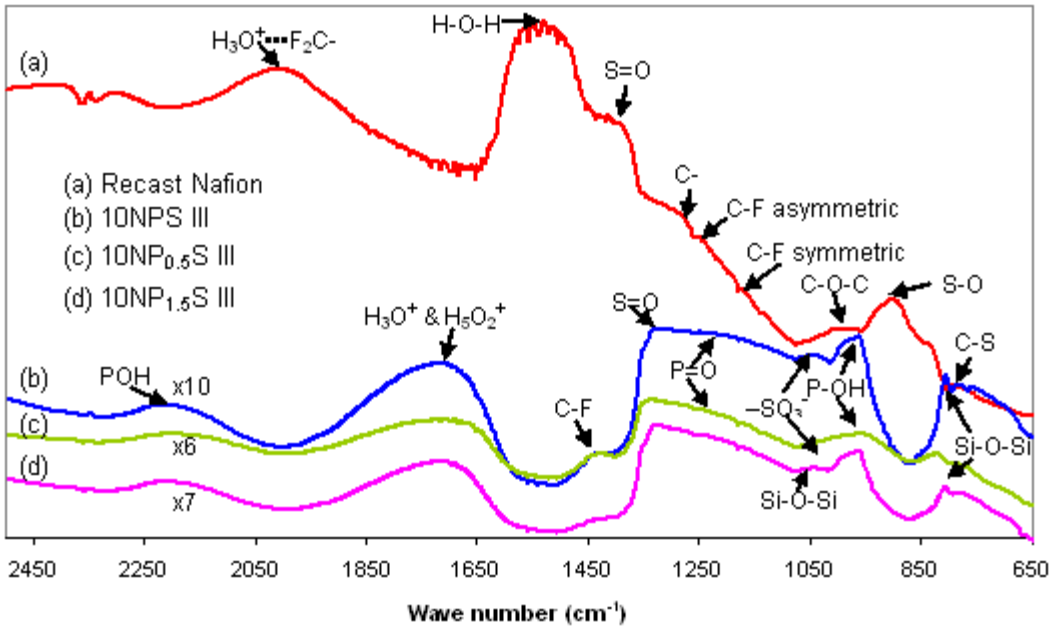

Figure **5-13**: FT-IR spectra of 10NPS composite membranes with different P:Si ratios.

5.3 PEM fuel cell performance

Hydrophilic inorganic particles were reported to be more pronounced in improving the membrane electrochemical performance in a fuel cell [49, 53, 55, 86]. Figure **5-14** shows the PEM fuel cell performance (cell voltage as a function of current density) and ionic resistance of our newly developed NPS composite membranes with different synthesis methods and different P-SiO_2 contents, in a H_2/air fuel cell at 120 °C and different RH[4]. More data of the fuel cell performance at low temperatures of 30 and 80 °C were included in the Appendix **B**. Clearly, the current densities of Nafion/10 % P-SiO_2 composite membranes appeared much higher than pure recast Nafion owing to the decreased membrane resistance in the former. Table **5-5** lists the resistance of composite membranes at different RH. The reduction of the cell resistance was more obvious at low RH: at 50 % RH, compared with Nafion, the cell resistance was around 40 % lower for 10NPS I and 20 % lower for 10NPS II; at 20 % RH, the reduction was around 30 % for both 10NPS I and 10NPS II. This demonstrated that uniformly dispersed P-SiO_2 particles with high water retention ability improved the proton mobility and bridged the proton exchange sites of the SO_3H groups in Nafion [53]. However, when the P-SiO_2 content increased to 50 %, the cell resistance increased by around 50 % compared with Nafion. The agglomerates in high content of inorganic additives blocked the Nafion pores for water sorption and impeded proton transport.

[4] I acknowledge the participation of Dr. Lee to measure the fuel cell performance of NPS composite membranes.

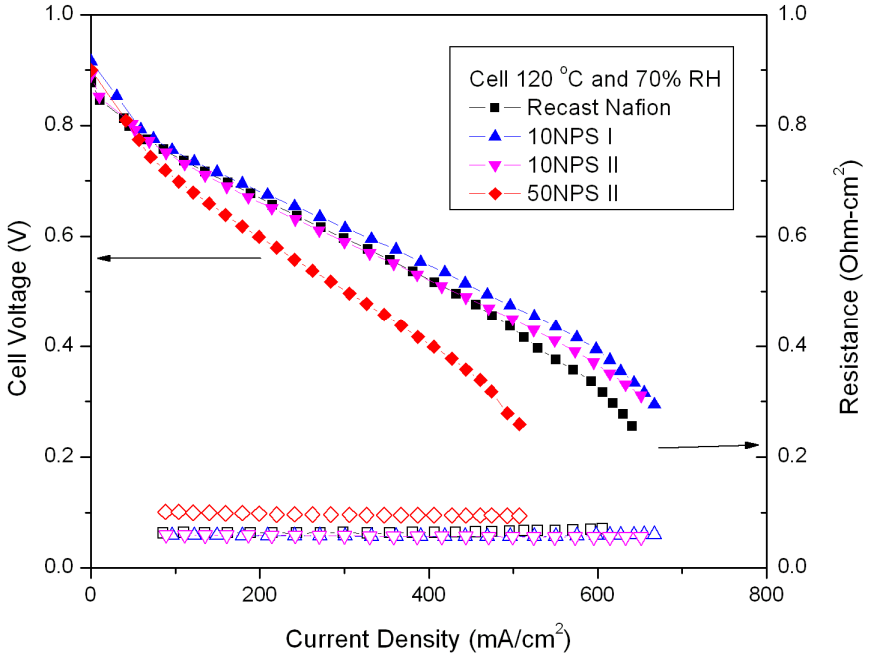
Cell 120 °C and 70% RH
Recast Nafion
10NPS I
10NPS II
50NPS II
Cell Voltage (V)
Resistance (Ohm-cm²)
Current Density (mA/cm²)
0.0
0.2
0.4
0.6
0.8
1.0
0
200
400
600
800

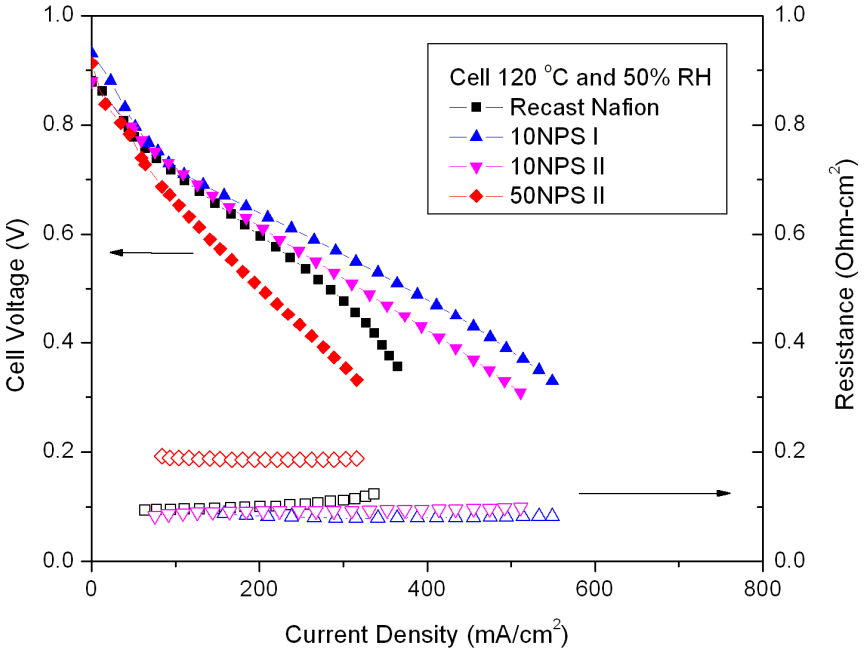
Cell 120 °C and 50% RH
Recast Nafion
10NPS I
10NPS II
50NPS II
Cell Voltage (V)
Resistance (Ohm-cm²)
Current Density (mA/cm²)
0.0
0.2
0.4
0.6
0.8
1.0
0
200
400
600
800

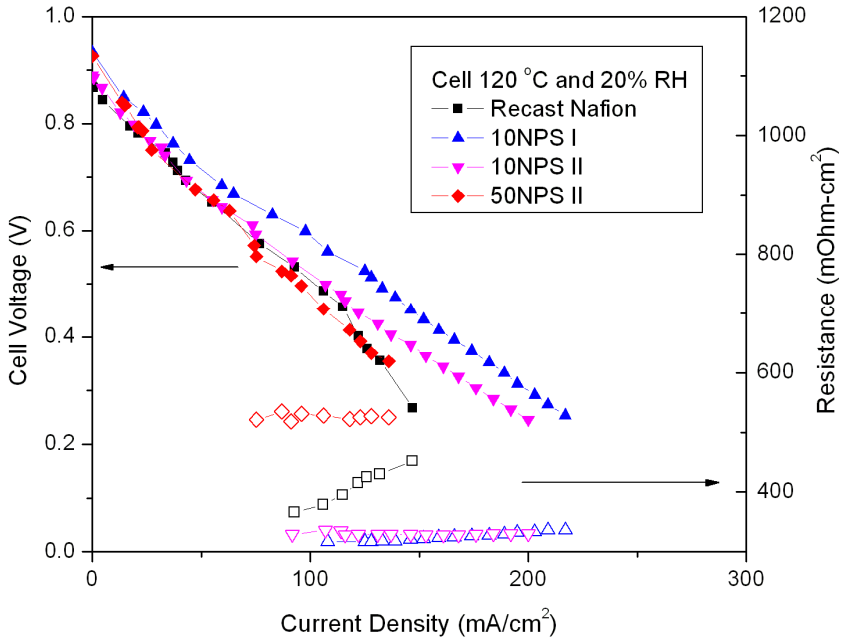

Figure **5-14**: PEM fuel cell performance and resistance of recast Nafion and Nafion/P-SiO_2 composite membranes, in a H_2/air fuel cell at 120 °C and different RH.

Table **5-5**: The resistance of NPS composite membranes at 120 °C and different RH.

RH (%)	Resistance (Ω cm^2)			
	Nafion	10NPS I	10NPS II	50NPS II
20	0.409	0.325	0.33	0.526
50	0.103	0.081	0.092	0.187
70	0.065	0.058	0.057	0.096

The characteristic shape of the voltage/current density graphs of Figure **5-14** resulted from three main irreversibilities: activation polarization, ohmic loss, and concentration loss. The activation polarization is caused by the slowness of the reaction taking place on the surface of the electrodes; to drive the chemical reaction that transfers the electrons to or from the electrode consumes a proportion of the voltage [87]. The ohmic loss comes from the resistance of the electrodes, the interconnections, and the electrolyte. It is a large source of performance loss at high current density. The ohmic loss increases linearly with the current density. The concentration loss results from the limitation of reactant transport in the electrode. The cell potential (V) *vs*. current density (i) behavior follows the equation as [50]

$$V = V_0 - A\ln i - Ri \qquad [5\text{-}1]$$

where V_0 is the open circuit voltage (V_0 = 1.23 V for H_2/air fuel cell), R is the resistance, Ω cm^2, and A is the Tafel slope.

When nothing limits the gas and ion transport in the electrode, in the low current density region, the feature of this behavior meets the Tafel equation [87]

$$\Delta V_{act} = A\ln(i) \qquad [5\text{-}2]$$

where ΔV_{act} is overvoltage and is defined as

$$\Delta V_{act} = V_0 - V - Ri \qquad [5\text{-}3]$$

In the Tafel equation, the Tafel slope represents how fast the overvoltage drops with the current density and indicates the kinetic of the electrochemical reaction. When A is higher, the reaction is slower.

Figure **5-15** shows the overvoltage *vs.* current density in a semi-log plot for Nafion and NPS composite membranes at 120 °C and different RH. Table **5-6** lists the ohmic loss and Tafel slopes for these membranes specifically at 120 °C and 50 % RH. 10NPS composite membranes demonstrated lower ohmic loss and Tafel slopes than Nafion, which explained their improved

PEM fuel cell performance. Apparently, 10NPS composite membranes proved to be kinetically active in the reaction. 50NPS composite membrane displayed a substantial high ohmic loss and a steeper Tafel slope. The bigger Tafel slope suggested the lower kinetic of the electrochemical reaction. An increased inorganic additive content might diminish the catalyst activity on the surface of the composite membrane. In a word, the high resistance of the membrane and reduced catalyst activity caused the dramatic drop of cell voltage in the 50NPS II. At 120 °C and 70 % RH, Tafel slops for Nafion and 10NPS composite membranes showed similar values. The high mobility of protons in electrolytes and at the membrane-electrode interface under high water content does not affect the oxygen reduction reaction [53].

Table **5-6**: The ohmic losses and kinetic parameters for Nafion and NPS composite membranes at 120 °C and 50 % RH.

	Nafion	10NPS I	10NPS II	50NPS II
Ohmic loss at 200 mA cm^{-2} (mV)	20.0	16.6	18.3	37.2
Tafel slope (mV/decade)	111	108	109	120

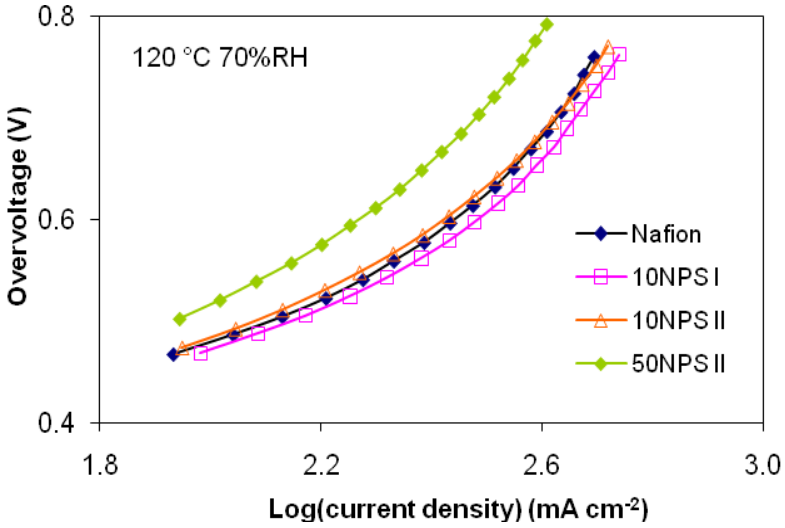

(a)

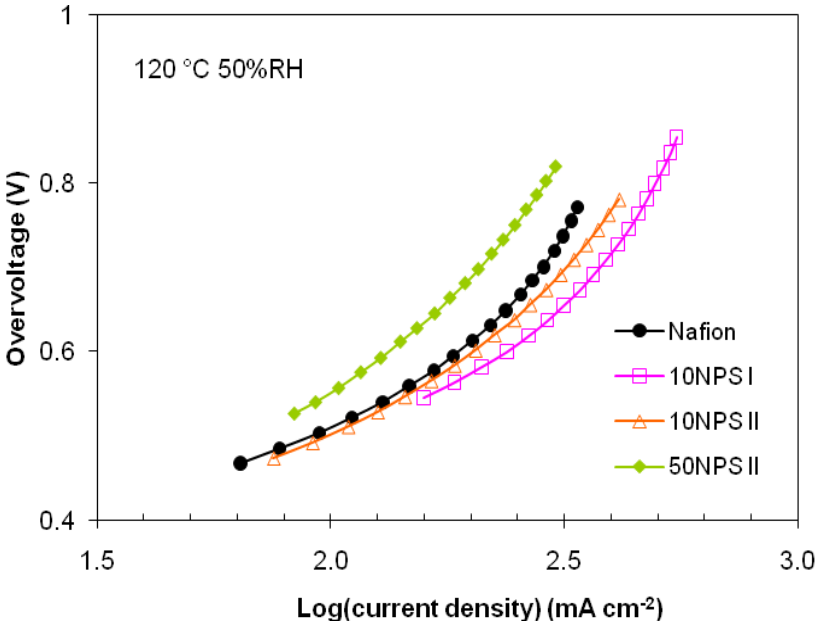

(b)

Figure **5-15**: Tafel plots for Nafion and PSN composite membranes at 120 °C and 70 % (a) and 50 % RH (b).

Chapter 6

Proton Transport Modeling of Composite Membranes

6.1 Modified simple rule of mixtures

The proton conductivity of composite membranes combining the conductivity of the polymer electrolyte and the inorganic additive are rarely described in literature. In the study, we proposed a simple model based on the rule of mixtures to better understand the proton conductivity from all components. This proposed model, based on the assumption that inorganic additives were uniformly dispersed within Nafion clusters, was applied with composite membranes that were synthesized by merely mixing inorganic powders with the Nafion solution (method III). The obtained results were compared with experimental data.

The simulation discovered that the contribution of the inorganic conductivity on the membrane conductivity depended on the inorganic phase properties, such as specific surface area (SSA) and IEC. When the inorganic material SSA (A) was large (A > 500 m^2 g^{-1}), inorganic particles proved to be well mixed within the Nafion matrix. The proton conductivity of composite membranes followed the simple rule of mixtures, which is:

$$\sigma = x_i \sigma_i + x_n \sigma_n \qquad [6\text{-}1]$$

where x_i is the weight percent of the inorganic additive, σ_i is the proton conductivity of the inorganic pellet, x_n is the weight percent of Nafion, and σ_n is the proton conductivity of Nafion. An example is the Nafion/SBA-15 composite membrane. SBA-15 presented to have a large surface area of 629 m^2 g^{-1} (Table **4-1**). When mixed around 10 % of SBA-15 particles with 90 % of Nafion solution, the model calculated the proton conductivity of the cast membrane by taking a sum of 10 % of the proton conductivity of SBA-15 and 90 % of the proton conductivity of

Nafion. We compared the calculated conductivity of the composite membrane with measured values at 120 °C and different RH. Figure **6-1** shows the comparison. Table **6-1** lists the standard deviation between calculated results and experimental data. Observation indicated that the calculated membrane conductivity using the rule of simple mixtures was consistent with measured data in the wide range of RH. The standard deviation was less than 1.2 mS cm^{-1} for the whole set of the data.

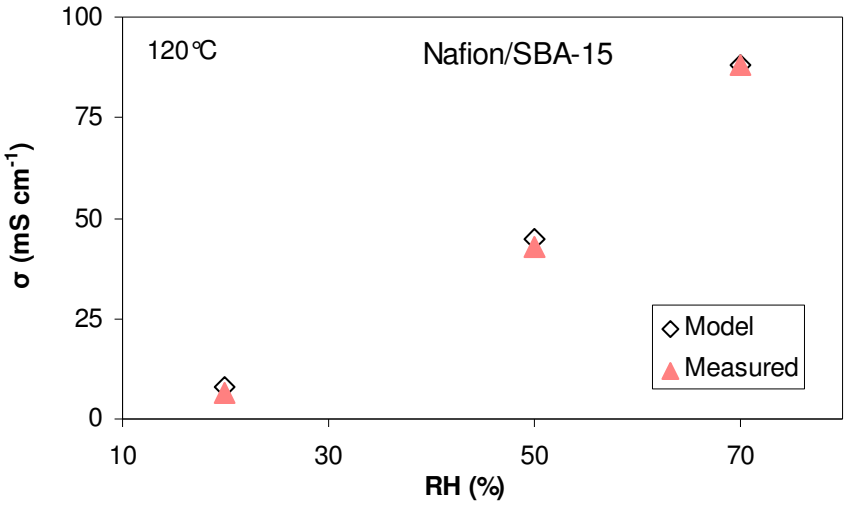

Figure **6-1**: Comparison of the obtained proton-conductivity of the membrane Nafion/SBA-15 using simple rule of mixtures with experimental data at 120 °C and different RH.

When the SSA of inorganic additives was small, the model used the effective proton conductivity of Nafion and inorganic additives in calculation. This effective proton conductivity was induced by considering the limited interaction between Nafion clusters and inorganic additives because of small surface area of inorganic materials. We observed that when the surface acid site density (= IEC/A) of the inorganic additive was less than 10^{-7} mol cm^{-2}, the acidity of

Nafion played dominant function and strongly affected the proton conductivity of composite membranes. Under this circumstance, the membrane conductivity was proposed to be calculated by the following expression

$$\sigma = x_i\sigma_i + ax_n\sigma_n \qquad [6\text{-}2]$$

where a is a modification parameter to emphasize the domination of Nafion acidity, and $a \approx Value(IEC_{Nafion})$. Figures **6-2** and **6-3** show examples of calculation by using this equation. Table **6-2** lists the inorganic phase properties and modeling parameters in the calculation. Sulfated ZrO_2 was measured to have a small surface area of 4.72 $m^2\ g^{-1}$ and a low IEC of 0.22 mmol g^{-1}. When mixed it with Nafion, the proton conductivity of the composite membrane was mainly from Nafion acidic groups. Similarly, the composite membrane of Nafion/P-SiO_2 with the P:Si ratio of 0.5 reflected the same characteristic. The standard deviations between calculated values and experimental data for these membranes at 120 °C and different RH (Table **6-1**) were found to be low enough (< 3 mS cm^{-1}) to prove the accuracy of the calculation. The modification parameter, *a*, proclaimed to be applicable for the whole range of RH at 120 °C.

When the surface area of the inorganic additive was small, but the IEC was relatively high and the surface acid site density was greater than 10^{-7} mol cm^{-2}, the small surface area of the inorganic materials jeopardized the contribution of its acidity. Then, the conductivity of the composite membrane was proposed to be calculated with

$$\sigma = bx_i\sigma_i + x_n\sigma_n \qquad [6\text{-}3]$$

where b is a modification parameter to represent the loss of the conductivity in the inorganic additive, and $b \approx IEC_{Nafion} / IEC_{inorganic}$. Figure **6-4** shows an example of the modeling results with membrane Nafion/P-SiO_2 with a P:Si ratio of 1.5. The simulation revealed that the high IEC of P-SiO_2 with the P:Si ratio of 1.5 only contributed around 23 % of its proton conductivity within the composite membrane owing to the low SSA. Thus, in order to improve the proton

conductivity of composite membranes, inorganic conductors with a high acidity need to be modified to increase the surface area. Also, it drives us to develop new composite membrane fabrication method to improve the interaction between inorganic acidic functional groups and Nafion side-chains. The table proved that the proposed modification parameter, *b*, fitted well in a wide range of RH. The calculation with different composite membranes confirmed that the proposed equations, based on the modified rule of mixtures to calculate the composite membrane conductivity, deemed to be accurate for further application.

Table **6-1**: Standard deviation (SD, mS cm^{-1}) between calculated results (CR) and experimental data (ED) in the calculation of modified simple rule of mixtures for Nafion-based composite membranes with 10 % inorganic additives at 120 °C and different RH.

RH (%)	20			50			70		
	ED (mS/cm)	CR (mS/cm)	SD (mS/cm)	ED (mS/cm)	CR (mS/cm)	SD (mS/cm)	ED (mS/cm)	CR (mS/cm)	SD (mS/cm)
Nafion/ SBA-15	6.50	7.73	0.87	42.90	44.55	1.16	88.30	88.19	0.08
Nafion/ S-ZrO_2	6.30	8.27	1.39	44.80	47.66	2.03	96.50	94.36	1.51
Nafion/ P:Si=0.5	8.70	8.62	0.06	51.00	50.51	0.35	103.50	99.30	2.97
Nafion/ P:Si=1.5	6.70	8.13	1.01	40.20	45.92	4.04	89.80	90.60	0.56

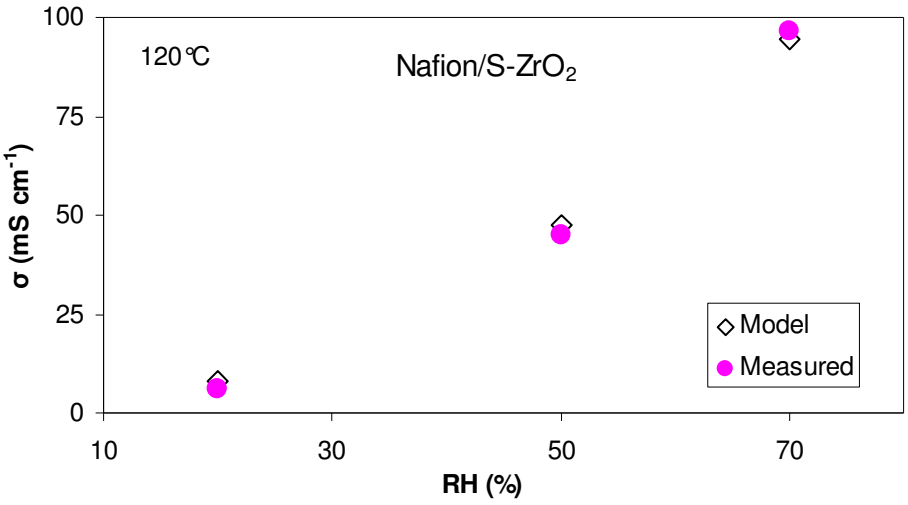

Figure **6-2**: Comparison of the calculated proton conductivity of the membrane Nafion/S-ZrO_2 to experimental data at 120 °C and different RH.

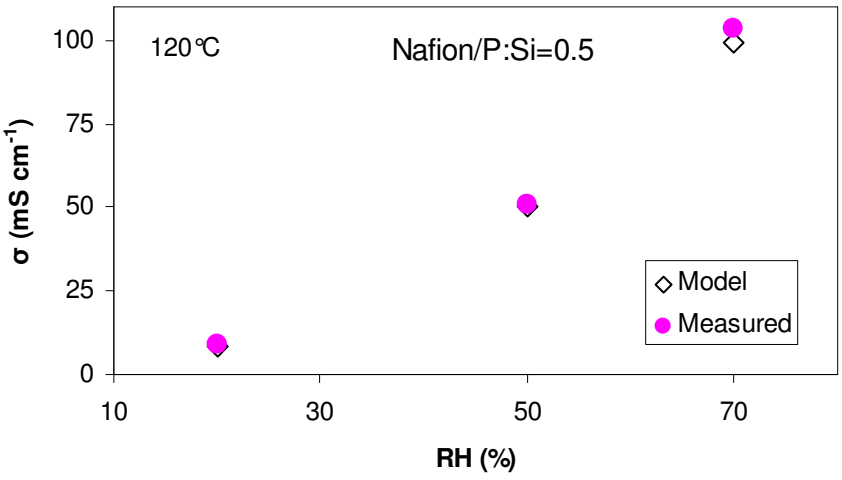

Figure **6-3**: Comparison of the calculated proton conductivity of the membrane Nafion/P-SiO_2 with a P:Si ratio of 0.5 to experimental data at 120 °C and different RH.

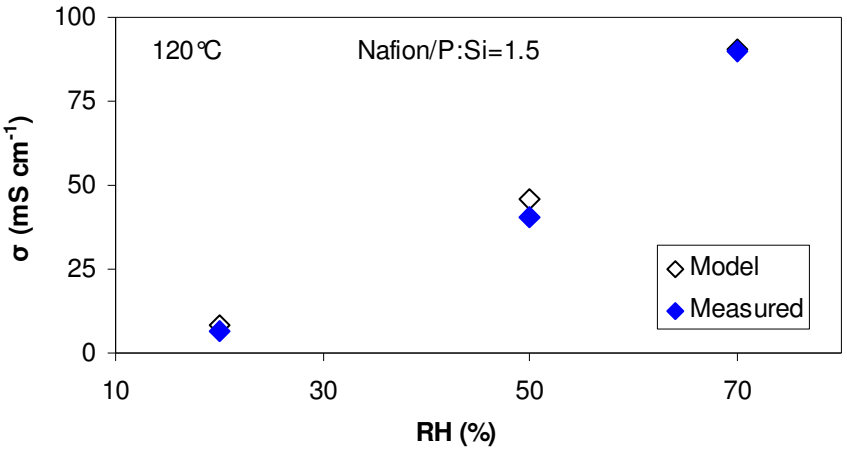

Figure **6-4**: Comparison of the calculated proton-conductivity of the membrane Nafion/P-SiO_2 with a P:Si ratio of 1.5 to experimental data at 120 °C and different RH.

Table **6-2**: The inorganic phase properties and modeling parameters for the modified rule of mixtures.

		S-ZrO_2	P-SiO_2 (P:Si)		SBA-15	Nafion
			0.5	1.5		
Surface Area ($m^2 g^{-1}$)		4.72	9	3	629	
IEC (mmol g^{-1})		0.22	2.66	4.75	0.8	1.07
Surface acid site density (10^{-7} mol cm^{-2})		0.05	0.30	1.58		
x_i (%)					9.09	
x_n (%)						90.91
Modification parameter	a ≈ Value(IEC_{Nafion})	1.07	1.07			
	b ≈ IEC_{Nafion} / $IEC_{inorganic}$			0.23		

6.2 Developed proton-transport modeling of composite membranes

We adopted a theoretical proton-transport model that simulated the proton conductivity of Nafion to describe the proton transport in Nafion-based composite membranes. The basic theory was described in the Chapter **2.2**. This model was based on the dusty-fluid model for transport and the percolation model for structural aspects. The generalized Stefan-Maxwell equations, or equivalently Spiegler's frictional model were applied [61]. This study defined the parameters that involved in the model for inorganic additives from their physical-chemistry characteristics and from the literature study.

In the Nafion-based composite membranes, similarly, proton-transport is through surface hopping, Grotthuss diffusion, and vehicle diffusion. The key effect of the additives is to provide additional surface functional sites for water adsorption. Thus, the acidity and the amount of water adsorbed of composite membranes are increased. However, the particles also provide an additional obstruction to the proton bulk diffusion (Grotthuss and vehicle diffusion). The enhancement of the proton bulk diffusion depends on whether bulk water and bulk proton concentrations are increased. On the basis of this fundamental understanding, we generalized the following assumptions:

(1) The protons were transported mainly through Grotthuss mechanism and vehicle mechanism;

(2) The sulfonic acid groups from Nafion and the acid groups from inorganic additives were spatially uniform with an electroneutrality within the membrane;

(3) The hydronium ions were the only charge-carrying species;

(4) The effective continuum diffusion coefficients for water (species 2) and the hydronium ion (species 1) in the membrane matrix (species M) were the same, that was $D_{1M}^{e} = D_{2M}^{e}$;

(5) The concentration gradient of hydronium ions was zero; and

(6) No convection in the flow process.

The final equation used to describe the proton conductivity of a composite membrane is [34]

$$\sigma = (\varepsilon - \varepsilon_0)^q \left(\frac{\lambda_{H+}}{1+\delta_{AH}+\delta_{ZH}}\right)(c_{AH,0}\alpha_{AH} + c_{ZH,0}\alpha_{ZH}) \quad [6\text{-}4]$$

where ϵ is the volume fraction of water in hydrated membrane, or wet porosity, ϵ_0 is the percolation threshold volume fraction of water in a hydrated membrane, q is the Bruggeman or critical exponent proposed to be 1.5, λ_{H+} is the equivalent conductivity of the proton at infinite dilution, δ_{AH} is the ratio of mutual to Nafion matrix effective diffusion coefficients, δ_{ZH} is the ratio of mutual to inorganic additive matrix effective diffusion coefficients, $c_{AH,0}$ is the acid-group concentration of the Nafion membrane, α_{AH} is the degree of acid-group dissociation in the Nafion membrane, $c_{ZH,0}$ is the acid-group concentration of inorganic particles, and α_{ZH} is the degree of acid-group dissociation in inorganic additives. In literature, the equation **6-4** was given without further data analysis and confirmation. In our study, this equation was explored with substantial calculation and experimental data confirmation. All of these parameters are defined as follows.

The volume fraction of water in hydrated membrane ϵ corresponding to the water loading, λ is [34]

$$\varepsilon = \frac{\lambda}{\frac{\overline{V}_M}{\overline{V}_2} + \lambda} \quad [6\text{-}5]$$

where $\overline{V}_2$ is the partial molar volume of water taken roughly as 18 cm^3 mol^{-1}, and $\overline{V}_M$ is the partial molar volume of the composite membrane, calculated by

$$\overline{V}_M = \overline{V}_{Nafion}(1-x_i) + x_i\overline{V}z \quad [6\text{-}6]$$

The partial molar volume of Nafion, $\overline{V}_{Nafion}$, corresponding to EW and the dry membrane density ρ_0 is

$$\overline{V}_{Nafion} \approx \frac{EW}{\rho_0} \quad [6\text{-}7]$$

For the Nafion used in our research EW = 1100 g mol^{-1} and ρ_0 = 2.05 g cm^{-3} [61]. Thus, $\overline{V}_{Nafion}$ = 537 cm^3 mol^{-1}. The partial molar volume of the inorganic additive, $\overline{V}z$, is calculated as [34]

$$\overline{V}z = d_Z / (6c^*_{ZH_0}) \quad [6\text{-}8]$$

where $c^*_{ZH_0}$ is the surface acid site density of the additive (mol cm^{-2}) and d_Z is the additive particle size (cm). $c^*_{ZH_0}$ is calculated by

$$c^*_{ZH_0} = IEC_Z / A \quad [6\text{-}9]$$

Table **6-3** shows the character parameters of inorganic additives and calculated parameters. The water loading λ was estimated from a Brunauer-Emmett-Teller (BET) finite layers model [13, 34, 41, 61]. Table **6-4** presents the water loading λ and the volume fraction of water in the membrane ϵ at different RH. The percolation threshold volume fraction of water in the membrane ϵ_0 was accepted as 0.06 based on the previous discussion [88]. Table **6-5** lists the parameter values employed in the model.

The equivalent conductivity of the proton at infinite dilution λ_{H+} is assumed as the equivalent conductivity of hydronium ions in water. At 25 °C, it is 349.8 S cm^2 [61]. The temperature (T) dependence of equivalent conductivity is estimated to be [61]

$$\lambda_{H+} = \lambda_{H+,298} \exp[-\frac{E_\eta}{R}(\frac{1}{T} - \frac{1}{298})] \quad [6\text{-}10]$$

with the activation energy for viscosity of water $E_\eta \approx 14$ kJ mol^{-1}. At 120 °C, the equivalent conductivity of the proton is calculated to be around 1771.5 S cm^2.

The ratio of mutual to Nafion matrix effective diffusion coefficients δ_{AH} is defined as [61]

$$\delta_{AH} = D_{12}^e / D_{1M}^e = \zeta_{12} / \zeta_{1M} = (K_1 / K_0)(D_{12} / D_{1M}) \quad [6\text{-}11]$$

As introduced in Chapter **2.2**, $D_{12}^e = K_1 D_{12}$, $D_{1M}^e = K_0 D_{1M}$, K_1 is the DFM structural constant for the mutual diffusion coefficient, K_0 is the DFM structural constant for the membrane matrix diffusion coefficient, D_{12} is the mutual diffusion coefficient for hydronium ions and water (cm^2 s^{-1}), D_{1M} is the diffusion coefficient for interaction of hydronium ions and the membrane (cm^2 s^{-1}), ζ_{12} is the friction coefficient for interaction between hydronium ions and water (J s cm^{-5})(cm^3 mol^{-1})^2, and ζ_{1M} is the friction coefficient for interaction between hydronium ions and the membrane matrix (J s cm^{-5})(cm^3 mol^{-1})^2. The value of δ_{AH} depends on the diffusion of species of hydronium ions and water within the tortuous membrane. It is difficult to be more quantitative at the current stage. Thus, δ_{AH} is treated as a fitted parameter depending upon the level of hydration. At 120 °C, δ_{AH} was fitted as 5.5 for vapor-equilibrated conductivity [61]. Similarly, the ratio of mutual to inorganic additive matrix effective diffusion coefficients δ_{ZH} is defined as

$$\delta_{ZH} = D_{12}^e / D_{1Z}^e = \zeta_{12} / \zeta_{1Z} \quad [6\text{-}12]$$

where ζ_{1Z} is the friction coefficient for interaction between hydronium ions and the inorganic additive. The value of δ_{ZH} was fitted to be 0.6 referencing the literature value for liquid-equilibrated conductivity [61].

The acid-group concentration of Nafion membrane $c_{AH,0}$ is defined on the basis of per unit volume of pore solution [61]

$$c_{AH,0} = \frac{1}{\lambda \bar{V}_2} \quad [6\text{-}13]$$

Since the acid-group concentration of Nafion varies with the water loading λ. At different RH, the calculated values of $c_{AH,0}$ are presented in Table **6-4**.

The degree of acid-group dissociation in the Nafion membrane α_{AH} is calculated with [61]

$$\alpha_{AH} = \frac{(\lambda+1) - \sqrt{(\lambda+1)^2 - 4\lambda(1-1/K_{A,C})}}{2(1-1/K_{A,C})} \quad [6\text{-}14]$$

where $K_{A,C}$ is the equilibrium constant for proton solvation in terms of concentrations. The temperature dependence of the acid-group dissociation constant is

$$K_{A,C} = K_{A,C,298} \exp[-\frac{\Delta H^0}{R}(\frac{1}{T} - \frac{1}{298}) \times 10^{-3}] \quad [6\text{-}15]$$

where $K_{A,C,298}$ is the equilibrium constant for proton solvation at 25 °C and ΔH^0 is the enthalpy change for proton solvation (kJ mol^{-1}). Unfortunately, the $K_{A,C,298}$ value for Nafion was not found in literature. It was reported that the Hammett acidity function of Nafion is similar to that for 100 % sulfuric acid. Thus, the solvation reaction of sulfuric acid was used to simulate that of the sulfonic acid groups in Nafion. A value of 6.2 for $K_{A,C,298}$ was adopted [61]. At 120 °C, $K_{A,C}$ was calculated to be around 6.16. The heat of adsorption of water vapor in Nafion was found to be 52.3 kJ mol^{-1} at $\lambda < 4$ [61]. The value $\Delta H^0 = -52.3$ kJ mol^{-1} was applied. The degree of acid-group dissociation in inorganic additives α_{ZH} was assumed roughly to be 0.3 ~ 0.4 based on our knowledge in the proton conductivity calculation using simple rule of mixtures

that around 30 % of acidity of P-SiO_2 with a P:Si ratio of 1.5 contributed to the membrane conductivity when the SSA of inorganic materials was small. When the surface area of inorganic additives was high a value of 0.4 for α_{ZH} was used, for example in Nafion/SBA-15 composite membrane.

Assuming the inorganic particles are in the shape of a sphere the concentration of acid groups on the surface of particles $c_{ZH,0}$ is calculated by

$$c_{ZH,0} = c^{*}_{ZH_0} /(2/3d_Z) \qquad [6\text{-}16]$$

The structural effects considering the space-filling aspect and tortuosity of the membrane are represented by K_1/K_0, which depends on the RH. The interaction between hydronium ions, water, and membrane matrix depends upon the difference in collision frequencies of hydronium ions and water and that of hydronium ions and the composite membrane matrix is described by δ_{AH} and δ_{ZH}. The developed proton-transport model taking into account structural effects and the interaction between hydronium ions, water, and Nafion matrix was applied to simulate the proton transport in our newly synthesized Nafion-based composite membranes. Figures **6-5** and **6-6** show the modeled results in a whole range of RH from 20 to 90 % at 120 °C. Experimental data at each RH were compared with those calculated ones. Table **6-6** lists the standard deviations in comparison for test membranes. Overall, the modeled results were well correlated with a variety of experimental data in a wide range of RH. The standard deviation for more than 80 % of modeled points was less than 3 mS cm^{-1}. The developed proton-transport model for composite membranes is applicable to predict the membrane proton conductivity under varied RH.

In this model, we referenced the parameters to define the properties of Nafion membrane from literature description. The inorganic additive parameters employed in the model were developed from the physical-chemistry characteristics of inorganic materials, except the ratio of mutual to inorganic additive matrix effective diffusion coefficients (δ_{ZH}), the degree of acid-

group dissociation in inorganic additives (α_{ZH}), and the particle size of additives (d_z). The value of δ_{ZH} was fitted based on the literature discussion; the value of α_{ZH} was assumed from our knowledge of inorganic phase performance in the composite membranes. Both values appeared justifiable. The quantity of the inorganic particle size was estimated in composite membrane SEM images, which would bring the major error for proton-transport model simulation. Furthermore, a potential limitation of applying this model exists in that the concentration of additives has to be low (< 20 %) to keep the suitable structure model of Nafion. Also, when the inorganic additive content is high, the parameters, describing the inorganic particles, have to be modified. For example, agglomerates make the particle size distribution non-uniform.

Table **6-3**: Characteristic parameters and calculated parameters of inorganic additives in the composite membrane proton-transport modeling.

Parameter	Units	$S\text{-}ZrO_2$	$P\text{-}SiO_2$ (P: Si)			SBA 15
			0.5	1	1.5	
$c^*_{ZH_0}$	mol cm^{-2}	4.66E-09	2.96E-08	8.12E-08	1.58E-07	1.27E-10
d_Z	cm	6.00E-06	7.00E-06	1.00E-05	5.00E-05	8.00E-05
$\overline{V}_Z$	$cm^3\ mol^{-1}$	4.66E-15	3.45E-14	1.35E-13	1.32E-12	1.69E-15
$\overline{V}_M$	$cm^3\ mol^{-2}$	488	488	488	488	488
$c_{ZH,0}$	mol cm^{-3}	1.17E-03	6.34E-03	1.22E-02	4.74E-03	2.38E-06

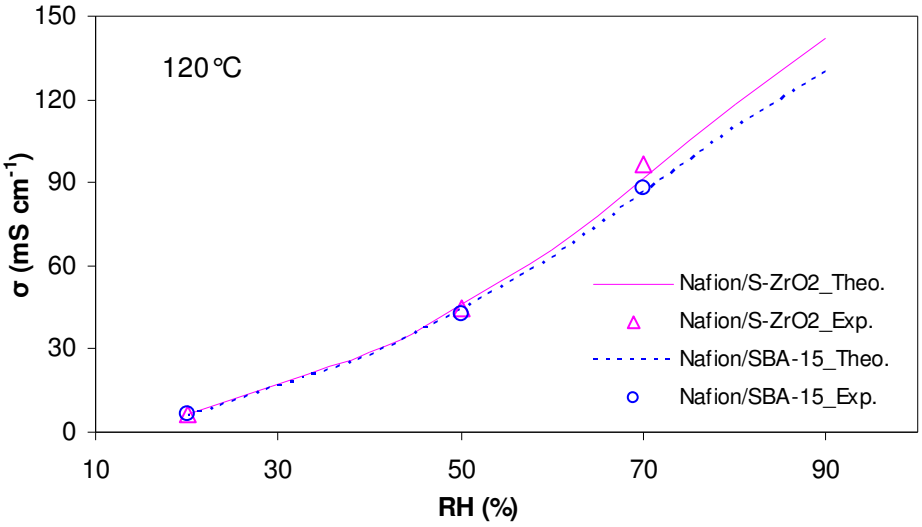

Figure **6-5**: Comparison of results between developed proton transport modeling and experimental measurements at 120 °C for composite membranes of Nafion/S-ZrO_2 and Nafion/SBA-15.

Table **6-4**: Characterization parameters of Nafion in the composite membrane proton-transport modeling.

Parameter \ RH (%)	20	40	50	60	70	80	90	100
λ	2.06	2.8	3.4	4.2	5.5	7.4	10	14
ϵ	0.071	0.094	0.111	0.134	0.169	0.214	0.269	0.341
$c_{AH,0}$ mol cm^{-3}	2.70E-02	1.98E-02	1.63E-02	1.32E-02	1.01E-02	7.51E-03	5.56E-03	3.97E-03
$\alpha_{AH,0}$	0.891	0.926	0.942	0.955	0.967	0.976	0.983	0.988

Table **6-5**: Parameter values employed in the model for composite membranes.

Parameter	Value	Units	Reference
EW	1100	g mol^{-1}	Taken as Nafion 117
ρ_0	2.05	g cm^{-3}	Thampan et al. 2000
ϵ_0	0.06		Morris and Sun 1993
q	1.5		Thampan et al. 2005
$\bar{V}_2$	18	cm^3 mol^{-1}	
$\lambda_{H+,298}$	349.8	S cm^2	Thampan et al. 2000
E_η	14	kJ mol^{-1}	Activation energy for viscosity of water
δ_{AH}	5.5		Fitted for Nafion at vapor-equilibrated conductivity
δ_{ZH}	0.6		Fitted for inorganic at liquid-equilibrated conductivity
α_{ZH}	0.3 ~ 0.4		Assumed for inorganic acid groups dissociation
$K_{A,C,298}$	6.2		Thampan et al. 2000
ΔH^0	-52.3	kJ mol^{-1}	Thampan et al. 2000

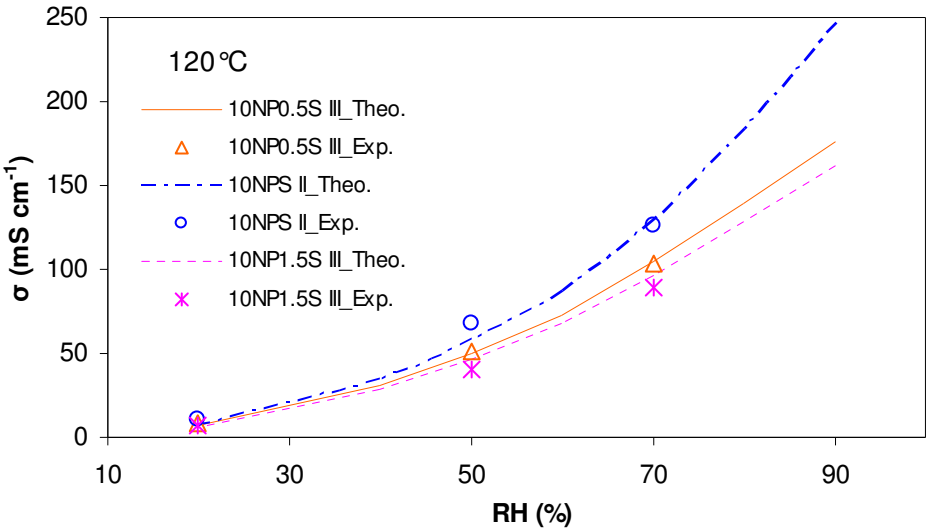

Figure **6-6**: Comparison of results between developed proton transport modeling and experimental measurements at 120 °C for composite membranes of Nafion/P-SiO_2.

Table **6-6**: Standard deviation (mS cm^{-1}) between calculated results and experimental data for developed proton-transport model at 120 °C and RH from 20 to 70 %.

RH (%)	N/S-ZrO_2	10$NP_{0.5}$S III	10NPS II	10$NP_{1.5}$S III	N/SBA-15
20	0.27	1.15	2.20	0.21	0.04
50	0.94	0.49	5.90	3.47	1.33
70	3.60	0.53	3.52	1.67	0.74

In addition, we applied this proton transport model to illustrate the effect of inorganic properties on the membrane proton conductivity. It has been reported that a smaller size of filler is more favorable in the property enhancement of the composite membrane [28]. Likewise, the deduction of the proton conductivity, $\Delta\sigma$, at 120 °C was simulated when increased the particle size of inorganic additives by one order of magnitude in composite membranes. Figure **6-7** shows the results. Calculation revealed that the proton conductivity decreased around 5 ~ 30 % at 70 % RH, 3 ~ 21 % at 50 % RH, and 2 ~ 15 % at 20 % RH for both Nafion/sulfonated-inorganic and Nafion/phosphonated-inorganic composite membranes with different inorganic additives. To the contrary, the proton conductivity reduction for Nafion/SBA-15 composite membrane seemed to be around 0 at all RHs when varied the particle size of SBA-15. The main reason for this different performance of inorganic additives proved from the different concentration of acid groups on the surface of particles $c_{ZH,0}$ (Table **6-3**). The higher acid-group concentration of inorganic additives the larger is the degree of effect on the proton conductivity of composite membranes investigated. Thus, the study proposed a new route in rational design of a high proton-conductive composite membrane, which was to increase the acidity of inorganic materials and to decrease their particle sizes.

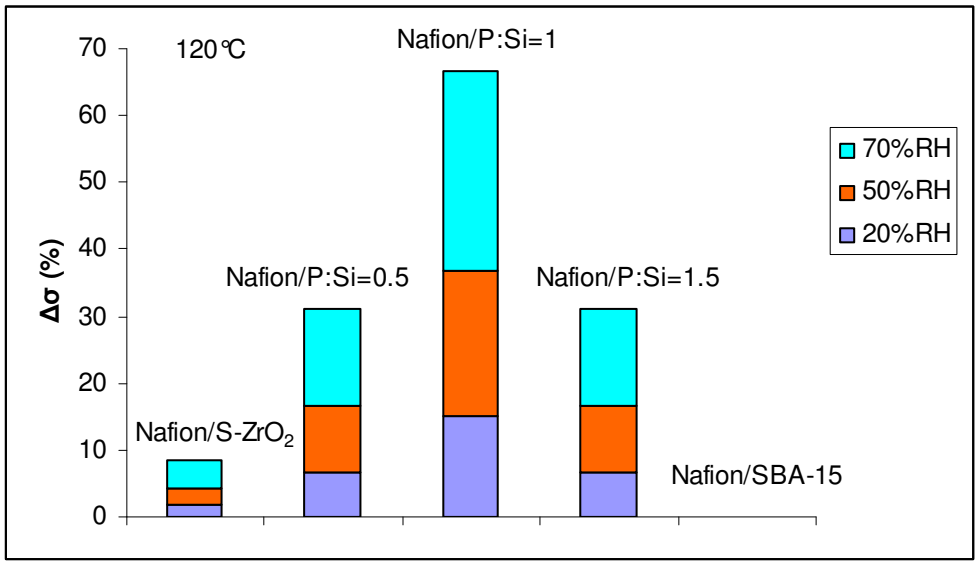

Figure **6-7**: The proton conductivity reduction ($\Delta\sigma$) with an increase of the particle size by one order of magnitude in composite membranes at 120 °C and different RH.

Chapter 7

Research Summary

To develop a desired proton-exchange membrane that can provide a high conductivity of approximately 100 mS cm^{-1} under hot and dry conditions (120 °C and 50 % RH) is not likely unless the fundamental understanding of transport mechanisms in functioning electrolyte membranes is realized. This complex experimental and theoretical study explored a number of already known and new proton-conductive inorganic materials as functional components in Nafion-based composite membranes, which provided knowledge to allow the deliberate design of improved or new PEMs. The experimental findings and fundamental understandings are generalized in the following Conclusions section.

7.1 Conclusions

1. A two-electrode through-plane inorganic conductivity measurement method has been developed. With the newly constructed conductivity cell and introduced BekkTech saturator, we realized the conductivity measurement of inorganic materials over a wide range of temperature from 25 to 120 °C and RH from 1 to 100 % reliably. The contribution of electrons in the conductivity was quantitatively defined at the same time.

2. A well known inorganic proton conductor, α-ZP, was proposed as a standard material (similar to Nafion for PEM) for future testing and calibrating the newly developed conductivity cells on the basis of literature study and laboratory measurements.

3. The study investigated the proton conductivity of solid acid materials, such as sulfated zirconia (S-ZrO_2), phosphosilicate gels (P-SiO_2), and sulfonic functionalized SBA-15,

over a wide range of RH. For the first time, their impedance characteristics were obtained and discussed to better understand the proton transfer process under different conditions.

4. Sulfated zirconia presented a high proton conductivity of 10 mS cm^{-1} under fully hydrated conditions at elevated temperatures owing to SO_x groups existing on the ZrO_2 surface. As the RH was increased, the proton transport in the S-ZrO_2 pellet changed from the kinetically sluggish behavior to the dynamic mass transfer mechanism.

5. Phosphosilicate gel with a P:Si ratio of 1.5 has a better conductivity than that with the P:Si ratio of 0.5. In our laboratory measurements, it was investigated that the former reached a high proton conductivity of 100 mS cm^{-1}, which was higher than that of Nafion. Nafion NRE 212 shows a conductivity of 80 mS cm^{-1} at the same temperature of 120 °C and 70 % RH. Silicon phosphate oxide ($Si_5O(PO_4)_6$) in phosphosilicate gels forms an isolated phosphoric acid and Si-O-POH groups, which facilitate the proton conductivity at high RH. The structure of phosphosilicate gels allows the enhancement of the water retention at 120 °C and reduced RH. Based on the impedance spectroscopy analysis, it was found that the phosphosilicate gels are primarily proton-conductive materials and conduct protons as pure ion conductors.

6. Sulfonic-functionalized SBA-15, containing surface siloxane Si-O-Si-OH and sulfonic -SO_3H groups, have a relatively low proton conductivity. However, its large surface area is suitable to improve the proton distribution in composite membranes when it is used as an additive. The AC impedance plots and DC polarization curves indicate that SBA-15 might partially conduct electrons. By calculating the transport numbers of protons and electrons, we found that the electron conductivity contributed less than 1% of the proton conductivity at different RH. SBA-15 has been regarded as a proton-conductivity dominant material.

7. Nafion-based proton-conductive composite membranes with different functionalized solid acid additives have been synthesized by different methods. The research found that functionalized solid acid particles, including S-ZrO_2, SBA-15, MCM-41, S-SiO_2, and P-SiO_2,

increased the acidity of the membrane. The proton conductivity of composite membranes was directly correlated with their acidity.

8. Membranes with poor proton conductivity presented to have low values of membrane water uptake. However, the membrane proton conductivity was not proportional to the membrane water uptake. The interaction between the inorganic matrix and the membrane cluster affects the membrane conductivity.

9. Inorganic additive properties, such as conductivity, surface area, and acidity, affect the conductivity of composite membranes. Modeling simulation showed that the acid-group concentration on the surface of inorganic particles significantly affected the proton conduction of composite membranes. This suggests a new route in rational design of a high proton-conductive composite membrane, which is to enhance the acidity of inorganic materials via surface modification, and at the same time to increase the specific surface area of particles.

10. The way to synthesize a composite membrane by merely mixing inorganic powders with Nafion solution can not improve the membrane conductivity owing to particle agglomerates.

11. New composite membrane fabrication methods have been developed. They are in-situ formation of P-SiO_2 particles in Nafion matrix by dispersing P-SiO_2 gels in Nafion solution (method I), and poly-condensation of tetraethoxysilane and phosphoric acid within Nafion clusters (method II). Both methods realized uniform distribution of particles in the Nafion matrix when the inorganic additive doping concentration was low. When the hydrophilic inorganic particles have high surface area, they trapped water molecules on the surface, which facilitated the proton transport by providing extra acid sites and decreasing the transport distance between H_3O^+ ions.

12. Hydrophilic inorganic materials are more promising with respect to enhancing the electrochemical performance when they are introduced into composite membranes. Newly developed Nafion/10 % P-SiO_2 composite membranes have shown greater current densities than

Nafion membrane with 40 % lower of the cell resistance. Those P-SiO_2 particles in Nafion preserved a thin layer of absorbed water and increased the proton concentration on the membrane surface, which decreased Tafel slopes of composite membranes.

13. Increased inorganic additive content (> 10 %) decreased the membrane conductivity and worsened the membrane fuel cell performance owing to particle agglomerates and reduced Nafion content.

14. This project developed the first proton-transport model that was based on the rule of mixtures. The model incorporated proton conductivities of inorganic materials and Nafion into the calculation separately. Two modification parameters were proposed to define the effective proton conductivity of the Nafion and inorganic additives. The modeled results were quite consistent with experimental data. The calculation indicated that the standard deviation between modeled results and experimental data was less than 3 mS cm^{-1} for a variety of composite membranes in a wide range of RH from 20 to 70 % at 120 °C.

15. A theoretical proton-transport model, based on the generalized Stefan-Maxwell equations, has been developed. The model took into account structural effects and the thermodynamic equilibrium of membranes. The fitted, assumed, and calculated inorganic parameters were argued to be justifiable. We concluded that this model can be applied for future research to predicat the proton conductivity of composite membranes over a wide range of RH up to 100 %.

7.2 Suggestions for future research

A new rational approach to design membrane materials needs to be developed to meet the application target, which requires the new membrane to have the proton conductivity of at least 100 mS cm^{-1} at elevated temperatures (100 - 130 °C) and dry conditions. One schematic of new

membrane materials is proposed where the inorganic additive works as the catalyst. This catalyst promotes water generation under hot conditions. Therefore, the membrane realizes self-humidifying process and can retain necessary water molecules for the proton transport.

Composite membrane fabrication techniques require further development to attain the desired additive particle size and distribution. In situ formation of inorganic particles in the membrane cluster is promising. The new fabrication technique aims to decrease the particle size i.e., increase the particle surface area. Moreover, with respect to the membrane PEM fuel cell performance, the fabrication technique can make the thickness of the membrane as thin as possible to shorten the proton transfer path.

The mechanism of the ionic motion in composite inorganic-organic membranes is needed to be investigated systematically. The function of inorganic groups, including sulfonated and phosphonated groups, and of the interaction between inorganic particles and organic matrix is examined. Membranes will be characterized by means of different methods to better understand structure - property relationships. Some examples of these methods are TEM, FT-IR, and solid state NMR.

New phosphoric acid functionalized mesoporous inorganic materials with different structures (wormhole, hexagonal and cubic) and high acidity can be synthesized. These materials, with ordered pores and high surface area, are expected to improve the interaction of the inorganic phase with the organic matrix.

BIBLIOGRAPHY

1. Li, Q., et al., *The CO Poisoning Effect in PEMFCs Operational at Temperature up to 200°C.* Journal of The Electrochemical Society, 2003. **150**(12): p. A1599-A1605.
2. Ciureanu, M. and H. Wang, *Electrochemical Impedance Study of Electrode-Membrane Assemblies in PEM Fuel Cells I. Electro-oxidation of H_2 and H_2/CO Mixtures on Pt-Based Gas-Diffusion Electrodes.* Journal of the Electrochemical Society, 1999. **146**(11): p. 4031-4040.
3. EERC. *R&D Plan for the High Temperature Membrane Working Group*. 2008 [cited; Available from: http://www1.eere.energy.gov/hydrogenandfuelcells/htmwg.html
4. Alberti, G., et al., *Polymeric proton conducting membranes for medium temperature fuel cells (110-160°C).* Journal of Membrane Science, 2001. **185**(1): p. 73-81.
5. Alberti, G. and M. Casciola, *Composite Membranes for Medium-Temperature PEM Fuel Cells.* Annu. Rev. Mater. Res., 2003. **33**: p. 129-154.
6. Hogarth, W.H.J., J.C. Diniz da Costa, and G.Q. Lu, *Solid acid membranes for high temperature (> 140°C) proton exchange membrane fuel cells.* Journal of Power Sources, 2005. **142**(1-2): p. 223-237.
7. Yuan, J., H. Pu, and Z. Yang, *Studies on Sulfonic Acid Functionalized Hollow Silica Spheres/Nafion® Composite Proton Exchange Membranes.* Journal of Polymer Science: Part A: Polymer Chemistry, 2009. **47**: p. 2647-2655.
8. Herring, A.M., *Inorganic-polymer composite membranes for proton exchange membrane fuel cells.* Polymer Reviews, 2006. **46**(3): p. 245-296.

9. Park, Y.-S. and Y. Yamazaki, *Low methanol permeable and high proton-conducting Nafion/calcium phosphate composite membrane for DMFC.* Solid State Ionics, 2005. **176**: p. 1079-1089.

10. Saccà, A., et al., *Nafion-TiO_2 hybrid membranes for medium temperature polymer electrolyte fuel cells (PEMFCs).* Journal of Power Sources, 2005. **152**: p. 16-21.

11. Alberti, G., et al., *Novel Nafion-zirconium phosphate nanocomposite membranes with enhanced stability of proton conductivity at medium temperature and high relative humidity.* Electrochimica Acta, 2007. **52**(28): p. 8125-8132.

12. Santurri, P.R., J. Mausar, and B. Decker, *Microstructural Design and Development of High Performance Polymer Electrolyte Membranes*, in *2008 Annual Progress Report*. 2008.

13. Choi, P., et al., *Consideration of Thermodynamic, Transport, and Mechanical Properties in the Design of Polymer Electrolyte Membranes for Higher Temperature Fuel Cell Operation.* Journal of Polymer Science: Part B: Polymer Physics, 2006. **44**: p. 2183-2200.

14. Hamlen, R.P., *Ionic Conductivity of Zirconium Phosphate.* Journal of the Electrochemical Society, 1962. **109**(8): p. 746-749.

15. England, W.A., et al., *Fast Proton Conduction in Inorganic Ion-Exchange Compounds.* Solid State Ionics, 1980. **1**: p. 231-249.

16. Andersen, E.K., et al., *α-zirconium hydrogenphosphate, monohydrate: preparation, chemical properties and ac conductivity.* Solid State Ionics, 1982. **7**(4): p. 301-306.

17. Subramanian, M.A., B.D. Roberts, and A. Clearfield, *On the Proton Conductor $(H_3O)Zr_2(PO_4)_3$.* Materials Research Bulletin, 1984. **19**(11): p. 1471-1478.

18. Casciola, M. and D. Bianchi, *Frequency response of polycrystalline samples of α-$Zr(HPO_4)_2$•H_2O at different relative humidities.* Solid State Ionics, 1985. **17**(4): p. 287-293.

19. Heed, B., et al., *Proton conductivity in fuel cells with solid sulphate electrolytes.* Solid State Ionics, 1991. **46**(1-2): p. 121-125.

20. Stein, E.W., A. Clearfield, and M.A. Subramanian, *Conductivity of group IV metal sulfophosphonates and a new class of interstratified metal amine-sulfophosphonates.* Solid State Ionics, 1996. **83**(1-2): p. 113-124.

21. Alberti, G., et al., *Protonic conductivity of layered zirconium phosphonates containing -- SO_3H groups. III. Preparation and characterization of γ-zirconium sulfoaryl phosphonates.* Solid State Ionics, 1996. **84**(1-2): p. 97-104.

22. Alberti, G., et al., *Proton conductivity of mesoporous zirconium phosphate pyrophosphate.* Solid State Ionics, 1999. **125**(1-4): p. 91-97.

23. Hogarth, W.H.J., et al., *Proton conductivity of mesoporous sol–gel zirconium phosphates for fuel cell applications.* Journal of Materials Chemistry, 2005. **15**: p. 5.

24. Matsuda, A., et al., *Proton conductivities of sol-gel derived phosphosilicate gels in medium temperature range with low humidity.* Solid State Ionics, 2002. **154-155**: p. 687-692.

25. Carrière, D., et al., *Proton conductivity of colloidal nanometric zirconium phosphates.* Solid State Ionics, 2003. **162-163**: p. 185-190.

26. Hara, S. and M. Miyayama, *Proton conductivity of superacidic sulfated zirconia.* Solid State Ionics, 2004. **168**(1-2): p. 111-116.

27. Marschall, R., et al., *Proton conductivity of sulfonic acid functionalized mesoporous materials.* Microporous and Mesoporous Materials, 2007. **99**: p. 190-196.

28. Jin, Y.G., et al., *Porous Silica Nanospheres Functionalized with Phosphonic Acid as Intermediate-Temperature Proton Conductors.* Journal of Physical Chemistry C, 2009. **113**: p. 3157-3163.

29. Colomban, P., *Proton conductors-solids, membranes and gels materials and devices*, ed. A.R. West and H. Baxter. 1992, New York: Cambridge Univeristy Press.

30. Alberti, G. and M. Casciola, *Solid state protonic conductors, present main applications and future prospects.* Solid State Ionics, 2001. **145**(1-4): p. 3-16.

31. Shao, Z.G., et al., *Hybrid Nafion-inorganic oxides membrane doped with heteropolyacids for high temperature operation of proton exchange membrane fuel cell.* Solid State Ionics, 2006. **177**(7-8): p. 779-785.

32. Otomo, J., et al., *Phase transition behavior and proton conduction mechanism in cesium hydrogen sulfate/silica composite.* Journal of Physics and Chemistry of Solids, 2005. **66**(1): p. 21-30.

33. Tatsumisago, M., et al., *Preparation of proton conductive composites with cesium hydrogen sulfate and phosphosilicate gel.* Solid State Ionics, 2005. **176**(39-40): p. 2909-2912.

34. Thampan, T.M., et al., *Systematic Approach to Design Higher Temperature Composite PEMs.* Journal of The Electrochemical Society, 2005. **152**(2): p. A316-A325.

35. Lvov, S., et al. *New Proton Conductive Composite Materials with Co-continuous Phases Using Functionalized and Crosslinkable VDF/CTFE Fluoropolymers*. in *The 2007 DOE Hydrogen Program Review Meeting*. 2007. Arlington, VA.

36. Melero, J.A., R.v. Grieken, and G. Morales, *Advances in the Synthesis and Catalytic Applications of Organosulfonic-Functionalized Mesostructured Materials.* Chemical Reviews, 2006. **106**: p. 3790-3812.

37. Marschall, R., J. Rathouský, and M. Wark, *Ordered Functionalized Silica Materials with High Proton Conductivity.* Chemistry of Materials, 2007. **19**: p. 6401-6407.

38. Marschall, R., et al., *Nanoparticles of Mesoporous SO_3H-Functionalized Si-MCM-41 with Superior Proton Conductivity* Small, 2009. **5**(7): p. 854-859.

39. Steininger, H., et al., *Intermediate temperature proton conductors for PEM fuel cells based on phosphonic acid as protogenic group: A progress report.* Physical Chemistry Chemical Physics, 2007. **9**: p. 1764-1773.

40. Mauritz, K.A. and R.B. Moore, *State of Understanding of Nafion.* Chemical Reviews, 2004. **104**: p. 4535-4585.

41. Choi, P., N.H. Jalani, and R. Datta, *Thermodynamics and Proton Transport in Nafion.* Journal of The Electrochemical Society, 2005. **152**(3): p. E84-E89.

42. Pereira, F., et al., *Advanced Mesostructured Hybrid Silica-Nafion Membranes for High-Performance PEM Fuel Cell.* Chemistry of Materials, 2008. **20**: p. 1710-1718.

43. Ye, G., C.A. Hayden, and G.R. Goward, *Proton Dynamics of Nafion and Nafion/SiO Composites by Solid State NMR and Pulse Field Gradient NMR.* Macromolecules, 2007. **40**(5): p. 1529-1537.

44. Aparicio, M. and L.C. Klein, *Synthesis and Characterization of Nafion/60SiO_2-30P_2O_5-10ZrO_2 Sol-Gel Composite Membranes for PEMFCs.* Journal of The Electrochemical Society, 2005. **152**(3): p. A493-A496.

45. Aricò, A.S., et al., *Influence of the acid-base characteristics of inorganic fillers on the high temperature performance of composite membranes in direct methanol fuel cells.* Solid State Ionics, 2003. **161**: p. 251-265.

46. Adjemian, K.T., et al., *Silicon Oxide Nafion Composite Membranes for Proton-Exchange Membrane Fuel Cell Operation at 80-140°C.* Journal of The Electrochemical Society, 2002. **149**(3): p. A256-A261.

47. Miyake, N., J.S. Wainright, and R.F. Savinell, *Evaluation of a Sol-Gel Derived Nafion/Silica Hybrid Membrane for Proton Electrolyte Membrane Fuel Cell Applications I. Proton Conductivity and Water Content.* Journal of the Electrochemical Society, 2001. **148**(8): p. A898-A904.

48. Baglio, V., et al., *Composite Mesoporous Titania Nafion-Based Membranes for Direct Methanol Fuel Cell Operation at High Temperature.* Journal of the Electrochemical Society, 2005. **152**(7): p. A1373-A1377.

49. Baglio, V., et al., *Nafion-TiO_2 composite DMFC membranes: physico-chemical properties of the filler versus electrochemical performance.* Electrochimica Acta, 2005. **50**: p. 1241-1246.

50. Chalkova, E., et al., *Nafion/TiO_2 Proton Conductive Composite Membranes for PEMFCs Operating at Elevated Temperature and Reduced Relative Humidity.* Journal of The Electrochemical Society, 2005. **152**(6): p. A1035-A1040.

51. Baglio, V., et al., *Influence of TiO_2 Nanometric Filler on the Behaviour of a Composite Membrane for Applications in Direct Methanol Fuel Cells.* Journal of New Materials for Electrochemical System, 2004. **7**: p. 275-280.

52. Chalkova, E., et al., *Nafion/Zirconium Phosphate Composite Membranes for PEMFC Operating at up to 120°C and down to 13% RH.* Journal of The Electrochemical Society, 2007. **154**(2): p. B288-B295.

53. Si, Y., H.R. Kunz, and J.M. Fenton, *Nafion-Teflon-$Zr(HPO_4)_2$ Composite Membranes for High-Temperature PEMFCs.* Journal of The Electrochemical Society, 2004. **151**(4): p. A623-A631.

54. Kim, Y.-T., et al., *Nafion/ZrSPP composite membrane for high temperature operation of PEMFCs.* Electrochimica Acta, 2004. **50**(2-3): p. 645-648.

55. Costamagna, P., et al., *Nafion 115/zirconium phosphate composite membranes for operation of PEMFCs above 100 °C.* Electrochimica Acta, 2002. **47**(7): p. 1023-1033.

56. Meng, F., et al., *Structural and transport effects of doping perfluorosulfonic acid polymers with the heteropoly acids, $H_3PW_{12}O_{40}$ or $H_4SiW_{12}O_{40}$.* Electrochimica Acta, 2007. **53**(3): p. 1372-1378.

57. Navarra, M.A., F. Croce, and B. Scrosati, *New, high temperature superacid zirconia-doped Nafion™ composite membranes.* Journal of Materials Chemistry, 2007. **17**: p. 3210-3215.

58. Tung, S.-P. and B.-J. Hwang, *Preparation and Characterization of Nafion®/Hydrated Phosphor-Silicate Hybrid Membranes for the Direct Methanol Fuel Cell.* Fuel Cells, 2006. **1**: p. 32-39.

59. Yang, C., et al., *Approaches and technical challenges to high temperature operation of proton exchange membrane fuel cells.* Journal of Power Sources, 2001. **103**(1): p. 1-9.

60. Fedkin, M.V., et al., *Understanding the Water Retention of Composite PEMs Based on Surface Chemistry of Inorganic Fillers.* ECS Transactions, 2008. **11**(27): p. 189-198.

61. Thampan, T., et al., *Modeling of Conductive Transport in Proton-Exchange Membranes for Fuel Cells.* Journal of The Electrochemical Society, 2000. **147**(9): p. 3242-3250.

62. Choi, P., N.H. Jalani, and R. Datta, *Thermodynamics and Proton Transport in Nafion II. Proton Diffusion Mechanisms and Conductivity.* Journal of The Electrochemical Society, 2005. **152**(3): p. E123-E130.

63. Cohen, E.R., et al., *Quantities, Units and Symbols in Physical Chemistry*. Third ed. 2007, Cambridge: The Royal Society of Chemistry.

64. BekkTech, *General Information on Membrane Conductivity*. 2007.

65. Ciureanu, M., S.D. Mikhailenko, and S. Kaliaguine, *PEM fuel cells as membrane reactors: kinetic analysis by impedance spectroscopy.* Catalysis Today, 2003. **82**: p. 195-206.

66. Thangadurai, V., R.A. Huggins, and W. Weppner, *Use of simple ac technique to determine the ionic and electronic conductivities in pure and Fe-substituted $SrSnO_3$ perovskites.* Journal of Power Sources, 2002. **108**: p. 64-69.

67. Bard, A.J. and L.R. Faulkner, *Electrochemical Methods: Fundamentals and Applications.* 2004: John Wiley & Sons, Inc.

68. Clearfield, A., et al., *On the Mechanism of Ion Exchange in Crystalline Zirconium Phosphates. I. Sodium Ion Exchange of α-Zirconium Phosphate.* The Journal of Physical Chemistry, 1969. **73**(10): p. 3424-3430.

69. Laporta, M., M. Pegoraro, and L. Zanderighi, *Perfluorosulfonated membrane (Nafion): FT-IR study of the state of water with increasing humidity.* Physical Chemistry Chemical Physics, 1999. **1**: p. 4619-4628.

70. Troup, J.M. and A. Clearfield, *On the Mechanism of Ion Exchange in Zirconium Phosphates. 20. Refinement of the Crystal Structure of α-Zirconium Phosphate.* Inorganic Chemistry, 1977. **16**(12): p. 3311-3314.

71. Alberti, G., et al., *Layered and Pillared Metal (IV) Phosphates and Phosphonates.* Advanced Materials, 1996. **8**(4): p. 291-303.

72. Alberti, G., et al., *Proton-conducting Solid Dispersions of Silica and Zirconium Phosphate Pyrophosphate.* Journal of Materials Chemistry, 1995. **5**(11): p. 1809-1812.

73. Casciola, M., F. Marmottini, and A. Peraio, *ac conductivity of α-layered zirconium phosphate in the presence of water vapour at 100-200°C.* Solid State Ionics, 1993. **61**(1-3): p. 125-129.

74. Jerus, P. and A. Clearfield, *Ionic conductivity of anhydrous zirconium bis(monohydrogen orthophosphate) and its sodium ion forms.* Solid State Ionics, 1982. **6**(1): p. 79-83.

75. Yadav, G.D. and J.J. Nair, *Sulfated zirconia and its modified versions as promising catalysts for industrial processes.* Microporous and Mesoporous Materials, 1999. **33**(1-3): p. 1-48.

76. Matsuda, A., et al., *Medium temperature range characterization as a proton conductor for phosphosilicate dry gels containing large amounts of phosphorus.* Electrochimica Acta, 2001. **47**(6): p. 939-944.

77. Margolese, D., et al., *Direct Syntheses of Ordered SBA-15 Mesoporous Silica Containing Sulfonic Acid Groups.* Chemistry of Materials, 2000. **12**: p. 2448-2459.

78. Melero, J.A., et al., *Direct Syntheses of Ordered SBA-15 Mesoporous Materials Containing Arenesulfonic Acid Groups.* Journal of Materials Chemistry, 2002. **12**: p. 1664-1670.

79. Zhao, D., et al., *Triblock Copolymer Syntheses of Mesoporous Silica with Periodic 50 to 300 Angstrom Pores.* Science, 1998. **279**: p. 548-552.

80. Chen, C.Y., et al., *Nafion/polyaniline/silica composite membranes for direct methanol fuel cell application.* Journal of Power Sources, 2007. **166**: p. 324-330.

81. Tung, S.-P. and B.-J. Hwang, *High proton conductive glass electrolyte synthesized by an accelerated sol-gel process with water/vapor management.* Journal of Membrane Science, 2004. **241**(2): p. 315-323.

82. Jin, Y., J.C. Diniz da Costa, and G.Q. Lu, *Proton conductive composite membrane of phosphosilicate and polyvinyl alcohol.* Solid State Ionics, 2007. **178**(13-14): p. 937-942.

83. Kim, D.S., et al., *Preparation and characterization of crosslinked PVA/SiO_2 hybrid membranes containing sulfonic acid groups for direct methanol fuel cell applications.* Journal of Membrane Science, 2004. **240**(1-2): p. 37-48.

84. Di Noto, V., et al., *New inorganic-organic proton conducting membranes based on Nafion® and [$(ZrO_2)\cdot(SiO_2)_{0.67}$] nanoparticles: Synthesis vibrational studies and conductivity.* Journal of Power Sources, 2008. **178**(2): p. 561-574.

85. Alberti, G. and M. Casciola, *Layered metalIV phosphonates, a large class of inorgano-organic proton conductors.* Solid State Ionics, 1997. **97**(1-4): p. 177-186.

86. Aricò, A.S., et al., *Surface properties of inorganic fillers for application in composite membranes-direct methanol fuel cells.* Journal of Power Sources, 2004. **128**: p. 113-118.

87. Larminie, J. and A. Dicks, *Fuel Cell Systems Explained*. 2003, West Sussex: John Wiley & Sons Ltd.

88. Morris, D.R. and X. Sun, *Water-Sorption and Transport Properties of Nafion 117 H.* Journal of Applied Polymer Science, 1993. **50**: p. 1445-1452.

Appendix A

Proton Conductivity of PVDF-CTFE/Nafion/α-ZP Composite Membranes

α-Zirconium phosphate was doped in the PVDF-CTFE/Nafion polymer matrix to develop proton conductive composite membranes. The proton conductivities of composite membranes with a series of composition are shown in Figure **A-1**. It was observed that the conductivities of composite membranes were proportional to the content of Nafion. α-ZP was seemed not to contribute to the conductivity of composite membranes.

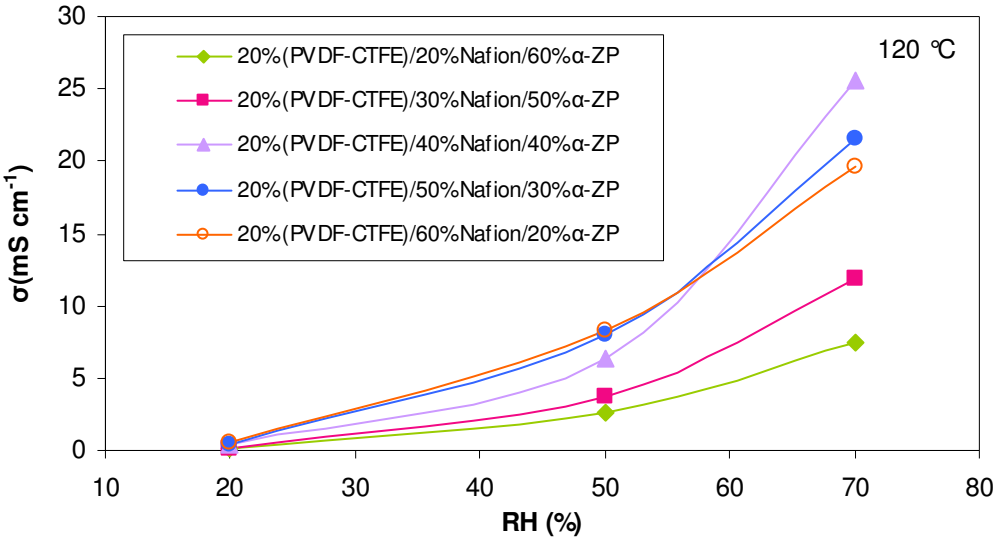

Figure **A-1**: Proton conductivities of PVDF-CTFE/Nafion/α-ZP composite membranes with a series of composition at 120 °C and different RH.

Appendix B

PEM Fuel Cell Performance of NPS Composite Membranes at Low Temperatures

The PEM fuel cell performance of NPS composite membranes at 30 and 80 °C under different RH is shown in the following figures.

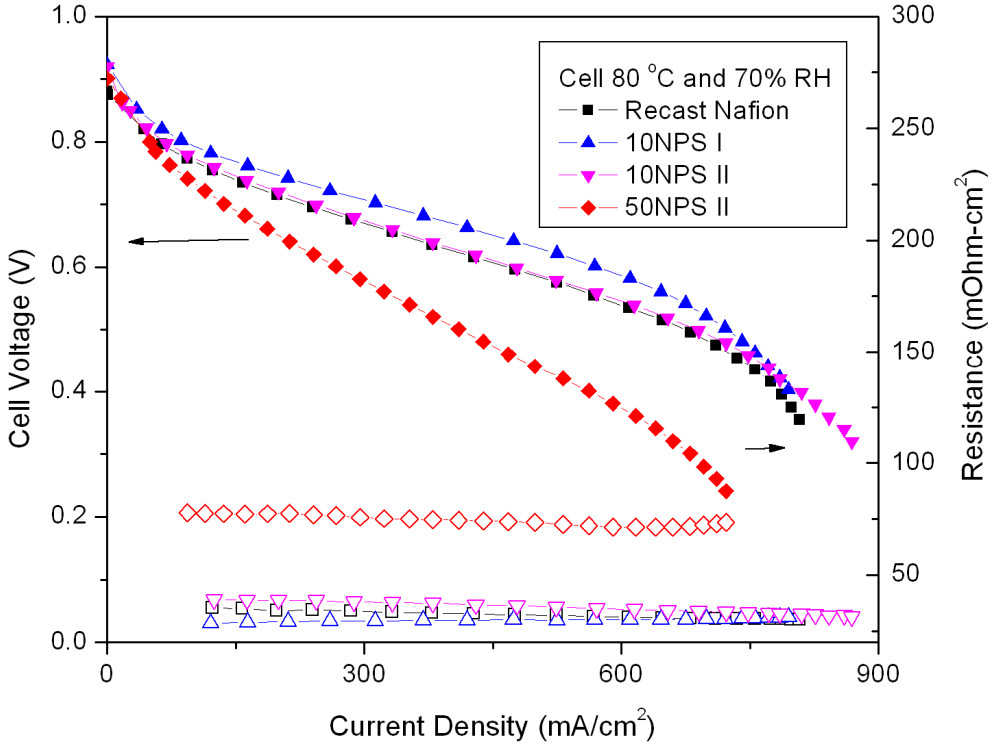

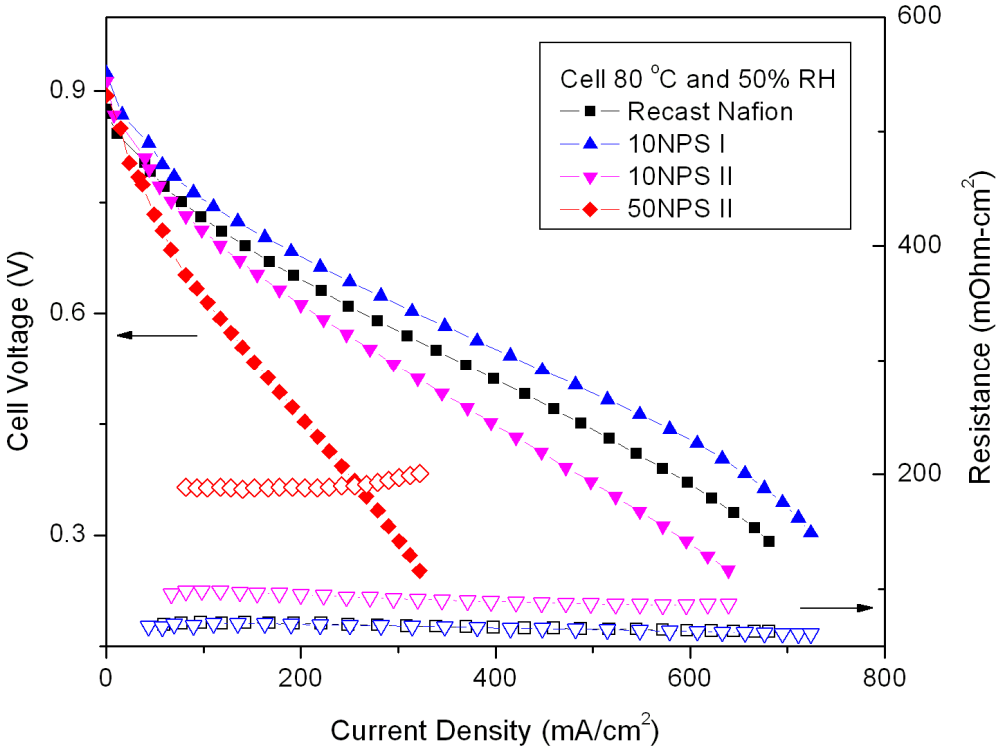
Cell 80 °C and 50% RH
Recast Nafion
10NPS I
10NPS II
50NPS II
Cell Voltage (V)
Resistance (mOhm-cm²)
Current Density (mA/cm²)
0.9
0.6
0.3
600
400
200
0
200
400
600
800

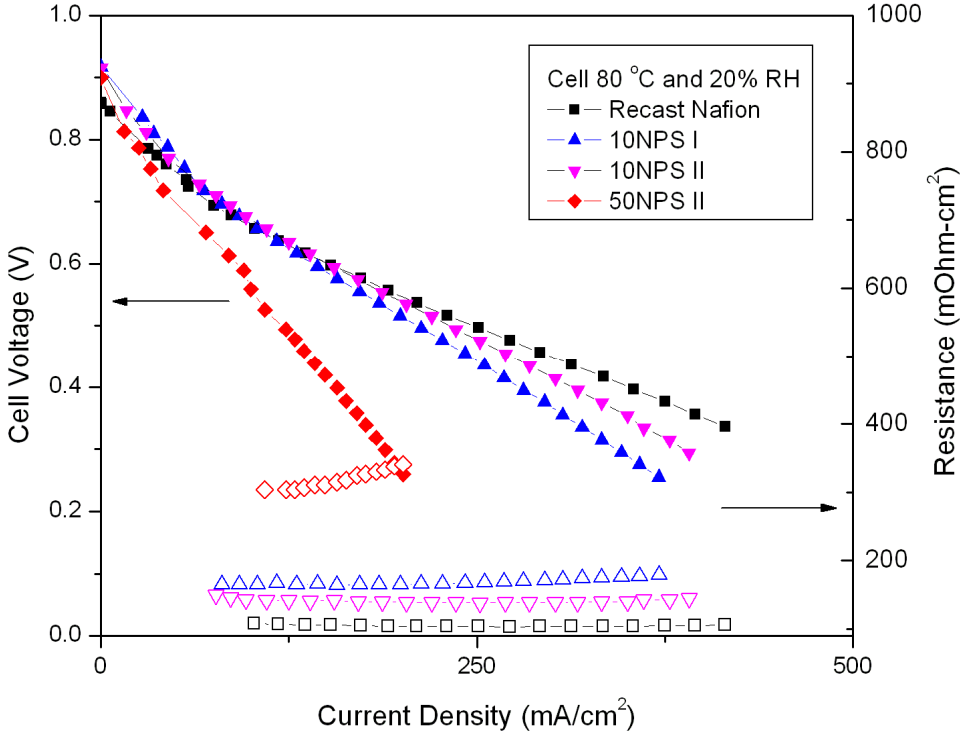
Cell 80 °C and 20% RH
Recast Nafion
10NPS I
10NPS II
50NPS II
Cell Voltage (V)
Resistance (mOhm-cm²)
Current Density (mA/cm²)
1.0
0.8
0.6
0.4
0.2
0.0
1000
800
600
400
200
0
250
500

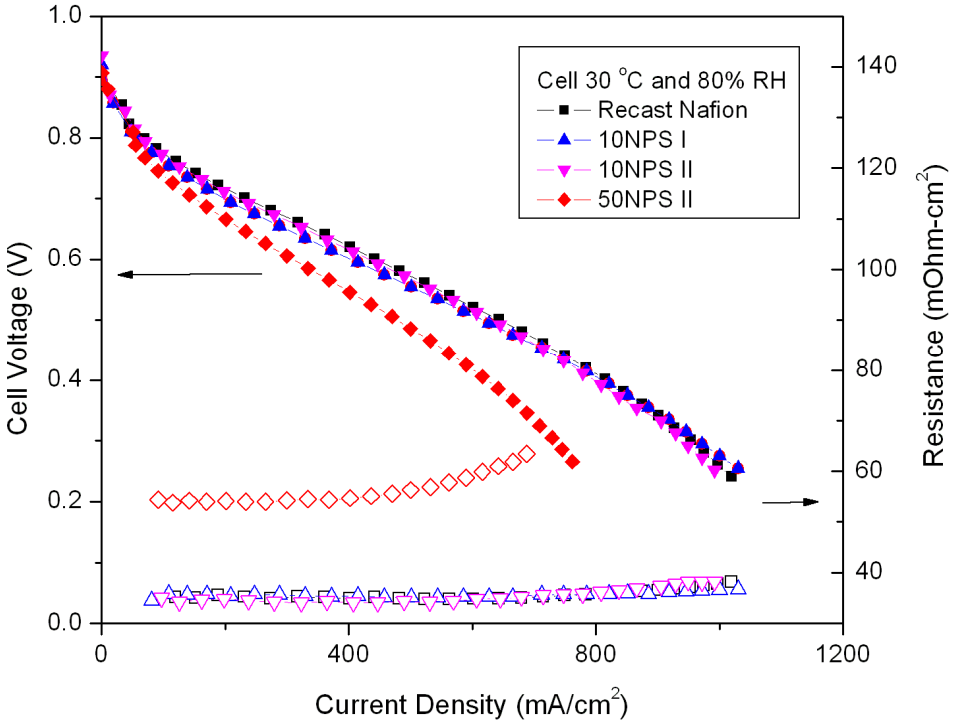

Figure **B-1**: PEM fuel cell performance and resistance of recast Nafion and Nafion/P-SiO_2 composite membranes, in a H_2/air fuel cell at 30 and 80 °C under different RH.

VITA

Chunmei Wang

Chunmei Wang was born on April 21, 1977, in Hami, Xinjiang province, China. She received her Bachelor of Engineering in Thermal Engineering from Changsha University of Electric Power, China, in 2001. After graduation, she continued her graduate study in Thermal Engineering in Huazhong University of Science and Technology, China. She carried out the fundamental studies on submicrometer particle formation and control in coal combustion systems and received her master's degree in 2004.

She found the interest in research. In Fall 2004, she applied to study in Chemical Engineering at University of North Dakota, Grand Forks, ND. She worked on the research project of low pressure impactors of BLPI and DLPI applied on environmental aspect of trace elements from combustion and published a paper in Aerosol Science and Technology in 2007. After receiving a master degree in Chemical Engineering, in Fall 2006, she joined the Ph.D. program of Energy & Geo-Environmental Engineering at the Pennsylvania State University. Her thesis was focused on the proton conductive materials for PEM fuel cells and was sponsored by the U.S. Department of Energy.

Chunmei has a happy family with two sisters. The family members are all in China. She loves kids and has been working as a volunteer to teach Chinese in the Happy Valley Chinese School for almost four years.